
THE UNIVERSITY *of* EDINBURGH

# Coupled process modelling with applications to radionuclide storage and disposal

Myles English BSc (Hons.), MSc


PhD Thesis
University of Edinburgh
2013

**Abstract**

Radioactive waste repositories, designed in accordance with the current UK concept, would be required to provide containment for thousands of years beneath hundreds of metres of rock. The physical processes, both geological and other processes, that might lead to migration of radionuclides are slow in comparison to human timescales — it is impractical to make an experiment of the whole system and so these systems are typically investigated through the use of numerical models. Predictive models are based on combinations of: assumptions, mathematical formulations and parameter values derived from experimental observations.

The Ventilation Experiment in the Opalinus Clay at Mont Terri, Switzerland, was designed to involve geological and other physical processes that would be active during the excavation and construction phases of a repository, and with consequences for the repository performance during the operational phase. The experiment consisted of a 10 m long tunnel of 1.3 m diameter through which air of known relative humidity was circulated in order to force drying and resaturation through the tunnel wall. Two such cycles over four years have been observed via installed instrumentation.

Several numerical models have been constructed of the ventilation experiment by different international teams under the DECOVALEX project using different approaches for cross-validation. Through participation in this project, a 1D model using Richards' Equation was developed that effectively reproduces the hydrodynamic, mechanical and conservative mass transport results. During the course of developing that model, many other domains, meshes, formulations and software versions were investigated.

Now that the field scale Ventilation Experiment can be reproduced with numerical models, the findings (assumptions, formulations, parameter values, computational methods and software) would be transferable to other argillaceous formations to enable predictive modelling of similar scenarios and contribute to the safe disposal of nuclear waste and other problems involving similar geological processes.

Work of this type fills the gap between laboratory scale experiments and regional scale modelling of geological systems. The gap is especially wide for low-permeability formations because the size and time-scale limitations effect the ability to make direct observations and measurements.

Two particular problems were also addressed in this work: that of the use relative permeability functions and also the computational treatment of the physical interface between the tunnel domain and the rock domain. A sensitive component in many models of unsaturated flow through porous media and covering a wide variety of applications, including reservoir engineering, is the representation of permeability at an unsaturated point ($k_x$) as a scaling of the saturated permeability ($\mathrm{k}_{sat}$) by introducing some function of the pressure head, or saturation as the relative permeability ($k_{rel}$) in the relation $k_x = \mathrm{k}_{sat} k_{rel}$. The choice of the particular function and its parameter values adds little to our understanding of the physical parameters. A solution is proposed to the second problem, of how to computationally represent, implement and manage the interface between two physical (i.e. spatial) domains. The scheme maps every part of the boundary of one domain onto the corresponding part of the boundary of the other domain, storing the state variables in shared memory and converting between physical components.

# Declaration and attribution of work

This thesis has been composed by myself and the the work is my own, unless otherwise attributed. This work has not been submitted for any other degree or professional qualification.

In section 6.2 I present results of modelling the Drying Test, all of which was the work of Christopher McDermott. The idea in section 6.1.2 for the calculation of mechanical deformation from the pore pressure came from Alex Bond.

My contributions to individual papers are stated here.

**Journal Paper 1** B. Garitte et al. (Feb. 2013). "Analysis of hydro-mechanical processes in a ventilated tunnel in an argillaceous rock on the basis of different modelling approaches". In: *Journal of Rock Mechanics and Geotechnical Engineering* 5 (1), pp. 1–17

**Contribution** This is one of the four main papers resulting from the four year project of Task A of DECOVALEX-2011. At a very late stage in production, during the final review of this paper, severe management issues came to light and the results presented in section 6.1, Modelling the Ventilation Experiment, were not included. Nonetheless, I contributed the majority of my research time to this project.

**Journal Paper 2** A. E. Bond et al. (Dec. 1, 2012). "Coupled hydro-mechanical—chemical process modelling in argillaceous formations for DECOVALEX-2011". en. In: *Mineralogical Magazine* 76 (8), pp. 3131–3143

**Contribution** Results were contributed from the OpenGeoSys model of the Ventilation Experiment, principally the mass transport of chloride. Most of the paper features the Quintessa model and their QPAC code and, as above, the OpenGeoSys model results are presented in section 6.1.

**Journal Paper 3** A. Bond, S. Benbow, et al. (Feb. 2013). "Reactive and non-reactive transport modelling in partially water saturated argillaceous porous media around the ventilation experiment, Mont Terri". In: *Journal of Rock Mechanics and Geotechnical Engineering* 5 (1), pp. 44–57

**Contribution** Results were contributed from the OpenGeoSys model of the Ventilation Experiment, principally the mass transport of chloride. Most of the paper features the Quintessa model and their QPAC code.

Signed:  Date: 24th September 2013

Myles English

## Acknowledgements

*Supervisors:*
Dr habil. Christopher McDermott MSc (University of Edinburgh)
Dr Alex Bond (Quintessa)

*Advisor:*
Prof. Wyn Williams (University of Edinburgh)

*Grant body:*
Nuclear Decommissioning Authority - *Radioactive Waste Management Directorate* (NDA-RWMD)

*For Alice, Murdo and Annie.*
*Yes Murdo, I have finished writing my book now.*

# CONTENTS

# LIST OF FIGURES

# LIST OF TABLES

# LIST OF ALGORITHMS

# NOMENCLATURE

| | | |
|---|---|---|
| $p^w$ | Water pressure | [Pa] |
| $\alpha$ | van Genuchten parameter (>0), inverse of the air entry value (bubbling pressure) | [$\mathrm{cm}^{-1}$] |
| $\bar{v}$ | Mean velocity | [$\mathrm{m\,s}^{-1}$] |
| $\bar{\Omega}$ | Union of a domain and its boundary | |
| $\mathbf{g}$ | Acceleration due to gravity | [$\mathrm{m\,s}^{-2}$] |
| $P_c$ | Capillary pressure | [Pa] |
| $\beta$ | Compressibility | [$\mathrm{Pa}^{-1}$] |
| $\Gamma_{\mathtt{D}}$ | Dirichlet boundary conditions ($\in \Gamma$) | |
| $\Delta t_{(\mathtt{t+1})}$ | Next time step | |
| $\Delta t_{(\mathtt{t-1})}$ | Previous time step length | |
| $\Delta t_{(\mathtt{t})}$ | Current time step length | |
| $\rho$ | Density | [$\mathrm{km}^3$] |
| $\rho_k^\gamma$ | Mass of $k$ per unit volume of $\gamma$ | [$\mathrm{kg\,m}^{-3}$] |
| $\Theta$ | Dimensionless fluid content | [-] |
| $\mathbf{v}$ | Macroscopic velocity | [$\mathrm{m\,s}^{-1}$] |
| $\mu$ | Dynamic viscosity | [Pa s] |
| $\epsilon$ | Maximum absolute residual for equivalence | |
| $\theta_r$ | Residual volume fraction | [-] |
| $\theta_s$ | Saturated volume fraction | [-] |
| $\mathbf{J}$ | Flux | [$\mathrm{kg\,m}^{-1}\,\mathrm{s}^{-1}$] |
| $\mathbf{J}_A$ | Advective flux | [$\mathrm{kg\,m}^{-1}\,\mathrm{s}^{-1}$] |
| $\mathbf{J}_D$ | Diffusive flux | [$\mathrm{kg\,m}^{-1}\,\mathrm{s}^{-1}$] |
| $\Gamma$ | Boundary of a domain | |
| $P_g$ | Gas pressure | [Pa] |
| $h$ | Hydraulic head | [m] |
| $k_{rel}^\gamma$ | Relative permeability of phase $\gamma$ | [-] |
| K | Hydraulic conductivity | [$\mathrm{m\,s}^{-1}$] |
| $\mathbb{D}$ | Diffusion coefficients tensor | |
| $\mathbb{R}$ | Set of real numbers. | |
| $\Gamma_{\mathtt{N}}$ | Neumann boundary conditions ($\in \Gamma$) | |
| $\Omega$ | Domain | |
| $\omega$ | Mass fraction | [-] |
| $\partial\Omega$ | Boundary of domain *Omega* | |
| $\mathbf{k}$ | Intrinsic permeability tensor | [$\mathrm{m}^2$] |
| $\phi$ | Porosity | [-] |
| $\Psi_b$ | Adsorption potential | [$\mathrm{J\,kg}^{-1}$] |
| $\Psi_o$ | Osmotic potential | [$\mathrm{J\,kg}^{-1}$] |
| $\Psi_p$ | Pressure potential | [$\mathrm{J\,kg}^{-1}$] |

| | | |
|---|---|---|
| $\Psi_t$ | Total potential | $[\mathrm{J\,kg^{-1}}]$ |
| $\Psi_z$ | Elevation potential | $[\mathrm{J\,kg^{-1}}]$ |
| $P$ | Pressure | [Pa] |
| $P^b$ | Bubbling pressure | [Pa] |
| $P_w^g$ | Equilibrium water vapour pressure | [Pa] |
| $S$ | Saturation | [-] |
| $S^g$ | Gas saturation | |
| $S^l$ | Liquid saturation | |
| $S^\gamma$ | Saturation with phase $\gamma$ | [-] |
| $S_{res}$ | Residual saturation | [-] |
| $\varepsilon$ | Strain | [L/L] |
| $t_{\texttt{max}}$ | Duration of problem | |
| $B$ | Bulk modulus | |
| $k_o$ | matching point at saturation | $[\mathrm{cm\,d^{-1}}]$ |
| $L$ | Length | |
| $l$ | pore-connectivity parameter (van genuchten) | |
| $m$ | van Genuchten parameter | |
| $M_a$ | Molar mass of air (28.97) | $[\mathrm{g\,mol^{-1}}]$ |
| $M_w$ | Molar mass of water (18.01528) | $[\mathrm{g\,mol^{-1}}]$ |
| $n$ | van Genuchten parameter (>1) | |
| $N_A$ | Avogadro's constant ($6.022\,142 \times 10^{23}$) | $[\mathrm{mol^{-1}}]$ |
| $p^b$ | Bubbling pressure | [Pa] |
| $p^{gws}$ | Saturation vapour pressure | [Pa] |
| $p_l^w$ | Pressure of liquid water | [Pa] |
| $q$ | Discharge, volumetric | $[\mathrm{m^3\,s^{-1}}]$ |
| $R$ | Universal gas constant (8.31432) | $[\mathrm{pJ\,K^{-1}\,mol^{-1}}]$ |
| $s$ | Distance in direction of flow | [m] |
| $T$ | Thermodynamic temperature | [K] |
| $t_{\texttt{wc}}$ | Wall clock time | |
| $wc$ | Water content | [% dry mass] |
| $Y$ | Young's Modulus | |

**Superscripts**

| | |
|---|---|
| $\gamma$ | Phase |
| $g$ | Gas phase |
| $l$ | Liquid phase |

**Subscripts**

| | |
|---|---|
| 0 | Initially (i.e. at time = 0) |
| $a$ | Air component |
| $k$ | Component/species (e.g. air, water) |
| $s$ | Soil component |
| $w$ | Water component |

**Other Symbols**

| | |
|---|---|
| $\nabla \cdot$ | Divergence operator: $\frac{\partial}{\partial x} + \frac{\partial}{\partial y} + \frac{\partial}{\partial z}$ |

$\emptyset$ Empty set

$\nabla$ Gradient operator

**Abbreviations**

CFD Computational fluid dynamics

CPU Central processing unit

CT X-ray computed tomography

DECOVALEX development of coupled process models and their validation against experiments

DGD Deep geological disposal

EDZ Excavation damaged zone

FDM Finite difference method

FEM Finite element method

GPGPU General purpose graphics processing unit

HLW High level waste

HPC High performance computing

ILW Intermediate level waste

LILW-LL Low and intermediate level waste — long lived

LILW-SL Low and intermediate level waste — short lived

LLW Low level waste

MPI Message passing interface

PA Performance assessment

PDE Partial differential equation

PSD Particle size density

RHS Right hand side

SF Spent fuel

SpBiCGStab Single precision biconjugate gradient stabilised

VE Ventilation experiment

Chapter 1

# OVERVIEW

This PhD project investigated by numerical modelling the behaviour of a clay tunnel, as it underwent several cycles of forced drying and resaturation during an *in situ* field scale experiment — the *Ventilation Experiment*). It was anticipated that modelling the basic experiment would be relatively straightforward and that along the way it would be worthwhile to investigate features of the experiment, the models and the wider subject of coupled process modelling. Modelling the Ventilation Experiment in a simple way was a significant challenge in itself and formed a large majority of the work.

Radioactive waste repositories would be required to provide containment for thousands of years beneath hundreds of metres of rock and the geological and other physical processes that might lead to migration of radionuclides are slow in comparison to human timescales — it is not possible to make an experiment of the whole system (Neretnieks, 2004). For these reasons, and the complexity of the interactions of the processes, the system is investigated by the use of numerical models.

Models are based on combinations of: assumptions, mathematical formulations and parameter values derived from experimental observations, at a smaller scale than the problem being modelled. Geological processes are scale dependant so it is desirable to experiment on a scale as close as possible to that of the problem to be modelled. The Ventilation Experiment was designed to involve geological and other physical processes that would be active during the excavation and construction phases of a repository, and with consequences for the repository performance during the operational phase.

The combination of the very high level of accuracy required (because of the consequences of the accumulation of errors over the timescales considered), with the complexities (as will be shown later), means that several numerical models were constructed by different international teams using different approaches for validation, under the DECOVALEX[1] project. The results of the DECOVALEX collaboration have been published in a special issue journal[2].

The purpose in reproducing the field scale Ventilation Experiment using a numerical model is so that the findings (assumptions, formulations, parameter values, computational methods and software) are transferable to other argillaceous formations to enable predictive modelling of different scenarios over the lifetime of a repository. In this sense, the modelling system may be used as a calibrated tool.

Work of this type fills the gap between laboratory scale experiments designed to determine rock properties and regional scale modelling of geological systems. The gap is especially wide for low-permeability formations because of the physical size and timescale limitations that effect the ability to make observations and measurements (Neuzil, 1986).

[1] Described in chapter 3.
[2] Journal of Rock Mechanics and Geotechnical Engineering (2013, Vol. 5, No.1)

The findings contribute ultimately to the safe future disposal of nuclear waste and other problems involving similar geological processes. The results of work such as this have important applications from both the UK and international perspectives since the challenge of demonstrating the safe disposal of nuclear waste is significant and common to several countries.

Aspects of the Ventilation Experiment have been modelled before (e.g. by Zheng et al. (2008), who found that the rock undergoes desaturation and oxidation) however not so thoroughly as to capture all the main features. A review of much of the available literature is made in chapter 2.

The main modelling work was done using OpenGeoSys (Kolditz, Bauer, et al., 2012). Many different models (combinations of meshes, dimensions, formulations, parameter values) were attempted before the Ventilation Experiment could be represented realistically and, although these models do not contribute directly to the final results, they nonetheless manifested some interesting problems of numerical modelling and are described in section 5.3.

A consequence of having to manage so many different models, their results, and the presentation of those results every six months at DECOVALEX workshops, was the development of a framework to facilitate the reproducibility of any set of results from a minimum of information. A brief explanation of this framework is given in section 5.2.

**Thesis structure** Relevant literature is reviewed next in chapter 2, chapter 3 describes the setup of the Ventilation Experiment itself that is the central theme of this project. The theoretical background is covered in chapter 4 and describes the mathematical and numerical basis to the wider modelling work in chapter 5 and section 6.1, Modelling the Ventilation Experiment. The conclusions are in chapter 7.

Chapter 2

# LITERATURE REVIEW

The topics covered in the relevant literature are closely interrelated and so the reviews here are only approximately arranged under headings.

**Field scale experiments** Several nuclear waste disposal scenarios (varying repository designs and host rocks) have been investigated by coupled process modelling, mainly as part of the DECOVALEX project, of which a summary is given in Appendix A. Underground sites, most of them home to more than one field scale *in situ* test, have included Grimsel (fractured crystalline rock), Switzerland; Yucca Mountain (fractured tuffs), Nevada, USA; Kamaishi Mine (fractured granite), Japan; the Underground Research Laboratory of Atomic Energy of Canada Ltd (granite) at Pinawa, Manitoba; Tournemire and Bure (argillite), France; Mol (clay), Belgium and Mont Terri, Switzerland (see e.g. Alonso and Alcoverro, 2005; Guo and Dixon, 2006; Kalbacher, Mettier, et al., 2007; C. McDermott et al., 2008; Nguyen et al., 2001; Rutqvist, Börgesson, Chijimatsu, Hernelind, et al., 2009; C.-F. Tsang et al., 2005; Zhang et al., 2008). Two examples that indicate the scale of these types of experiments are:

- When **the Yucca Mountain Drift Scale Test** (DST) began it was designed to undergo four years of heating followed by four years of cooling. Instrumentation consisted of 3700 sensors in 147 boreholes (totalling of 3.3 km of drilling) (Mariner, 2004). Yucca Mountain has also been the site of the Large Block Test and Single Heater Test.
- The **FEBEX test at Grimsel**, Switzerland (a European Commission Project) included an *in situ* experiment whereby heaters, simulating HLW canisters, were encased in bentonite blocks and inserted into horizontal drifts in granitic rock (Alonso and Alcoverro, 2005).

Using ABAQUS and a 3D fully coupled THM finite element model, Börgesson and Hernelind (2005) model the near field for the whole duration of the FEBEX experiment; from excavation onwards, to some time after the emplacement of 'waste'. They postulate the existence of a **skin zone** between the bentonite and the granite — with implications for the (argillaceous) EDZ in the Opalinus Clay. Coupling is by a "*staggered solution technique*" — the initial thermal analysis is used for input to the hydromechanical analysis (which effects the thermal properties) and the procedure is repeated until there is no change in output over each time step. This seems to be a hybrid of coupling schemes (described in section 4.3.2): hydromechanical processes are associated in a system matrix (a *monolithic* scheme), however the thermal process is solved first (making it a *partitioned* scheme). A factor is used to alter the vapour flow diffusivity to account for the decreased vapour flux at high and low saturations. Water transport is governed by the pore water pressure (i.e. advection dominates) in the FEBEX experiment (Börgesson and Hernelind, 2005), unlike in the Opalinus Clay, and a vapour transport calculation is used

too. They use the modified van Genuchten formula with experimentally derived parameter values. Relative humidity is found, where $U_w$ is the porewater pressure, by

$$RH = \exp(U_w/135022)\,.$$

Börgesson and Hernelind (2005) conclude that fully coupled HM models are required for determining the water pressure response to excavation during the construction phase and fully coupled THM models are required for the prediction of the hydration and stress development in the bentonite buffer.

Chijimatsu et al. (2005) modelled the Prototype Repository Project (PRP) comprised of an experimental back filling of galleries containing 'waste' at the Kamaishi Mine, Japan, using an extended version of THAMES — a fully coupled THM finite element code.

Guo and Dixon (2006) model the Tunnel Sealing Experiment (TSX) at the Underground Research Laboratory, Canada, using a half-domain FE mesh orthogonal to the long axis of the tunnel to investigate the response of bulkheads sealing a tunnel containing 'waste'.

Argillaceous rocks at Tournemire have also been studied extensively; part of DECOVALEX THMC (Task C) was concerned with the EDZ in the Toarcian Marls and Argillites of this terrane. One of the EDZs studied is around a tunnel that was excavated in 1881: Maßmann et al. (2009) use Richards' Approximation[1] for unsaturated single phase flow and identify intrinsic permeability and relative permeability as more important than mechanical deformation and seasonal influences, although the authors acknowledge that the simulated saturation values are not reproduced accurately. Deformation mechanisms are found to be specific to each site and the theory of *propagation of fractures* is preferred over the *continuum mechanical* approach that is seen as limited[2].

**Coupled processes** Coupled process modelling has been applied in many different geological fields: Feng et al. (2004) investigated applications in oil and gas reservoir engineering, coal mining and geotechnical engineering in permafrost regions, C. I. McDermott, Randriamanjatosoa, et al. (2006) modelled heat extraction and related effects from geothermal sources, Zhu et al. (2007) modelled gas flow, deformation, and sorption/desorption of methane in a coal seam, Gessner et al. (2009) modelled hydrothermal systems related to a geothermal resource and mineralisation of an ore body.

Radioactive waste disposal is possibly the most complex application of coupled process modelling. Hudson et al. (2001) gives a full account of the process of storage of nuclear waste and relates THM processes to phases of the nuclear waste storage lifetime through excavation – operational – post-closure stages. They give a good overview of the role of coupled THM models in the Performance Assessment (PA) of nuclear waste repositories Hudson et al. (2001, p. 157):

> "A predictive THM capability is required to support repository design because precedent practise information is insufficient. Many aspects of THM processes and modelling are now well understood and there is a variety of numerical codes available

[1] Richards' Approximation of unsaturated flow assumes that the compressibility of the gaseous phase can be accommodated in a lumped parameter — *storativity*, that includes all compressibility effects (e.g. squeezing a sponge releases water).

[2] Fractures are part of the superset of geological features called *discontinuities* i.e. the clay does not deform without bound but rifts instead.

to provide solutions for different host rock and repository conditions. However, modelling all the THM mechanisms in space and time is extremely complex and simplifications will have to be made if only because it is not possible to obtain all the necessary detailed supporting information. Therefore, an important step is to clarify the THM modelling requirement within the PA context. This will help to indicate the complexity of THM modelling required and hence the models, mechanisms, type of computing, supporting data, laboratory and in situ testing, etc. required. An associated transparent and open audit trail should be developed."

Soler (2001) investigates the potential effects of coupled transport processes in radioactive waste repositories using the Opalinus Clay as the hypothetical host rock. With a simple 1D model that considers advection, chemical diffusion, thermal and chemical osmosis, and ignoring conservation of fluid mass, he shows that thermal osmosis could have a "strong impact" on solute and fluid transport if the coefficient is greater than $1 \times 10^{-12}\,\mathrm{m^2\,K^{-1}\,s^{-1}}$, compared with the range for compacted clays of $1 \times 10^{-14}$ to $1 \times 10^{-10}\,\mathrm{m^2\,K^{-1}\,s^{-1}}$ derived from experiment, and could therefore have an effect on the state of the engineered containment (Soler, 2001, p. 75). All the other processes considered are shown to have minor or negligible effects. The hydraulic gradient was constant throughout the simulation however this prevents the feedback of changes in the concentration gradients (Garavito et al., 2006). Soler then constructs 2D and 3D models (not reported in detail) of coupled thermal osmosis and advection processes as a square domain centred on a warm canister of waste. Including the conservation of fluid mass this time, the model effectively runs out of water at the canister because of the thermo-osmotic flow away from it, this then alters the hydraulic gradient field and the advective component of flow towards the canister cancels out the thermo-osmotic component — the final result is no net effect due to thermo-osmotic coupling. The possibility of large and rapidly changing temperature gradients shortly after the emplacement of canisters is identified as a necessary topic for further study.

Coupled chemical processes proximal to canisters containing nuclear waste are investigated by Johnson and King (2008) and Senger et al. (2008) who model the corrosion of the metal canister as it draws water out of the surrounding Opalinus Clay. Shao et al. (2009) model the reactive transport of radium in the near-field of a nuclear waste repository. Bourgeat et al. (2009) present a formulation for isothermal multiphase flow (liquid and gas) of water and hydrogen components in a rigid porous medium that accounts for the appearance and disappearance of one of the phases. The gas may arise through corrosion of the metallic canister containing radioactive waste.

A. Gens et al. (2002) assess factors controlling interactions between fractured crystalline rock and a bentonite clay buffer material at the Grimsel Rock Laboratory[3] and find that vapour diffusion, permeability and the retention curves of both materials influence the interactions. The characteristics of the retention curve (whether it is hysteretic or not) have a large influence on the results, the main factor being whether the rock desaturates or not. They point out that the difference between unsaturated and desaturated regions is so great that it raises the question of whether it is valid to consider averaged rock properties.

Kolditz and De Jonge (2004) use a formulation involving equations of state for phase changes from Clausius-Clapeyron's and Henry's Laws and assuming local thermodynamic equilibrium states between the phases. They compare two numerical coupling schemes: partitioned and

[3]Reporting on the FEBEX test.

monolithic. The monolithic scheme was found to be more correct and precise for calculating gas pressure and incorporating swelling effects makes a significant difference in saturation profile. They note that process interactions are especially complex in clays due to swelling and suction, there is no research on numerical stability analysis of codes modelling non-isothermal behaviour in swelling materials.

Xie et al. (2007) use a two stage method to model the pressure arising solely from swelling of expansive clays — free extension followed by back-compaction. They use the multiphase model developed in Kolditz and De Jonge (2004). The free-extension stage is based on diffuse double layer theory thus linking micro scale parameters to macro scale effects. A partitioned iterative scheme is used — the Picard method (section 4.3.3) is used to resolve multiphase flow and the Newton-Raphson method (section 4.3.3) is used to resolve elasto-plastic deformation. In general there are two types of clay models: those that treat the clay particles as a single solid phase, and those that treat the particles as swelling.

Several studies are interesting because of particular findings in numerical modelling or techniques used. Rutqvist, Börgesson, Chijimatsu, Kobayashi, et al. (2001) review the implementations of THM coupled process models in four modeling software systems: ROCMAS, THAMES, FRACON and AQCLAY. The balance, constitutive and equilibrium constraints were tabulated for comparison.

El-Kadi and Ling (1993) looked at the application of Péclet and Courant Number criteria to finite element simulations based on Richards' Equation and found that defining criteria through theoretical analysis was not possible due to the nonlinearity. They note that a reference solution with a very fine mesh is needed to assess the accuracy of the solutions.

Jiao and Hudson (1995) introduce a *fully coupled model*, whereby:

- a *binary interaction matrix* is assembled by listing the state variables along the leading diagonal and the relations between them are entered in the off-diagonal positions,
- the uncoupled matrix is then transformed, by the use of graph theory to analyse the interactions between the state variables, into the fully-coupled *global interaction matrix*.

Zhou (1998, p. 12) uses a numerical inversion scheme to obtain time-domain solutions for a cylindrical cavity (similar to the Ventilation Experiment model).

Two interesting studies mix statistical methods with coupled process modelling. A. S. Mayer and Huang (1999) use MODFLOW (which uses the Finite Difference Method) and MT3D (a transport solver) and a coupled-process parameter inversion model based on the maximum likelihood estimation method. Korsawe et al. (2006) compare the Galerkin FEM (for which an analytical solution is known) to a least-squares mixed FEM when applied to consolidation in porous media. Their benchmark problem involves a fully saturated elastic porous medium. The computation is programmed into Rockflow software — a relative of OpenGeoSys.

Class et al. (2002) use a primary variable switching technique; if a phase disappears the primary variable 'saturation' is replaced by a 'mole fraction'. Krabbenhøft (2007) presents an alternative that is simpler to implement.

In C. I. McDermott, Xie, et al. (2007) a *geomechanical process facies* approach was used to model coupled processes dominant in different subdomains of the same system. The hybrid analytical and numerical approach allows only the most important processes to be modelled for each facies thus saving computational effort in some areas of the model and where, otherwise the whole process would be calculated even if it was not relevant, and redistributing the effort

to facies where other processes are operating. A case study reported is the injection of cold water into fractures of the hot dry rock geothermal resource at Spa Urach, Germany, and the coupled behaviour of the fracture system heat exchanger in response. The concept of geomechanical process facies (or geoprocess facies) and the hybrid modelling technique are a method of upscaling processes to allow realistic representation in a model of a system at a scale greater than that at which the process is defined. The problem of upscaling pore- and atomic-scale processes inherent in modelling a repository for nuclear waste over the required space and time scales, would be aided by a geoprocess facies approach.

Freiboth et al. (2008) presents a model where the main interest is in multiphase flow and transport in a deforming cohesive soil, rather than the deformation itself, so a short-cut in the calculation is possible. They present a *phenomenological model concept* — "in terms of the processes responsible for soil deformation, since the effects of deformation on flow and transport are only considered by constitutive relations that allow an adaptation of the hydraulic properties". The advantage is significant reduction in computational effort. The new model (MUFTE) is validated by comparison with two other codes that include the whole mechanical scheme.

**Multiphase flow** There are many published papers on multiphase flow through porous media, often with subtle differences, it would be useful to have a tree diagramme showing which formulations inherit from others. Nonetheless, a relevant selection are reviewed here.

Bennethum et al. (1997) describes the *hybrid mixture theory* (HMT) that leads to a method for formulating constitutive restrictions (i.e. *closures*) that are thermodynamically admissible.

C. T. Miller, Christakos, et al. (1998) reviews many approaches to the problem of multiphase flow. They use a standard formulation approach in order to allow the comparison of many different formulations by factoring them by their *continuum balance equations* and *closure relations*[4]. There are mainly two concepts in use for formulating the balance equations: *phase-related* and *compositional* approaches. The compositional approach is advantageous for multiphase-multicomponental processes with phase changes (Gawin, Baggio, et al., 1995; A. A. Gens et al., 1998; Xie et al., 2007). It is based on balancing the species rather than the phases and seeks a solution that includes the volume fraction *and* the composition of each phase, as a function of space and time. In their conclusions, (C. T. Miller, Christakos, et al., 1998) say that Object Oriented (OO) methods and High Performance Computing (HPC) are important tools in the investigation of multiphase flow phenomena.

Sanavia et al. (2006, Appendix 1) Contains a good description of the formulation of the problem and equations of state variables. They say that capillary pressure may be applied as a state variable following advances in thermodynamic theory at the macro scale (Sanavia et al., 2006, p. 346). They use averaging techniques from M. Hassanizadeh and Gray (1979); M. Hassanizadeh and Gray (1980).

Gawin and Sanavia (2009) describe the physics of desaturation of a porous medium caused by air degassed from liquid water during *cavitation*. The scenario studied is the development of localised shear bands in undrained sands. Where $P_l$ is the liquid pressure, $T$ is temperature $P_c$ is capillary pressure and $P^b$ is the bubbling pressure and $p^{gws}$ is the saturated vapour pressure, cavitation starts where $P_l^w \leq p^{gws}(T)$ and then $P_c > P^b$ leading to desaturation. They observed $P_c \sim P_l^w < P_{atm}$ — close to cavitation pressure, and cavitation occurring, at the onset of shear

[4]Closure relations — *equations of state* and *constitutive relations*.

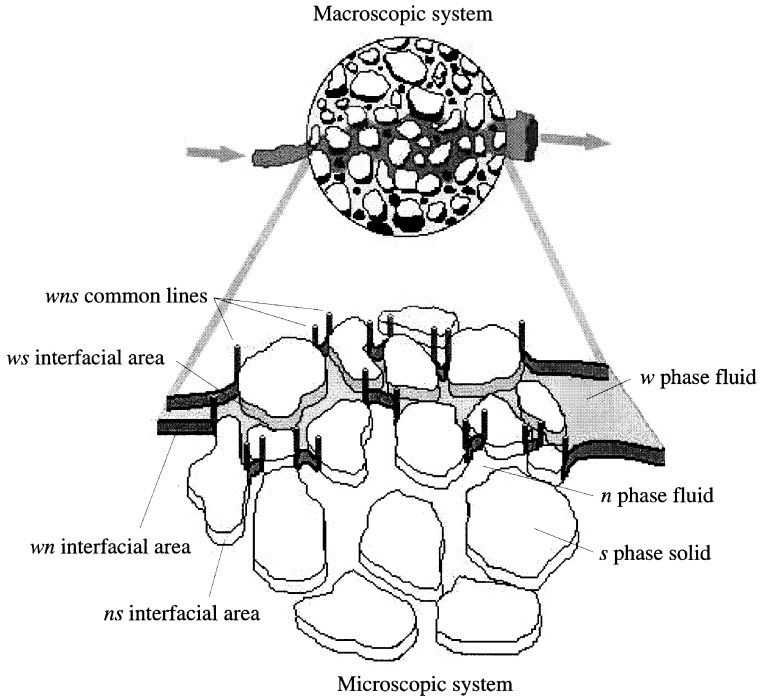


Figure 2.1: "Depiction of a three-phase system at a macroscale point (top) and from the microscale perspective (bottom) with notation employed to identify phases, interfaces, and the common line." *(From Gray, 1999, p. 526).*

band formation. They identify the coupled nature (after being initialised by cavitation) of the process of 'desorption' of air from water → further desaturation → further cavitation, and go on to investigate the phenomena using a fully coupled multiphase model using the mass balance equations, Equations 4.19 and 4.22.

**Relative permeability, capillarity and hysteresis** Romero et al. (1999) experiment with samples of Boom Clay to provide information on the morphology of the porous medium and factors influencing hydraulic states. The main objective is to define an entrance pore size region separating intra-aggregate (unaffected by mechanical loading and containing fairly immobile water) and inter-aggregate (loading results in a reduction of interconnected macropores, effecting free water) porosities. They find that intra-aggregate water to be 54 % to 59 % of the total volume of soil water at low porosity packing and 28 % to 38 % at high porosity packing. During sample preparation (by static compaction) for the main work, they note a striking constancy in soil suction when loading causes higher saturations. It is only when close to becoming saturated that the suction becomes a function of water content. This is because (in those samples) the compaction effects the macroporosity that does not contain free water and *"degree of saturation changes are only associated to macroporosity changes under constant intra-aggregate water content"*. They use several different techniques to delimit 'trapped' and 'free' porosity. In some of the packings from *"one- to two-thirds of water behaves more like a solid than a fluid"* (Romero et al., 1999, p. 127).

Jerauld and Salter (1990) explain behaviour based on pore-scale phenomena — *"changes in the patterns of hysteresis often attributed to consolidation can be understood in terms of changes in aspect ratio"*.

Blunt (2001) Reviews the recent major advances in pore network models arising from progress in multiphase flow and transport in porous media. They focus on models of wettability and three-phase flow writing that it is *"almost universal practice in the oil industry"* to estimate relative permeability for oil, water, gas systems using empirical models with no physical basis. Predictive models incorporating pore-networks (e.g. those of Jerauld and Salter (1990)) are improvements on those based on pore-space geometry and percolation.

Gray and S. M. Hassanizadeh (1991a) highlights difficulties with negative absolute pressure of water (positive capillary pressure) and inadequate explanations for hysteresis in $P_c$–$S$ relations. They point out that the capillary pressure is used to represent the thermodynamic energy state of the liquid, composed in part of matric potential[5] — itself composed from soil liquid pressure potential and the attractive forces of the solid phase on the liquid. The problem is how to resolve adsorption effects and pressure at the macroscale. The authors account for hysteresis in capillary pressure and relative permeability by allowing them to depend on interfacial area as well as saturation.

Gray and S. M. Hassanizadeh (1991b) maintain that "relative wettability of the water and air phases is an important dependent thermodynamic variable which contributes to the hysteretic nature of the capillary pressure versus saturation curve".

R. D. Miller (1994) answers the negative liquid pressure 'paradox' of Gray and S. M. Hassanizadeh (1991a) by demonstrating that within a *porous medium* the stability of phases is different to that observed in simplified situations.

Couture et al. (1996, p. 311) points out that there is no consensus (in 1996) on the effect of flow direction of one phase on the relative permeability of another. Estimating the relative phase permeability ($k^{\gamma}_{rel}$) as a function of saturation ($S^{\gamma}$) is done either by capillary pressure measurements or as a power function of saturation (e.g. in Chijimatsu et al. (2005)). Geoscience methods are problematic because the saturation to which the relative permeability corresponds must be measured and assumes that no mass transfer between the phases occurs. The measured saturation depends on the thermodynamic equilibrium between the two fluids. Consequently arbitrary functions are used to provide the relative permeability.

C. T. Miller, Christakos, et al. (1998) notes that the use of Forcheimer's Equation instead of the extension of Darcy's Law to accommodate multiphase flow, is more rigorous. They provide a critique of the experiments used to derive p-S-k relations.

The *Coleman and Noll* method — a *closure scheme* using the 2$^{\text{nd}}$ law of thermodynamics[6] as a constraint type-relationship to derive constitutive relationships for the unknown exchange terms in the system of equations is used by Reggiani et al. (1999, p. 18).

Faisal Anwar et al. (2000) while investigating capillary pressure, directly and accurately measures the interfacial area (figure 2.2) for a porous medium made from glass beads using a surfactant adsorption technique.

X-Ray Computed Tomography (CT)[7] has been used by Schembre and Kovscek (2003) to measure two-phase relative permeability in argillaceous formations (although not the Opalinus Clay). The method is reported to be especially suitable for low-permeability rocks because it does not require that the system reaches steady state (the authors also point out that previously used unsteady-state techniques do not apply where there are high capillary forces) and is also

[5] *Matric potential* – the component of water potential due to adhesion to the soil.
[6] Entropy of a closed system will not decrease.
[7] 2D X-rays from a variety of angles computed into 3D images.

suitable for low saturations. These findings are useful in the current investigation into the meaning and use of relative permeability curves using Task A and the Opalinus Clay as a case study.

*Thermodynamically constrained averaging theory* (TCAT), a mathematically rigorous formulation that retains the connection to microscale processes at the macroscale, was initiated by Gray (1999) and developed through a series of papers: Gray and C. T. Miller (2005); Jackson et al. (2009); C. T. Miller and Gray (2005). The basic theme is that most multiphase flow formulations are over simplified by continuing to invoke Darcy's Law (section 4.2.2) inappropriately and assuming that relative permeability is a function of saturation. They argue that hysteresis is an effect caused by over simplification.

Meakin and Tartakovsky (2009) give a more recent review of the state of the art of multiphase fluid flow and reactive transport in porous media, and concentrate on pore-scale features. They state that hysteresis is caused by roughness impeding the advance and not the retreat of contact lines between phases and that determination of contact angles is an important barrier to accurate pore-scale models. Although dealing with a different scale than the TCAT series mentioned above, there is very little review of approaches based on thermodynamics.

**Capillary pressure** The common treatment of capillary pressure is that it is defined as the difference between the pressure phases (equation 4.5) and is a function of saturation. Capillary pressure has been investigated in the literature mainly via:

- thermodynamics
- interphase interfacial tension
- relative permeability

S. M. Hassanizadeh et al. (2002) comments on problems with the current (in 2002) treatments:

- on capillary pressure: *"the theoretical basis and practical implications...* [are] *poorly understood*"
- on interface dynamics within a network of pores: at the pore and pore-network scale, *"dynamic coefficients span about three orders of magnitude*".
- on hysteresis: *"dynamic effects are significant for air-water systems in drainage as well as imbibation*"
- on the assumption of equilibrium: *"even if there is equilibrium at the pore sale, the upscaling, in this case the volume averaging, of complex pore-sale processes will always introduce nonequilibrium effects*".

Reeves and Celia (1996) use a pore-scale network model with conical pore throats that shows a functional relationship between capillary pressure, saturation, and interfacial area.

In Bennethum et al. (1997), they favour the thermodynamical treatment of multiphase flow that *"involves averaging the field equations (e.g. conservation of mass, momentum balance, energy balance) and obtaining constitutive restrictions subject to the second law of thermodynamics*". They are critical of the extension of Darcy's Law to multiphase flow because *"an*

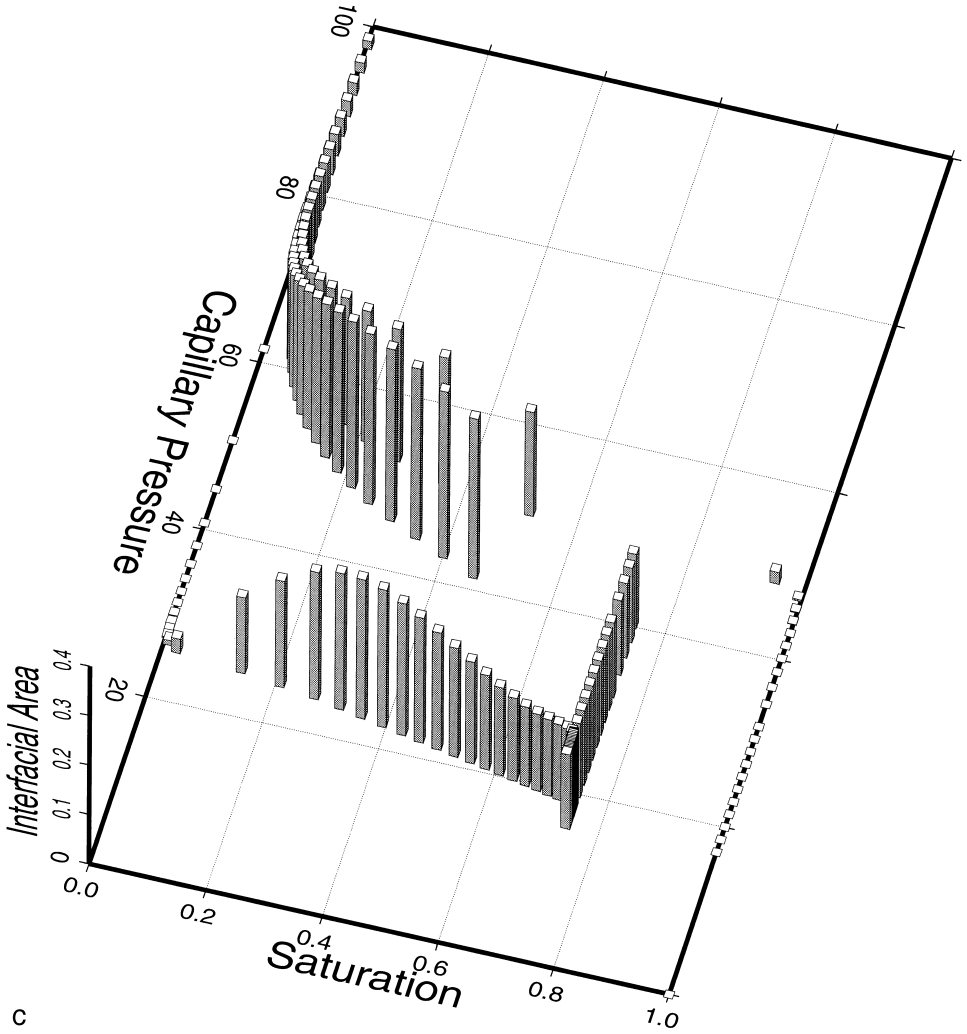


Figure 2.2: "Primary drainage and main hysteresis loop: ... capillary pressure versus saturation versus interfacial area." *(From Fig. 7(c) Reeves and Celia, 1996, p. 2351).*

*interaction potential is needed to show the vicinal fluid flows from regions of high volume fraction to low volume fraction. It is not enough to simply modify the permeability coefficient and presume that it is a function of the volume fraction*".

**Pore network models** Blunt (2001) reviews the use of pore network models in multiphase flow studies. Models now use a variety of pore shapes: circular, triangular, grain boundary, fractal, the advance being that rough or angular cross-sections allow the wetting phase to occupy the middle space and the non-wetting phase to occupy the crevices in the wall. The improvement has been demonstrated in several papers (Blunt, 2001, p. 198). One of the earliest was Mason and Morrow (1991) who used triangular pore spaces. The list of references at the back gives a short description for each. They say that at very low wetting phase saturation, adsorbed nanometres thick films have a *"significant impact"* on capillary pressure and that spatial correlation of pore sizes with scales of geologic structure leads to better connectivity and larger relative permeability.

Fischer and Celia (1999) predict relative permeability using a network model adjusted to

match capillary pressure measurements with functional relationships. They were able to make good and very good matches, using the pore-network model, to several soil parameters and characteristic drying and imbibation curves when compared with an analytical model. The approach is based on an algorithm for generating distributions of bond size and site size fitted to the retention curves.

**Opalinus Clay** Muñoz et al. (2003) found that bedding planes caused anisotropy and 'double structure' (meaning dual-porosity) in the Opalinus Clay. Dual-porosity (pores and discontinuities) is given as the explanation for hysteresis — during saturation flow is mainly in discontinuities as the matrix (the pores) fill, during desaturation the discontinuities drain first and the lower permeability matrix drains slowly.

In OECD Nuclear Energy Agency (2003, p. 283) they write that chemical osmosis "within a natural argillaceous formation is rather poorly understood" and yet further on say that "it can be neglected in comparison with other transport processes". However, S. Horseman et al. (2007) observed osmotic flow across laboratory samples of Opalinus Clay and measured the osmotic permeability to be $3.5 \times 10^{-22}\mathrm{m}^2$ and the hydraulic permeability to be $7.9 \times 10^{-21}\mathrm{m}^2$; an order of magnitude higher than others.

Pearson et al. (2003) reports geochemical analyses of samples from boreholes `BWS-A1`, `BWS-A4` and `BWS-A5` (just outside the VE). The work was compared by Fernández et al. (2007) with their own work to evaluate the effect of chemical processes (e.g. dissolution, precipitation) on hydromechanical rock properties (e.g. porosity, permeability).

**EDZ** In Su (2007, p. 5), reporting on a project to model the behaviour of an argillaceous rock during shaft sinking, a lesson learnt was that in order to model the near-field mechanical behaviour the effect of ventilation on water pressure within the adjacent rock mass requires further investigations.

The presence, geometry and connectivity of fracture networks around excavations has been related to excavation technique by Bossart et al. (2004). Investigating using fracture mapping and resin-impregnated overcores[8], they conclude that from most to least disturbance (in terms of fracture extent, fracture frequency and consistency of orientation) the order is: blasting, pneumatic hammer, rotary road-header, which is as would be expected.

Fracture transmissivity between repeated hydraulic tests is shown to decrease by two orders of magnitude over two years — the reason given is that of resaturation and subsequent self-sealing of fractures, whether by creep or by swelling of the fracture walls through osmosis. Later work backs up the self-sealing mechanism; in Blümling et al. (2007) a self-sealing fracture is observed in action using microfocus X-ray tomography and in other reports of results from geotechnical laboratory testing. Fernàndez-Garcia et al. (2007) has also reported work on the characterisation of the EDZ in the Opalinus Clay.

The strength of evidence for self-sealing of fractures observed at Mont Terri is such that the mechanism has been used as justification, on its own as well as with other evidence, for disregarding advective flow in fractures as a potential transport mechanism in the Callovo-Oxfordian (argillite) at Bure, France (Mazurek et al., 2008). Several mine-by tests were carried out in the Boom Clay at Mol, Belgium (see e.g. Barnichon and Volckaert, 2003).

[8]Resin is injected slowly at the base of a borehole, cured with heaters, then a wider diameter core barrel is drilled along the same axis to retrieve a *resin impregnated overcore* (Frieg et al., 1998).

**Previous models of the VE**

The Drying Test (described in section 3.6.7: The Drying Test) was modelled[9] by several researchers including C. McDermott (2009). The model and results are described later in section 6.2 DECOVALEX Step 0: modelling the Drying Test.

In the literature there exist previous models of the VE:

**G. Mayer et al. (2007)** modelled most of a desaturation-resaturation interval during the $5^{\text{th}}$–$7^{\text{th}}$ Phases (as per table 3.2) using the two phase flow code TOUGH2 (Pruess, 1991). They determined the undisturbed permeability of the Opalinus Clay to be $3 \times 10^{-20}\,\text{m}^2$, desaturation reached no further than 1.35 m from the tunnel wall, 95 % saturation reached no further than 0.4 m. The most sensitive parameters were the permeability ($k$) and the initial saturation ($S_o$) near the tunnel wall.

**Fernàndez-Garcia et al. (2007)** presented a hydrogeological model using the finite difference code MODFLOW and found that near-field water flux is driven significantly by desaturation processes (despite the small thickness of the zone of desaturation during the VE) and that determination of $k$ by representing the tunnel as a well function is not suitable. This is in contrast to the latest papers that say the whole Ventilation Experiment may be thought of as a large scale pumping test (Garitte et al., 2013).

**Zheng et al. (2004, 2008)** investigated the multicomponent reactive transport of the ventilation experiment using a 2D CODE_BRIGHT model (figure 2.3) assuming constant conditions along the length of the tunnel however experimental data shows this not to be the case (see figure 3.8). They used separate inverse hydrochemical model to estimate the initial chemical composition of pore water and quantified evaporation from the tunnel wall, upon which model results were highly dependent.

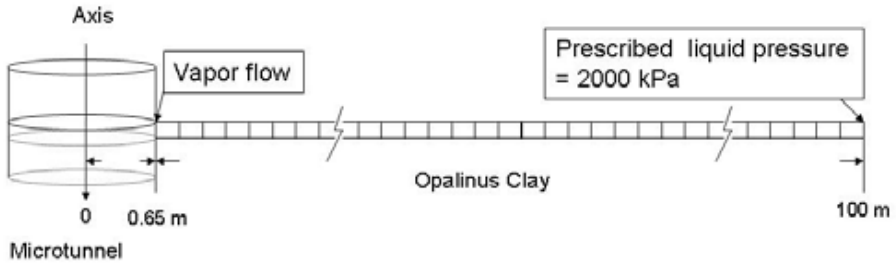


Figure 2.3: 2D rectangular mesh used by Zheng et al. (2008). *(After Fig. 37 Zheng et al., 2008, p. 34).*

[9]The work was part of DECOVALEX, Task A, Step 0.

Chapter 3

# DECOVALEX

## 3.1 Deep geological disposal

This PhD project is investigating, by computer simulation, the behaviour of a clay as it dries out and resaturates. The project is linked to an international collaborative project called DECOVALEX-2011 — *"development of coupled process models and their validation against experiments"*, that has provided a framework for a series of projects running since 1992 when it was established by waste management and national regulatory authorities (C.-F. Tsang et al., 2005). The purpose is to investigate aspects of the containment provided by the deep geological disposal concept. Each of the five rounds of the DECOVALEX project has looked at between four and six experiments of different scales and durations; there have been laboratory, large-scale laboratory and field scale experiments with some running for several years. The latest complete phase, DECOVALEX-2011, focused on argillaceous rocks. There are several subprojects ('Tasks') and part of this PhD project was to participate in Task A which was to model the Drying Test and the Ventilation Experiment. The phases and tasks of the DECOVALEX project so far are listed in Appendix A and much of the work has already been mentioned in the literature review of chapter 2. Coupled processes will be explained in section 3.5 and the Ventilation Experiment is described in section 3.6.

## 3.2 Radioactive waste

The products of radioactive decay (subatomic particles and gamma rays – *radiation*), can damage living cells by *ionisation* (electron removal from the atoms of molecules) and so the risks posed by natural and anthropogenic radioactive sources are assessed and controlled in the UK by the Health Protection Agency [1]. Controlled nuclear fission of uranium isotopes U-235 and U-238 for electricity generation produces radioactive spent fuel (SF) and waste. Spent fuel, both domestic and imported, can either be reprocessed to make fuel or designated as waste. Waste also arises from radioactive decay of other fissionable isotopes in research reactors and from military sources. The waste may be categorised as high, intermediate and low level waste (HLW, ILW, LLW). Low and intermediate level waste is considered together for some purposes as short lived and long lived (LILW-SL and LILW-LL).

The ionising effect on living tissue requires that waste of all categories must be isolated from living organisms until it has undergone enough radioactive decay that it is unlikely to cause harm. For HLW/SF this is taken to be $1 \times 10^5$ and $1 \times 10^6$ years (Gibb, 1999).

[1] Formerly the remit of the National Radiological Protection Board (NRPB).

The UK has (as of 2007) 1270 $m^3$ of HLW and 134 450 $m^3$ of LILW-SL/LL awaiting disposal for which there is no facility in the UK (Anon, 2008).

New sites for nuclear reactors are currently being considered in the UK for electricity production to begin in 2020. New nuclear power stations will (DTI, 2007):

- replace those (both fossil fuel and nuclear) that are scheduled to close,
- help to meet the target of 60% reduction in carbon dioxide emissions by 2050, and
- increase energy security by reducing imports of fossil fuels.

The increase in nuclear power generation is expected to lead to an increase in the volume of waste awaiting disposal.

## 3.3 Storage and disposal

Options for disposal aim for *isolation* of the waste by *containment* depending on the category and characteristics of the waste. LLW may be suitable for normal landfill. A number of geological storage designs have been proposed for HLW, some depend more on the nature of the waste than others[2] Internationally, deep[3] geological disposal (DGD) is the preferred policy of 25 out of 39 countries that produce radioactive waste — the remainder being undecided, and all of those favour *interim* storage rather than *indefinite* disposal (NDA, 2008). Retrievability of waste is desirable because of the potential to benefit from future advances in technology. The other main design criterion is containment. Evaluation of the proportion of containment that geological media can provide, requires adequate geological data on the characteristics of the host rock to be considered in the contexts of different repository designs. Various designs of DGD repositories have been proposed and are favoured by different countries (see figure 3.1 for the UK concept). The common design theme is of metal canisters containing HLW emplaced in drifts excavated into natural rock, the space between filled with a buffer material. The nature of the rock and the buffer material is critical for providing containment.

In the UK the host rock is likely to be granite or clay with a buffer material of bentonite.

Together, the buffer and the volume of host rock close to the canister is discussed as being in the *near field*, and the remainder of the host rock mass as being in the *far field*.

## 3.4 Scientific investigation to support safety cases

The nuclear waste problem requires factors to be considered ranging from the atomic scale (e.g. the waste itself) to the global scale (e.g. climate change — Chan et al. (2005) assess the implications of a glacial cycle). The size and complexity of the task of making a Safety Case[4] for DGD means that international collaborative projects are the main vehicle for investigation with various test formations in different countries being studied extensively over many years[5]. The tools and techniques developed in one geological terrane are then applied to others.

[2] e.g. *"very deep geological disposal"* proposed by Gibb (1999) proposed mixing ex-military fissile material with HLW to achieve the correct temperature for very deep self-disposal in boreholes by granite recrystallisation.

[3] Although 'deep' is not very deep in geological terms and means 300-1000m below ground.

[4] The set of arguments and analyses used to justify the conclusion that a specific repository system will be safe — (Lawrence et al., 2002).

[5] The literature review in chapter 2 mentions several studies.

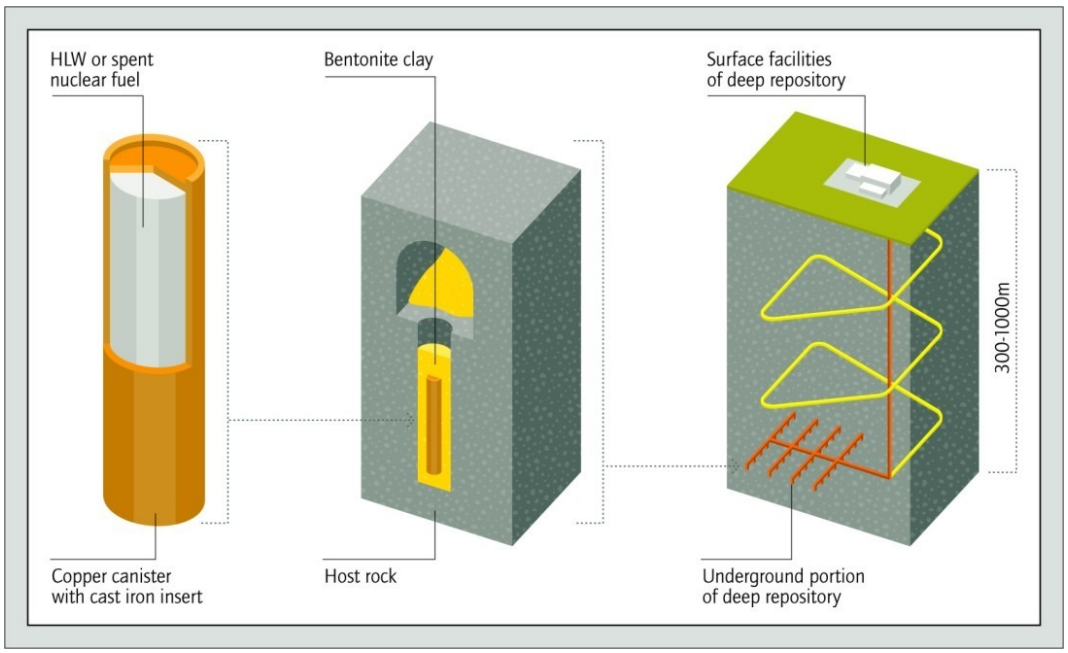


Figure 3.1: The geological repository concept for UK HLW/SF. To reduce mobility the liquid waste it is vitrified before being placed in metal canisters. Bentonite is used as the buffer material between the canister and the host rock. *(From Nirex, 2005, p. 13)*

Physical processes operate in geological media at a range of scales of measurement with the effect that a description of behaviour at one scale is not necessarily transferable to another. In recognition of this, experiments to investigate DGD have ranged in scale from laboratory through to field scales, and computer models. Field scale *in situ* experiments are more difficult and expensive to construct, control, execute and interpret and it could be an indicator of the importance of the information that they provide that so many have been completed. During an *in situ* experiment it may not be possible to completely enclose the problem with observations because there is not total control over the environment and some parameters of a process that is hypothesised to be acting may not be directly measurable so laboratory experiments and computer models can be used to add or derive further information.

Geological studies usually either look at the undisturbed nature of potential host rocks or at the nature and evolution of the near field containment during the construction and operational phases.

During the construction phase, a zone within the rock wall of the repository is altered from its natural state by physical processes, initiated by damage sustained during excavation. That zone, extending a certain thickness from the interior of the repository, is known conceptually as the *excavation damaged zone* (EDZ) (Hudson et al., 2001, p. 145). In clay host rocks the main process is drying from evaporation at the rock/air interface. Understanding the evolution and behaviour of the EDZ is critical for the performance of the near field containment (Rutqvist, Börgesson, Chijimatsu, Hernelind, et al., 2009).

DECOVALEX-2011 focuses on investigations of the near field and EDZ in argillaceous formations (C. F. Tsang et al., 2009).

## 3.5 Coupled processes

Two processes are said to be *coupled* where one process effects the initiation or progress of another process by a change in a shared parameter — determining the behaviour of one system may be impossible without the simultaneous study of the other (Jing et al., 1995; Zienkiewicz et al., 2005, p. 642). To illustrate this, here are two scenarios both starting with a clay host rock drying through evaporation (a *thermodynamic* process) at the air/rock interface during the construction of a repository:

- drying causes shrinkage and propagation of discontinuities (both *mechanical* processes) in the EDZ, this in turn cause an increase in the connectivity of the fracture network and so an increase in intrinsic permeability (a *hydraulic* property of the rock). The increased permeability causes an increase in the rate of transport of water (by *advection* and *diffusion* — *hydraulic* processes) to the rock's surface which could increase the availability of water for evaporation. In essence: **drying of the clay leads to an increased rate of drying**.

- drying develops a salinity gradient into the rock altering the composition of pore water and mineralogy, causing oxidation and precipitation (all *chemical* processes) leading to a reduction in porosity and permeability (*mechanical*). The reduction in permeability causes a decrease in the rate of transport of water (*hydraulic*) to the surface of the clay to be made available for evaporation (Fernández et al., 2007). The result being that **drying of the clay leads to a decreased rate of drying**.

The two scenarios are not distinct and can be mixed together in different ways. The overall behaviour is not easy to capture because of the complexity of the individual processes and the effects they have on one another due to changes in the rock's properties, i.e. the *coupling* between them.

C. F. Tsang (1991) describes *coupled behaviour* as *"changes in hydraulic and chemical properties of rock"* and outlines seven categories of coupled thermal, hydraulic, mechanical, and chemical (THMC) processes. One example given is of a nuclear waste heat source causing solute transport, precipitation and permeability change — THC coupled processes.

The *drying* of the EDZ implies that it is basically a flow problem. (S. T. Horseman et al., 1996, p. 185) has a concise definition of a *coupled flow process* as *"one in which flow of any kind ... is driven by the gradient of a potential not usually associated with that flow"* and constructs a matrix of coupled flow processes table 3.1. A damaged argillaceous host rock with an emplaced source (of both heat and ions) containing radioactive waste could potentially sustain any of these, and mechanical, processes. A graphical representation (figure 3.2) shows the possible coupling relationships between different classes of geological process and indicates recently published work concerned with those processes.

The determination of the phenomenological effect of coupled processes is most easily conducted by computer simulation.

This PhD project contributes directly to an understanding of the problems involved in determining the evolution of the near field containment for HLW during construction and operation of DGD repositories in the UK, or internationally. As such, it would enable more detail to be added to a Safety Case for a DGD facility.

| | Potential gradient X | | | |
|---|---|---|---|---|
| **Flow J** | Hydraulic | Temperature | Electrical | Chemical |
| Fluid | **Advection** *Darcy's Law* | Thermo-osmosis[a] | Electro-osmosis | Chemico-osmosis |
| Heat | Thermal filtration (Isothermal heat transfer) | **Thermal conduction** *Fourier's Law* | Peltier effect | Dufour effect |
| Current | Rouss effect | Seebeck or Thompson effect (Streaming current) | **Electrical conduction** *Ohm's Law* | Diffusion & membrane potentials |
| Ion | Streaming current | Sorét effect (thermal diffusion of electrolyte) | Electro-phoresis | **Diffusion** *Fick's Law* |

[a]Osmosis — refers to flow resulting from a gradient other than hydraulic.

Table 3.1: *"Matrix of direct (on-diagonal) and coupled (off-diagonal) flow phenomena. The off-diagonal processes are often known, collectively, as the Onsagerian coupled-flow processes, after the famous thermodynamicist."* (From S. T. Horseman et al., 1996; OECD Nuclear Energy Agency, 2003, p. 186).

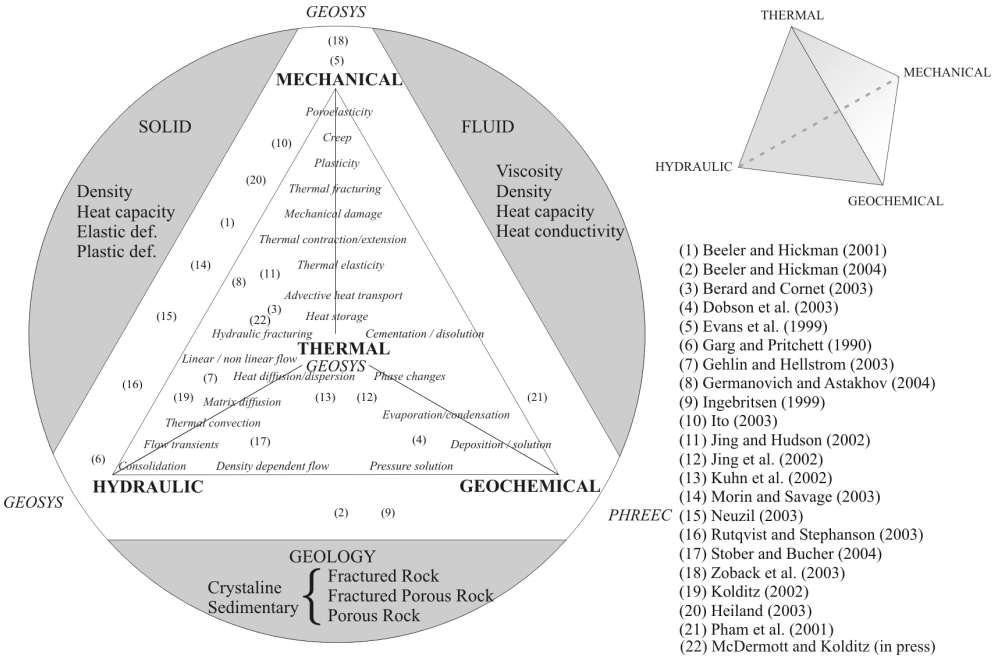


Figure 3.2: Examples of coupling in geosystems from recent studies./(From C. McDermott, 2007, Fig. 9)./

An understanding of coupled processes is required before the Safety Case can be completed for a repository in UK.

## 3.6 The Ventilation Experiment

### 3.6.1 Introduction

The main aim of the Ventilation Experiment (VE) is to observe *in situ* the consequences of desaturation of an argillaceous rock, in particular within the excavation damaged zone (EDZ). The experiment took place in the Mont Terri Rock Laboratory in northwest Switzerland (figure 3.3). The entire laboratory is within the *Opalinus Clay* lithology (figure 3.4). The VE is

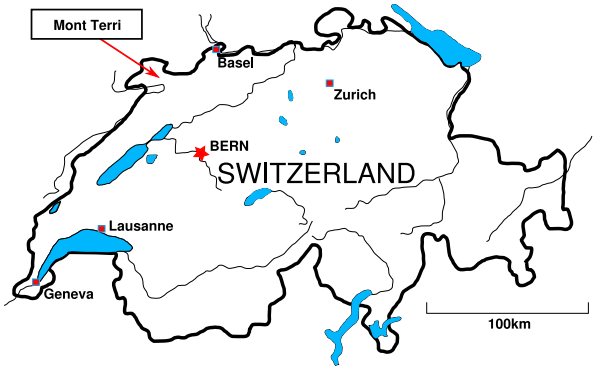


Figure 3.3: Location of Mont Terri in northwest Switzerland.

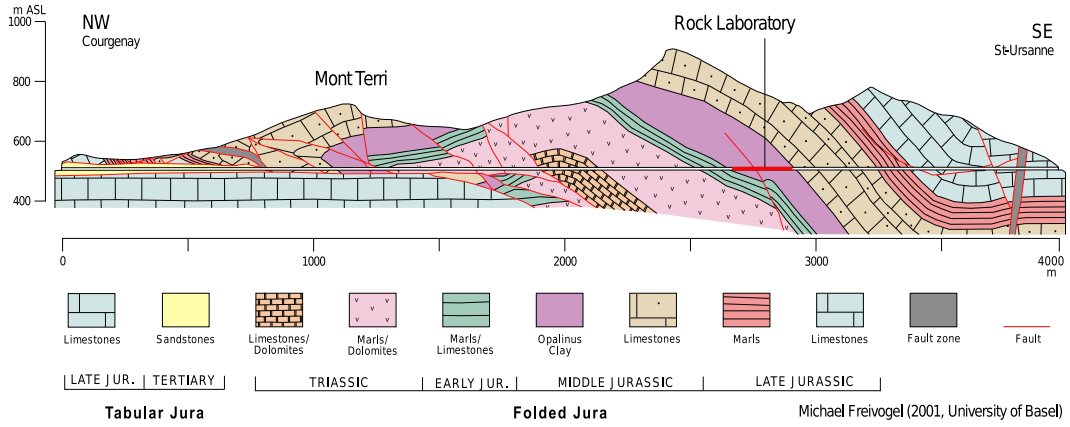


Figure 3.4: Cross section through Mont Terri showing the Rock Laboratory in the Opalinus Clay, the motorway tunnel and the regional geology (from Freivogel and Huggenberger, 2003).

centred on the raise bore (RB) microtunnel (Figure 3.5). The experiment setup, instrumentation, sampling and testing and results are described in this section and detailed descriptions of the VE are given in Matray and Coste (2003); J. C. Mayor et al. (2005); J.-C. Mayor et al. (2006).

### 3.6.2 Experiment setup

The experiment consisted of a section of a horizontal tunnel (known as the *"RB microtunnel"*). The section is 1.3 m in diameter by 10 m in length. Arrays of gauges were installed in radial

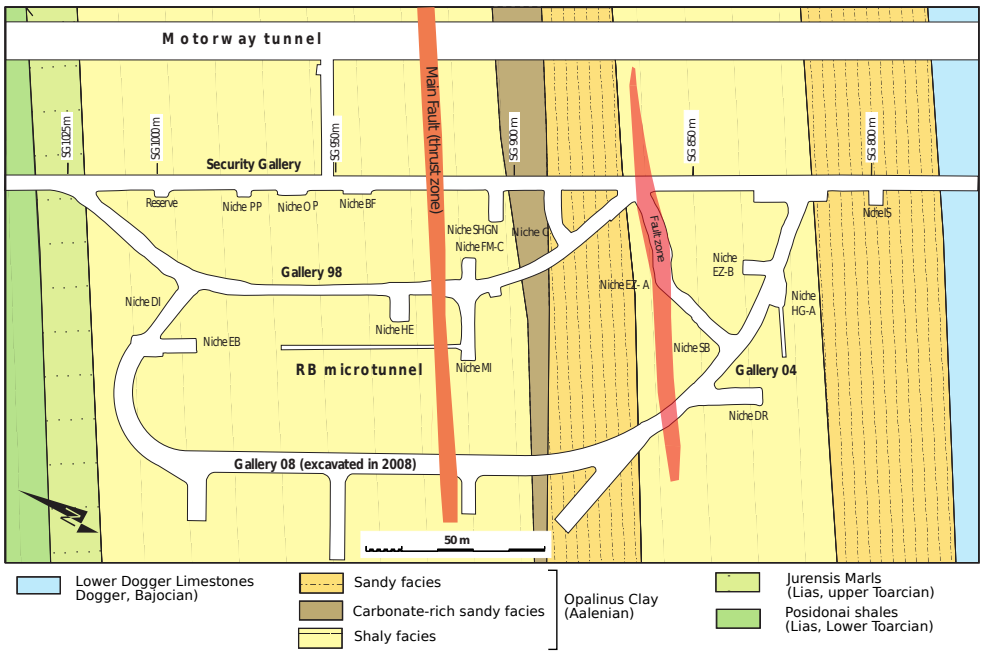


Figure 3.5: Geological map of the Mont Terri Rock Laboratory showing the local geology and the raise bore (RB) microtunnel in which the Ventilation Experiment (VE) was conducted. The microtunnel came about because of a 'fishing' operation to retrieve a tool that became stuck during drilling on a project belonging to a another team. The various niches contain other experiments run by various international consortia. *(Modified from mont-terri.ch.).*

fans of boreholes (i.e. drilled in planes orthogonal to the tunnel's long axis), to a maximum depth of 2 m, at 7 points down the long axis of the tunnel (see Figure 3.6).

The ends of the tunnel section were sealed off and air was circulated of varying relative humidity[6] and nearly constant temperature ($T \simeq 15\,^{\circ}\mathrm{C}$ to $16\,^{\circ}\mathrm{C}$). The relative humidity determined whether the clay surface began drying or resaturating. Evaluation of the suitable inflow rates and relative humidities to apply was made using measured evaporation rates (Matray and Coste, 2003).

Being open to the air of the underground laboratory for the time period between excavation in 1999 until it was sealed in June 2003, during which time there is no data for the test section itself, the rock in the test section has a poorly defined background hydromechanical history.

The seven phases of the experiment are shown in table 3.2.

### 3.6.3 Instrumentation

In total, 69 sensors, and 99 electrodes were installed in boreholes, see table 3.3.

### 3.6.4 Borehole tests

The mini piezometers were each subjected to one hydraulic pulse test to determine the hydraulic conductivity of the formation. The tests and results are reported in Solexperts (2003).

[6]Relative humidity is the amount of water vapour in a gaseous mixture of water and air.

| Period | Phase | Description | Start date | Duration (days) | Relative Humidity (%) |
|---|---|---|---|---|---|
| Background | $1^{st}$ | Microtunnel excavation | 1999-02 | 1277 | $\simeq$ 90 % |
| | $2^{nd}$ | Test section sealing | 2002-08-01 | 243 | $\simeq$ 93 % |
| | $3^{rd}$ | Equipment tests | 2003-04-01 | 102 | $\simeq$ 95 % |
| Desaturation | $4^{th}$ | $Q_{in}$ $\simeq$20m$^3$ h$^{-1}$ $RH_{in} \simeq$ 80 % | 2003-06-12 | 21 | $\simeq$ 84 % |
| | $5^{th}$ | $Q_{in}$ $\simeq$30m$^3$ h$^{-1}$ $RH_{in} \simeq$ 30 % | 2003-07-03 | 63 | $\simeq$ 47 % |
| | $6^{th}$ | $Q_{in}$ $\simeq$30m$^3$ h$^{-1}$ $RH_{in} \simeq$ 1 % to 3 % | 2003-09-04 | 147 | $\simeq$ 15 % |
| Resaturation | $7^{th}$ | $Q_{in}$ $\simeq$20m$^3$ h$^{-1}$ $RH_{in} \simeq$ 100 % | 2004-01-29 | 32 | $\simeq$ 92 % |
| | $8^{th}$ | Without ventilation | 2004-03-01 | 487 | $\simeq$ 95 % |
| Desaturation | $9^{th}$ | $Q_{in}$ $\simeq$40m$^3$ h$^{-1}$ $RH_{in} \simeq$ 1 % to 3 % | 2005-07-01 | | $\simeq$ 15 % |

Table 3.2: Time periods and ventilation phases of the VE. The flow rate ($Q_{in}$) and relative humidity ($RH_{in}$) of the air entering the test section of the tunnel was varied as shown. The last column shows the representative relative humidity in the test section. Other workers name Phases 0, I, II etc. *(After Fernández et al., 2007).*

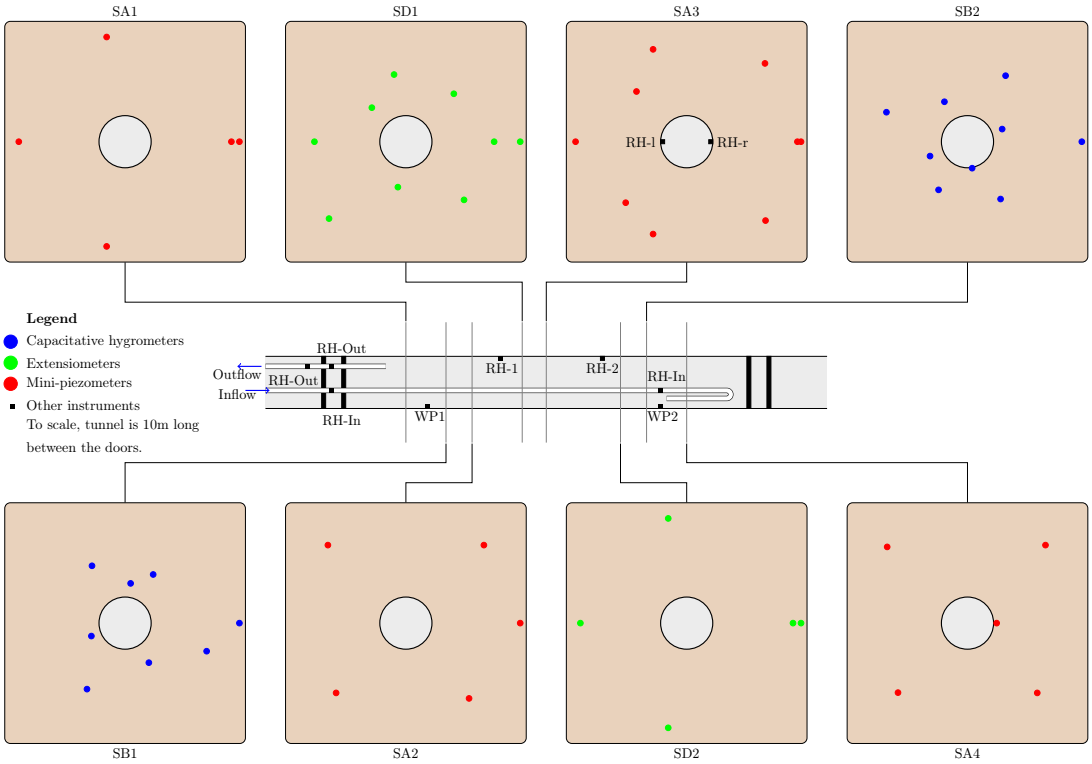


Figure 3.6: The setup of the VE showing locations of sensors in the Opalinus Clay and in the microtunnel. `WP1` and `WP2` are water pans, `RH-` sensors measure relative humidity. The drawing is to scale so that the density of monitoring can be understood.

Table 3.3: Sensors installed in the VE test section.

| Gauge type | No. | Measurement |
|---|---|---|
| mini-piezometers | 24 | Pore water pressure |
| capacitative hygrometers | 16 | Relative humidity |
| psychrometric hygrometers | 16 | Relative humidity |
| mini-extensiometers | 8 | Displacement |
| electrode chains | 5 (99 electrodes) | Electrical conductivity |

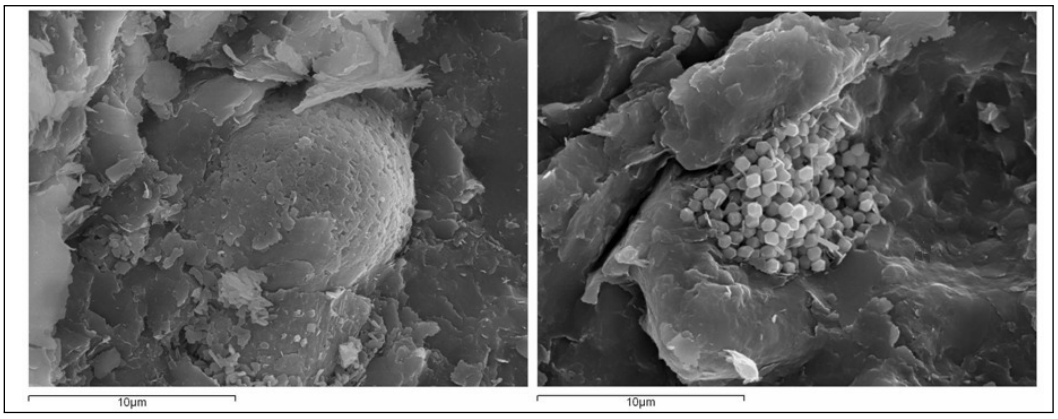


Figure 3.7: Scanning Electron Microscopy (SEM) photomicrographs of the Opalinus Clay. "a) Sample `BVE-99 m.0.65`. Fossil material ($CaCO_3$ biogenic material); b) `BVE-99 m.0.65`. Framboidal [raspberry like] Pyrite." *(From Fernández et al., 2007, Fig. 37, p. 34).*

### 3.6.5 Sampling

During the VE, the physical and chemical response (to a maximum depth of 2 m) was assessed by analysis of cores from small diameter boreholes.

- Cores from `BVE-82` (drilled July 2002, so pre-desaturation), `BVE-85` and `BVE-86` (drilled January 2004, post 1$^{st}$ desaturation) were logged and analysed for porosity, water content, sulphate and chloride. Reported by Traber (2003, 2004).
- A series of 7 boreholes from `BVE-96` to `BVE-102` were cored by Fernández et al. (2007), logged, and analysed for an extensive suite of geochemical parameters and included X-Ray Diffraction (XRD) and Scanning Electron Microscope (SEM) studies that provided detailed mineralogy (e.g. see figure 3.7).

### 3.6.6 Results

The data was supplied by the coordinators of Task A in many Microsoft Excel™ spreadsheets and it has been extracted into a PostgreSQL[7] database. Some data cleaning and shifting was necessary. figure 3.8 gives an overview of the *availability* and *quality* of the relative humidity data for the duration of the experiment. Pan evaporation data for Phase 1 is shown in figure 3.10.

Relative humidity within the tunnel walls, measured by capacitative and psychrometric hygrometers, show at the end desaturation periods, a zone down to a thickness of approximately 30 cm had been desaturated to <90%.

[7]PostgreSQL Global Development Group (2012)

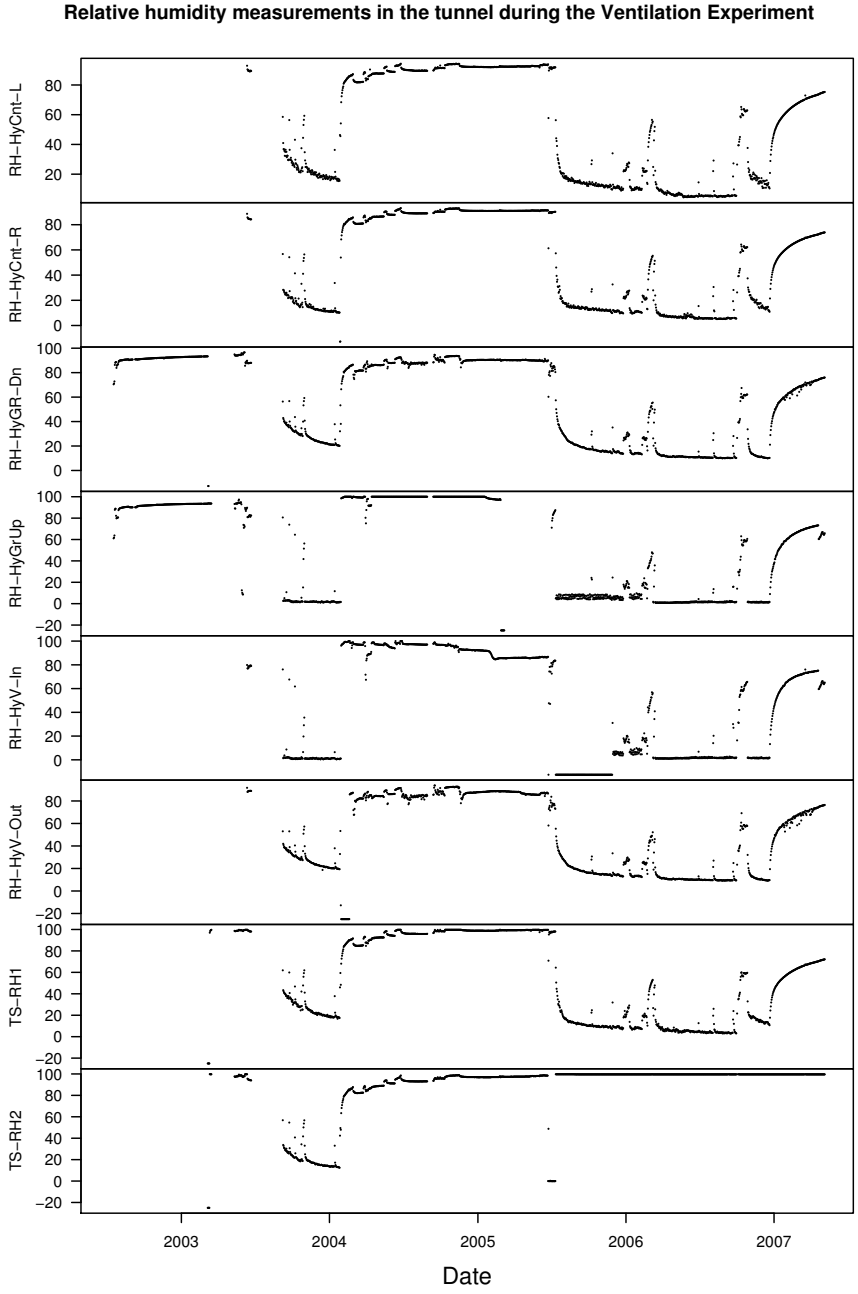


Figure 3.8: Raw relative humidity monitoring data from mid-2002 to mid-2007 showing the coverage and quality. An interesting feature is that during the period of high relative humidity centred around 2005, some sensors are trending upwards (e.g. `TS-RH1`) whereas others are trending downwards (e.g. `RH-HyV-In`). *(Data from* DECOVALEX-*2011).*

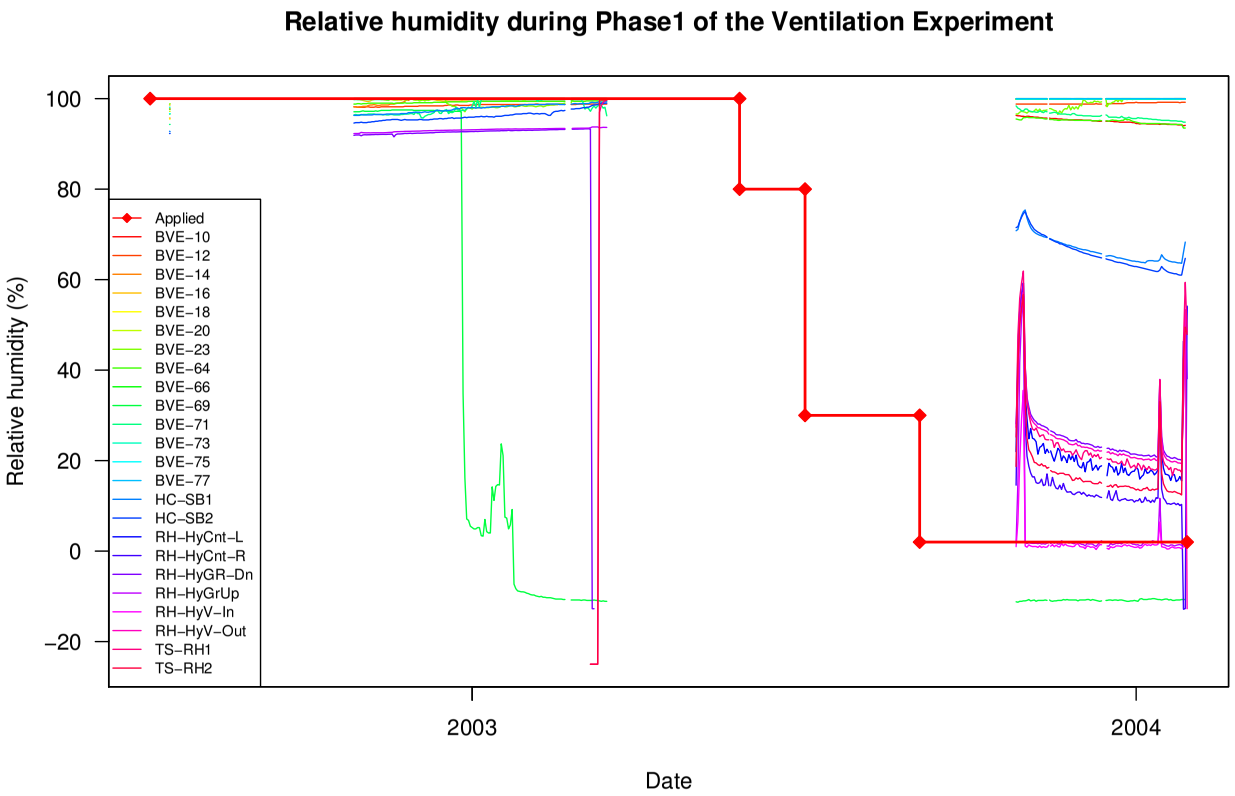


Figure 3.9: An overview of the available relative humidity (RH) monitoring data showing coverage and quality for the duration of the Phase 1 time interval of the Ventilation Experiment. Sensors are located in the air and the rock. The RH applied at the inflow end of the tunnel is shown (`Applied`). It can be seen that during the desaturation period (implied by the decrease in applied RH), all of the available data are in the second half of the period and that the data set may not have been cleaned (e.g. the RH axis goes negative).

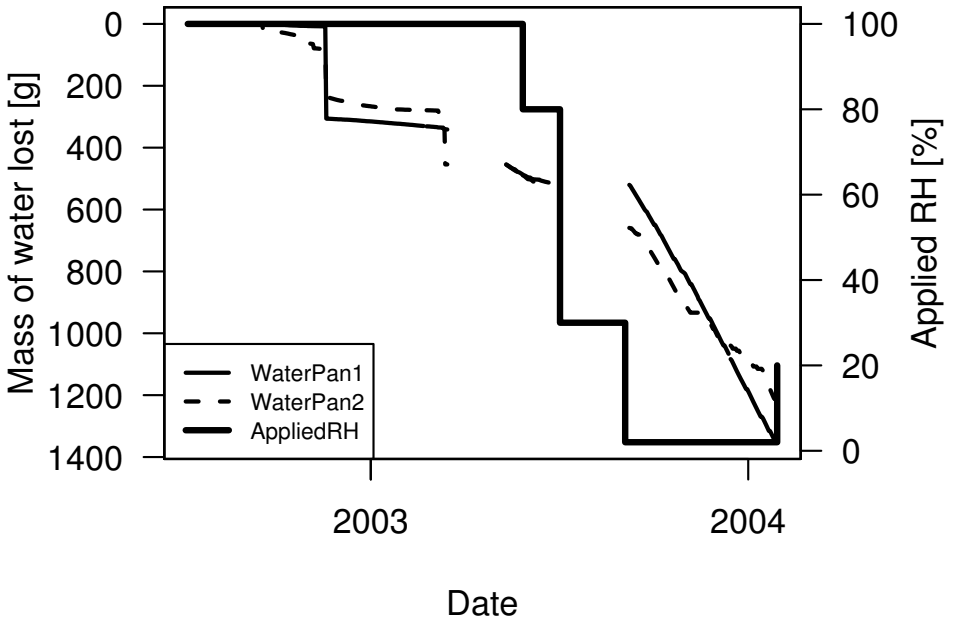


Figure 3.10: Free water evaporation from daily evaporation pan data for Phase 1 of the VE. `WaterPan2` is *up flow* from `WaterPan1` (as shown on `fig:ve_setup_sensors`). The RH applied at up flow end of the tunnel is shown (`AppliedRH`). During the period of 100 % RH, the rate of water loss from the down flow pan (`WaterPan1`) is greater so the rock must be removing water vapour from the tunnel.

### 3.6.7 The Drying Test

A small scale laboratory test in which three cylindrical samples of Opalinus Clay were dried from one end at 30 °C, RH≃33 % and air flow rate ≃0.5 m s$^{-1}$ for 142 days, described by Floría et al. (2002). The weight of water lost and the moisture content of samples was measured. The behaviour has been modelled by C. McDermott (2009) (and others, as part of the DECOVALEX project, see Garitte et al. (2013)) to determine scoping parameters for the modelling of the full VE. A description of the work and results is given in section 6.2 and has become known as the *Drying Test*.

### 3.6.8 Opalinus Clay

There are many data and property values available for Opalinus Clay contained in the reports shown in table 3.4. A summary of the *in situ* properties of the shaly facies of the Opalinus Clay

| Data | Sources |
|---|---|
| Physical properties | All those below. |
| Hydraulic properties | Floría et al. (2002), Muñoz et al. (2003), Sol-experts (2003) |
| Mechanical properties | Bock (2001) |
| Hydro-Mechanical coupling | Various |
| Hydro-Mechanical info from chemical reports. | Traber (2003), Traber (2004), Fernández et al. (2007), Noy et al. (2004) |

Table 3.4: Data sources for *Opalinus Clay*.

is given in table 3.5.

The formation is a stiff overconsolidated Mesozoic marine clay with a total thickness at Mont Terri of 160 m. The bottom half of the lithology consists of a shaly facies, then there is a 15 m thick sandy-limy facies, then a sandy shaly facies to the top. The shaly facies has small sandy lenses and a lower fracture density and is quite homogeneous (Thury, 2002).

There are several minor faults and the overthrusted Main Fault. Advective groundwater flow is negligible, both in undisturbed rock and in the Main Fault, by comparison with diffusion which is the predominant solute transport process (Croisé et al., 2004; Pearson et al., 2003; Thury, 2002). Hydraulic conductivity is fairly constant, showing no significant variation between the different facies and no enhancement near to tectonic features (Croisé et al., 2004).

Osmotic flow is thought to be slight due to a low membrane efficiency[8] (<12 %) (Croisé et al., 2004; OECD Nuclear Energy Agency, 2003), although S. Horseman et al. (2007) observed osmotic flow in laboratory samples, and hydromechanical coupled processes may be relevant when effective stress is lowered (Croisé et al., 2004) (e.g. by excavation).

Porewater chemistry is dominated by calcium, sodium, nitrate and chloride ions. Conditions are strongly reducing due to pyrite (≈1 %wt.) and siderite (Lawrence et al., 2002).

The excavation damaged zone (EDZ) varies depending on the excavation and drilling methods employed; in the Mont Terri Rock Laboratory, open fractures within 80cm from the tunnel wall are at least partly connected (Thury, 2002).

The presence, geometry and connectivity of fracture networks around excavations can be related to excavation technique and the process of fracture evolution can be explained in terms of stress fields, causing the roof and floor of a typical tunnel to have different fracture geometries than the side walls. The depth of the EDZ is shown to be related to the radius of the tunnel and the deeper parts of the EDZ are thought to be host to isolated, water-filled fractures (Bossart et al., 2004).

*Ex situ* (decompressed) samples of the clay swell — with deionised water, up to 9 % across the bedding, 10 times more than along it Thury (2002, p. 930). Self-sealing of fractures upon resaturation (whether by creep or by swelling of the fracture walls through osmosis) is an important mechanism (Blümling et al., 2007) and implies the exclusion of advective flow in fractures as a potential transport mechanism (as found in the Callovo-Oxfordian clay at Bure, France (Mazurek et al., 2008)).

The rate of tunnel stabilisation is related to the tunnel radius: a smooth pressure distribution around a 3.5m diameter galley is expected to take at least 10 years to stabilise — because the VE tunnel is 1.3m diameter it would be expected to stabilise faster, indeed it was noted (J.-C. Mayor et al., 2006) that the breakouts in that tunnel were smaller than elsewhere in the Mont Terri rock laboratory, indicating a shallower EDZ.

[8]Degree to which the clay acts as a perfect semi-permeable membrane.

| Parameter | Value | Units |
|---|---|---|
| Clay minerals: Illite, Chlorite, Kaolinite | 55 | wt% |
| Clay minerals: IS Illite/Smectite | 10 | wt% |
| Quartz (sand, silt) | 20 | wt% |
| Calcite (mainly fine shell fragments) | 10 | wt% |
| Feldspar, Siderite, Dolomite, Ankerite, Pyrite | 5 | wt% |
| Organic carbon | 0.2 | wt% |
| Physical porosity (water evaporation at 105 °C) | 12–18 | vol% |
| Mercury injection porosity (pores above 4 nm) | 5–10 | vol% |
| Hydraulic conductivity | $1–5 \times 10^{-13}$ | $\mathrm{m\,s^{-1}}$ |
| Seismic velocity (p-wave) | 2100–3700 | $\mathrm{m\,s^{-1}}$ |
| E-modulus perpendicular to bedding | 2000–5000 | MPa |
| E-modulus parallel to bedding | 5000–15000 | MPa |
| Swelling heave perpendicular to bedding | 7–9 | % |
| Swelling heave parallel to bedding | 0.5–1 | % |
| Porewater mineralisation (total dissolved solids) | 5000–20000 | $\mathrm{mg\,L^{-1}}$ |

Table 3.5: Key parameters of the shaly facies of the Opalinus Clay in which the test section of the VE is located. *(From Thury (2002)).*

Chapter 4

# THEORETICAL BACKGROUND

## 4.1 Introduction

In this chapter, the wider theoretical background of mathematical and numerical modelling is developed before the computational methods that have been employed are discussed in chapter 5, and before the applications of these theories and methods in section 6.1, Modelling the Ventilation Experiment.

A wide range of subjects have been covered in order to complete the work presented in this thesis. The depth to which these subjects have been followed varies because some of them stray far from their geological applications and others are difficult to understand without a high level of specialist knowledge in that area. As a background to the work presented so far, and a preface to the main work, these subjects will be covered here in varying degrees of detail appropriate to their involvement.

The next two chapters supports the remainder of the document by factoring out technical terms. Physical theories are described in mathematical form along with empirically derived equations. Alternatives are not discussed however the literature review in chapter 2 contains further comment. Symbols and notation used are consistent throughout this section; any repurposing will be stated. Unattributed material is considered to be established scientific knowledge.

The two most common mathematical models of unsaturated flow are those of multiphase flow and Richards' Equation. These will be derived from mass balance and constitutive equations, since they have both been used as models of the VE, however the final model of the VE uses Richards' Equation.

Central to the work is the Finite Element Method (FEM) and some time has been invested in understanding this. The selection of numerical methods to use for a particular purpose can be crucial to the efficiency, success or failure of finding an acceptable solution. Unfortunately the choice of numerical methods is generally difficult because of the mathematical background needed to understand their features, behaviour and implementation. Brief examples of numerical methods are covered.

The Drying Test was intended to form the preparatory work (Step 0) to modelling the Ventilation Experiment (VE) and so is described in section 6.2, the work is attributable entirely to C. McDermott (2009). Modelling the VE was the main work and so is discussed in the most detail, the process and the final results.

## 4.2 Mathematical modelling

### 4.2.1 Parts of a formulation

A model of the ventilation experiment may be constructed by describing the individual physical constituents (e.g. clay and water) in terms of behaviour and state, linking them by common variables and solving for measurable parameters (e.g. relative humidity, pressure) and then comparing with the experimental data.

A partial differential equation (PDE) for multiphase flow is outlined. The PDE would then be discretised using the finite element method, a general overview of which is given in section 4.3.1, and was the first formulation approximated by the earlier unsuccessful numerical models of the VE described in section 5.3.

In general, formulations of multiphase flow in porous media make use of the following types of equations (C. T. Miller, Christakos, et al., 1998):

**Balance equations** state the conservation of a continuous quantity (e.g. mass or momentum) across a domain.

**Field equations** hold for all materials without modifications (Bennethum et al., 1997).

**Constitutive relations** depend upon the material and involve coefficients which must be measured experimentally (e.g. Darcy's Law) (Bennethum et al., 1997).

**Equations of state** describe the equilibrium states in terms of pressure, volume and temperature.

Balance equations are defined continuously over a domain in a way that results in a system of equations with unknowns. Constitutive relations and equations of state are used to close the system of equations by supplying accessible parameters for some of the unknowns in the balance equations, for this reason they are also called *closure relations*.

It is the choices of constitutive relations that account for most of the variation, and introduce the most uncertainties, in models of flow in porous media.

### 4.2.2 Constitutive equations

#### Darcy's Law

By observing the flow of water through a cylinder of sand, Darcy (1856) found empirically that for water flowing through a saturated porous medium,

$$q = -\mathrm{K}\frac{dh}{ds}\,, \tag{4.1}$$

where $q$ is the volume of water per unit area passing through the end of the cylinder (the *specific discharge*), $h$ is the *hydraulic head* and $s$ is distance in the direction of flow. K is a constant of proportionality (the *hydraulic conductivity*) and is a property of both the porous medium *and* the water. Hydraulic head is defined as

$$h = z + P/\rho\mathbf{g} \tag{4.2}$$

where $z$ is the height above a datum (or *elevation head*), $\rho$ is the density of fluid, $P$ is the pressure in the fluid and $\mathbf{g}$ is the acceleration due to gravity[1]. The *pressure head* is $\psi = P/\rho\mathbf{g}$.

Where $\phi$ is the porosity as $\frac{\textit{volume of voids}}{\textit{volume of sample}}$ and $A$ is the area of the cross section of the cylinder orthogonal to the direction of flow, the velocity of water flowing though the pores is $\mathbf{v} = \frac{q}{\phi A}$. However, generalising in three dimensions for a fluid with *dynamic viscosity* $\mu$ and a porous medium with *intrinsic permeability* tensor $\mathbf{k}$ it is convenient to use a *macroscopic velocity* $\mathbf{v}$ (equivalent to the specific discharge though a unit square) and so the constitutive equation becomes

$$\mathbf{v} = -\frac{\mathbf{k}\rho g}{\mu}\nabla(\psi + z)\,. \tag{4.3}$$

Where the fluid in question is water then the (saturated) hydraulic conductivity is defined by

$$\mathbf{K} = \frac{\mathbf{k}\rho g}{\mu}\,.$$

### Pressure-saturation-permeability relations

Pressure-saturation-permeability ($P$–$S$–$k$) relations may be divided into (C. T. Miller, Christakos, et al., 1998):

- pressure–saturation ($P$–$S$) models,
- saturation–permeability ($S$–$k$) models,
- hysteresis models.

### Relative permeability

When more than one fluid phase $\gamma$ (e.g. gas and liquid: $\gamma \in \{g, l\}$) are sharing the porous medium the problem becomes one of *multiphase flow*[2]. To account for the reduction in permeability (of the porous medium) to a phase when that phase does not fully occupy the pore space, the intrinsic permeability is multiplied by a factor — the *relative permeability* $k^{\gamma}_{rel}$ of that phase (and assuming that the solid skeleton of the porous medium remains rigid):

$$\mathrm{K}^{\gamma} = k^{\gamma}_{rel}\mathrm{K}\,. \tag{4.4}$$

It is generally assumed[3] that $k^{\gamma}_{rel} = f(S^{\gamma})$ and that $\sum_{allphases} k^{\gamma}_{rel} = 1$, where the saturation of a phase $S^{\gamma}$ is defined as the fraction of the porosity occupied by the phase. Considering the complex microscale and pore scale process (e.g. interphase friction, interfacial tension, interparticle thin films[4]) this is a considerable simplification. Nonetheless there are several commonly used equations for $f(S^{\gamma})$.

[1] Thermodynamically, $h \equiv$ *mechanical energy per unit weight of water.*

[2] C. T. Miller, Christakos, et al. (1998) notes that this extension of Darcy's Law is not rigorously based and is not valid at high Reynold's Numbers ($Re = \frac{\rho\bar{v}L}{\mu}$, where $\bar{v}$ is the mean velocity through object of length $L$), i.e. turbulent flow conditions.

[3] In the FEBEX fractured rock study, referred to again in chapter 2) by Alonso and Alcoverro (2005) it is expressed as $\mathrm{K}_p = (S_{res})^d\mathrm{K}$ where $d$ is a parameter back calculated from infiltration tests.

[4] Thin films have a *chemical potential* that will be much more influential than the hydraulic potential in argillaceous rocks where advection is much less than diffusion.

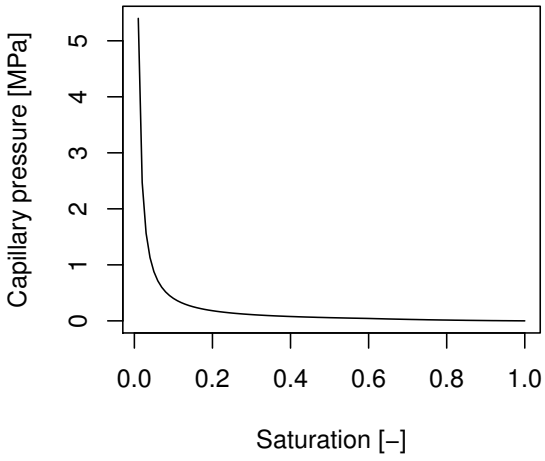


Figure 4.1: Capillary pressure - saturation curve for *Opalinus Clay*. The parameters for the curve were determined by experiment by Muñoz et al. (2003).

### Capillary pressure

*Surface tension* occurs at the interface between two fluid phases (*wetting* and *non-wetting*) and is caused by intermolecular attraction *within* each phase. At a contact surface between the interface and the solid phase, solid-fluid molecular attraction causes a concave meniscus on the interface of the wetting fluid. In a thin tube the surface tension will cause the wetting fluid phase to advance along the contact surface (the *capillary effect*), until equilibrium is found, according to

$$P_c = \frac{2wcos\theta}{r}$$

where $P_c$ is *capillary pressure* (or *suction*), $w$ is *surface tension* between wetting and non-wetting fluids (i.e. gas and liquid), $\theta$ is the wetting angle at the liquid/solid surface interface and $r$ is the effective radius of the interface. However, in porous media the underlying processes are more complicated and the equilibrium state is characterised by the empirical relationship (Reeves and Celia, 1996):

$$P_c \equiv P_{non-wetting} - P_{wetting} \tag{4.5}$$

and by $P_c^\gamma = f(S^\gamma)$ for which several functions are used (e.g. equation 4.8 of the van Genuchten retention curve, reformulated for pressure according to equation 4.2).

### Kelvin's Equation

Where the relative humidity ($RH$) of the air is the ratio in percent of the observed vapour pressure to the saturation vapour pressure (with respect to water at the same temperature and pressure), $\rho_w$ is the density of the water at 20 °C, $R$ is the universal gas constant, $T$ is the thermodynamic temperature, $M_w$ is the molar mass of water, Muñoz et al. (2003) calculate capillary pressure as:

$$P_c = \ln(RH) \times \rho_w \frac{RT}{M_w}\,. \tag{4.6}$$

**Water retention curve**

The relationship between capillary pressure (or *suction*) and water content can be described by a water retention curve. The drying behaviour of a porous medium is often different from the wetting behaviour (*hysteresis*) so the curve consists of a *drying path* and a *wetting path*. The curve may be said to be *characteristic* of the porous medium.

**Relative permeability-saturation functions**

In the following it is convenient to consider an air-water (i.e. a two phase, two component) system so that the phase qualifier ($\gamma$) may be omitted, for clarity, while noting that the RHS of

$$K = k\Big(\frac{\rho g}{\mu}\Big) \tag{4.7}$$

and the saturations could be phase-qualified at any point. The soil water retention according to the van Genuchten relationship is (from Genuchten, 1980; Schaap and Genuchten, 2005):

$$\Theta(h) = \begin{cases} \theta_r + \dfrac{\theta_s - \theta_r}{[1 + |10\alpha h|^n]^m} & \text{if } h \le 0, \\ \theta_s & \text{if } h > 0. \end{cases} \tag{4.8}$$

where $\Theta$ is the dimensionless fluid content (i.e. the water-filled volume fraction, also called the *effective saturation*), $\theta_r$ and $\theta_s$ are the *residual* (below which $\Theta$ effectively ceases to respond to changes in head) and *saturated* (where $k^\gamma_{rel} \equiv k^\gamma_{rel\,max}$) volume fractions, $n$ is a measure of the poresize distribution ($>1$) and $m = 1 - 1/n$. The relation that has become known as the Mualem-van Genuchten (or just van Genuchten) relation is then

$$k(\Theta) = \begin{cases} k_o \Theta^l \left[1 - (1 - \Theta^{1/m})^m\right]^2 & \text{if } h \le 0, \\ k_o & \text{if } h > 0. \end{cases} \tag{4.9}$$

where $K_o$ is the matching point at saturation (usually $K_o :\equiv K$), $L$ is a pore-connectivity parameter (usually $L := 0.5$) and $\Theta$ is the effective saturation, representing the range of saturations over which the formulations are practical, given by

$$\Theta(h) = \frac{\theta(h) - \theta_r}{\theta_s - \theta_r}; \quad 0 \le \Theta \le 1\,.$$

(from (4.4) and (4.9) it can be seen that for a multiphase system, $k^\gamma_{rel} = S_e^{\gamma\,L}(1 - (1 - S_e^{\gamma\,1/m})^m)$.)

The relation known as the **Modified Mualem-van Genuchten** is caused by a change in the water retention equation 4.8 to give

$$k(\Theta) = \begin{cases} K_o \Theta_e^L \left[\dfrac{1 - \Big((1 - \Theta^{1/m})\Big)^m}{1 - (1^{1/m})^m}\right]^2 & \text{if } h < h_s, \\ K_o & \text{if } h \ge h_s. \end{cases} \tag{4.10}$$

The ($P$–$S$–$k$) relations above are derived for the *equilibrium* state of a system and may have shortcomings when applied to dynamic systems. The investigation of the use and meaning

of such applications is an important aspect of the current work and is discussed further in section 6.2.

### 4.2.3 Multiphase flow formulation

First, continuum balance equations (of mass, energy, momentum) are used to describe the distribution of species and phases of interest, then closure relations are substituted to provide expressions for most of the unknowns so that the required (measurable) input and output parameters are involved.

This is one such approach, summarised from Kolditz and De Jonge (2004), Sanavia et al. (2006) and Wang, Park, et al. (2009), and was used to model the VE in some of the models in section 5.3.

The constitutive equations are formulated for the independent variables: capillary pressure $P_c$, gas pressure $P_g$ and temperature $T$.

#### Mass balance equation

Using the terms 'species' and 'components' interchangeably; for a multiphase, multispecies system a general species mass balance equation is (C. T. Miller, Christakos, et al., 1998, p. 79)

$$\frac{\partial}{\partial t}(\theta^\gamma \rho^\gamma \omega_k^\gamma) = -\nabla\cdot(\mathbf{j}_k^\gamma + \theta^\gamma \rho^\gamma \omega_k^\gamma \mathbf{v}^\gamma) + \mathcal{I}_k^\gamma + \mathcal{R}_k^\gamma + \mathcal{S}_k^\gamma \tag{4.11}$$

$\omega$ is a mass fraction, $\mathbf{j}$ is the nonadvective flux vector[5], $\mathbf{v}$ is a macroscopic phase velocity vector, $\mathcal{I}$ is a general interphase mass transfer term, representing the set of all possible transport pathways between binary groupings of phases, $\mathcal{R}$ is a general species reaction term, representing chemical and biological reactions, $\mathcal{S}$ is a solute source, representing mass added from outside the system, $\gamma$ is a phase qualifier, and $k$ a component (species) qualifier. It is worth noting at this stage that any mass of a component that transfers out of one phase (by diffusion or reaction) will transfer into another phase:

$$\sum_k \mathbf{j}_k^\gamma = 0\,, \tag{4.12a}$$

$$\sum_k \mathcal{R}_k^\gamma = 0\,. \tag{4.12b}$$

Consider fluid phases of gas $g$ and liquid $l$ ($\gamma \in \{g, l\}$) both comprised of $k$ components within a solid medium of porosity $\phi$ with no reactions between the phases (*conservative* transport). Noting that $\theta^\gamma \equiv \phi S^\gamma$ where $S^\gamma$ is the saturation of the solid phase with the $\gamma$ phase, and accounting for equation 4.3 in 4.11, the mass conservation of each component is

$$\frac{\partial}{\partial t}\left(\phi S^g \rho_k^g + \phi S^l \rho_k^l\right) + \nabla\cdot\left(\mathbf{J}_k^g + \mathbf{J}_k^l\right) = Q_k\,. \tag{4.13}$$

Sources, sinks and transfers between phases are lumped together in the RHS term, $\rho_k^\gamma$ means 'mass of $k$ per unit volume of $\gamma$', $\mathbf{J}_k^\gamma$ is total flux of $k$ in $\gamma$.

[5] Nonadvective transport is diffusion and dispersion.

Total flux is made up of advection ($\mathbf{J}_{A_k^\gamma}$) and diffusion ($\mathbf{J}_{D_k^\gamma}$) vectors:

$$\mathbf{J}_k^\gamma = \mathbf{J}_{A_k}{}^\gamma + \mathbf{J}_{D_k}{}^\gamma \tag{4.14}$$

from Darcy's Law (equation 4.3)[6]:

$$\mathbf{J}_{A_k}{}^\gamma = -\rho_k^\gamma \frac{\mathrm{K}k_{rel}^\gamma}{\mu^\gamma}\left(\nabla P^\gamma - \rho^\gamma \mathbf{g}\right) \tag{4.15}$$

from Fick's Law:

$$\mathbf{J}_{D_k}{}^\gamma = -\phi S^\gamma \rho^\gamma \mathbb{D}_k^\gamma \nabla\left(\frac{\rho_k^\gamma}{\rho^\gamma}\right) \tag{4.16}$$

where $\mathbb{D}$ is a tensor of diffusion coefficients. Since $\rho^\gamma = \rho_a^\gamma + \rho_w^\gamma$,

$$\mathbf{J}_{D_w}{}^\gamma + \mathbf{J}_{D_a}{}^\gamma = \mathbf{0} \tag{4.17}$$

from (4.12a): $\mathbb{D}_a^\gamma = \mathbb{D}_w^\gamma$, i.e. mass diffusing out of one phase goes into the other phase and *vice versa*.

Considering a water-air mixture so $k \in \{w, a\}$ and expanding the mass balance equation (4.13) with the flux defined in (4.14) based on equations (4.14), (4.15) and (4.16) above. For the water component, the diffusion part of the total flux is

$$\mathbf{J}_{D_w}{}^l = -\phi S^l \rho^l \mathbb{D}_w^l \nabla\left(\frac{\rho_w^l}{\rho^l}\right), \quad \mathbf{J}_{D_w}{}^g = -\phi S^g \rho^g \mathbb{D}_w^g \nabla\left(\frac{\rho_w^g}{\rho^g}\right). \tag{4.18}$$

Now, $\mathbb{D}_w^l = \mathbf{0}$ therefore, the **mass balance equation for the water component** can be written as

$$\begin{aligned}\frac{\partial}{\partial t}\left(\phi S^g \rho_w^g + \phi S^l \rho_w^l\right) - \nabla\cdot\left[\rho_w^l \frac{\mathrm{K}k_{rel}^l}{\mu^l}\left(\nabla P^l - \rho^l \mathbf{g}\right)\right] \\ - \nabla\cdot\left[\rho_w^g \frac{\mathrm{K}k_{rel}^g}{\mu^g}\left(\nabla P_g - \rho^g \mathbf{g}\right)\right] - \nabla\cdot\left[\phi S^g \rho^g \mathbb{D}_w^g \nabla\left(\frac{\rho_w^g}{\rho^g}\right)\right] = Q_w\end{aligned}$$

and since the capillary pressure $P_c$ is chosen as one of the two unknowns of (4.13) and $S^g = 1 - S^l$, this equation becomes

$$\begin{aligned}&\phi(\rho_w^l - \rho_w^g)\left(\frac{\partial S^l}{\partial T}\frac{\partial T}{\partial t} + \frac{\partial S^l}{\partial P_c}\frac{\partial P_c}{\partial t}\right) \\ &+ (1 - S^l)\phi\left(\frac{\partial \rho_w^g}{\partial T}\frac{\partial T}{\partial t} + \frac{\partial \rho_w^g}{\partial P^g}\frac{\partial P^g}{\partial t} + \frac{\partial \rho_w^g}{\partial P_c}\frac{\partial P_c}{\partial t}\right) \\ &- \nabla\cdot\left[\rho_w^l \frac{\mathrm{K}k_{rel}^l}{\mu^l}\left(\nabla(P_g - P_c) - \rho^l \mathbf{g}\right)\right] \\ &- \nabla\cdot\left[\rho_w^g \frac{\mathrm{K}k_{rel}^g}{\mu^g}\left(\nabla P_g - \rho^g \mathbf{g}\right)\right] - \nabla\cdot\left[\phi S^g \rho^g \mathbb{D}_w^g \nabla\left(\frac{\rho_w^g}{\rho^g}\right)\right] = Q_w\,.\end{aligned} \tag{4.19}$$

Similar to the previous procedure, the diffusion part of the total flux of air component can be written as

$$\mathbf{J}_{D_a}{}^l = -\phi S^l \rho^l \mathbb{D}_a^l \nabla\left(\frac{\rho_a^l}{\rho^l}\right), \quad \mathbf{J}_{D_a}{}^a = -\phi S^g \rho^g \mathbb{D}_a^g \nabla\left(\frac{\rho_a^g}{\rho^g}\right). \tag{4.20}$$

[6] Although empirically derived for a single phase system.

The density shift from air component to liquid $\rho_a^l$ is very small and can be omitted. Therefore, can assume $\mathbf{J}_{D_a^l} \approx 0$ and so the **mass balance equation for the air component** is:

$$\begin{aligned}\frac{\partial}{\partial t}\left(\phi S^g \rho_a^g\right) - \nabla\cdot\left[\rho_a^g \frac{\mathrm{K}k_{rel}^g}{\mu^g}\left(\nabla P_g - \rho^g \mathbf{g}\right)\right] \\ - \nabla\cdot\left[\phi S^g \rho^g \mathbb{D}_a^g \nabla\left(\frac{\rho_a^g}{\rho^g}\right)\right] = Q_a\,.\end{aligned} \tag{4.21}$$

Expanding the derivative term of (4.21) yields

$$\begin{aligned}&-\phi\rho_a^g\left(\frac{\partial S^l}{\partial T}\frac{\partial T}{\partial t} + \frac{\partial S^l}{\partial P_c}\frac{\partial P_c}{\partial t}\right) \\ &+ (1-S^l)\phi\left(\frac{\partial \rho_a^g}{\partial T}\frac{\partial T}{\partial t} + \frac{\partial \rho_a^g}{\partial P^g}\frac{\partial P^g}{\partial t} + \frac{\partial \rho_a^g}{\partial P_c}\frac{\partial P_c}{\partial t}\right) \\ &- \nabla\cdot\left[\rho_a^g \frac{\mathrm{K}k_{rel}^g}{\mu^g}\left(\nabla P_g - \rho^g \mathbf{g}\right)\right] - \nabla\cdot\left[\phi S^g \rho^g \mathbb{D}_a^g \nabla\left(\frac{\rho_a^g}{\rho^g}\right)\right] = Q_a\,.\end{aligned} \tag{4.22}$$

Mass balance equations (4.19) and (4.22) are exactly the same as that described in Sanavia et al. (2006). Expressions of *water vapour density* $\rho_w^g$ based on the Clapeyron Equation of perfect gas and Dalton's Law are

$$\begin{aligned}&P_a^g = \rho_a^g RT/M_a, \quad P_w^g = \rho_w^g RT/M_w \\ &P_g = P_a^g + P_a^w\end{aligned} \tag{4.23}$$

where $R$ is the universal gas constant, $M_w$ is the molar mass of water, $M_a$ is the molar mass of air. In unsaturated zones, the equilibrium water vapour pressure[7] $p_w^g$ can be derived from water vapour saturation pressure $P_{gws}$ and the Kelvin-Laplace equation

$$P_w^g = P_{gws}\exp\left(-\frac{P_c M_w}{\rho_w^l RT}\right) \tag{4.24}$$

which gives

$$P_{gws} = \frac{10^{-3} P_c M_w}{RT}\exp\left(19.84 - 4975.9/T\right). \tag{4.25}$$

**Energy balance equation**

Considering convective transport, i.e. the transport of heat by flow. The energy balance equation of the porous media is

$$\begin{aligned}&\rho C_p \frac{\partial T}{\partial t} + \rho^w C_p^w \frac{\mathrm{K}k_{rel}^w}{\mu^w}\left(-\nabla P^g + \nabla P_c + \rho^w \mathbf{g}\right)\nabla T \\ &\quad + \rho^g C_p^g \rho^g \frac{\mathrm{K}k_{rel}^g}{\mu^g}\left(-\nabla P^g + \rho^g \mathbf{g}\right)\nabla T + \nabla(K_e \nabla T) + Q_{\mathrm{T}} = 0\end{aligned} \tag{4.26}$$

where $C_p$ is the effective specific heat capacity, $K_e$ is the heat conductivity of the porous media.

[7] *Equilibrium vapour pressure* — pressure at which $p_k^g \equiv p_k^l$.

**Isothermal simplification**

When solving isothermal problems presented by (4.13), terms relating to temperature can be ignored so equations (4.19) and (4.22) become

$$\phi\rho_w^l\frac{\partial S^l}{\partial P_c}\frac{\partial P_c}{\partial t}-\nabla\cdot\left[\rho_w^l\frac{\mathrm{K}k_{rel}^l}{\mu^l}\left(\nabla(P_g-P^c)-\rho^l\mathbf{g}\right)\right]=Q_w\,, \tag{4.27}$$

$$\begin{aligned}-\phi\rho_a^g\frac{\partial S^l}{\partial P_c}\frac{\partial P_c}{\partial t}+(1-S^l)\phi\left(\frac{\partial\rho_a^g}{\partial P^g}\frac{\partial P^g}{\partial t}+\frac{\partial\rho_a^g}{\partial P_c}\frac{\partial P_c}{\partial t}\right)\\ -\nabla\cdot\left[\rho_a^g\frac{\mathrm{K}k_{rel}^g}{\mu^g}\left(\nabla P_g-\rho^g\mathbf{g}\right)\right]=Q_a\,.\end{aligned} \tag{4.28}$$

### 4.2.4 Richards' Equation

For a fluid moving through a saturated porous medium, the conservation of mass is (from (4.11)):

$$\frac{\partial\theta}{\partial t}+\nabla\cdot\mathbf{v}=f\,. \tag{4.29}$$

Substituting the multiphase version of the Darcy equation (4.3) into the conservation of mass (4.29) gives the Richards Equation:

$$\frac{\partial\theta}{\partial t}-\nabla\cdot(\mathbf{K}\nabla h)=f\,,$$

expanding the head term using (4.2):

$$\frac{\partial\theta}{\partial t}-\nabla\cdot(\mathbf{K}\nabla(\psi+z))=f\,.$$

Now the equation has two primary variables, $\theta$ and $\psi$ so recognising:

$$\frac{\partial\theta}{\partial t}=\frac{\mathrm{d}\theta}{\mathrm{d}\psi}\frac{\partial\psi}{\partial t}=C\frac{\partial\psi}{\partial t}\,,$$

where $\psi\mapsto C(\psi)$ is called the *specific moisture capacity* and is the slope of the graph of $\theta$ against $\psi$, substituting back into the main equation gives Richards' Equation with pressure head as the only primary variable:

$$C\frac{\partial\psi}{\partial t}-\nabla\cdot(\mathbf{K}\nabla(\psi+z))=f\,. \tag{4.30}$$

### 4.2.5 Osmotic potential

Thermodynamic treatment defines a total potential $\Psi_t$ ($\mathrm{J\,kg^{-1}}$) of water in soil, where each potential may have its own coefficient similar to K in Darcy's Law (equation 4.1) (S. T. Horseman et al., 1996, p. 89):

$$\Psi_t=\Psi_z+\Psi_p+\Psi_b+\Psi_o\,,$$

where the subscripts $z,p,b,o$ mean elevation, pressure, adsorption, osmotic. For $\Psi_o$ the constitutive equation is the same as Darcy's Law except the head gradient is a concentration gradient

across two regions of rock, the interface acting as a membrane, and the coefficient is called the *osmotic permeability* ($m^2$).

## 4.3 Numerical modelling

The partial differential equations of the mathematical model can be approximated using numerical methods to formulate a particular problem in matrix form. The benefit is that this enables the calculation of the field variables by computer. The overall objective is to get a solution to the problem, at the required accuracy, in the shortest real (*wall-clock*) time.

The finite element method (FEM) is described here briefly and generally; the actual FEM formulations of the multiphase flow equations (equation 4.27 and equation 4.28) are found in Kolditz and De Jonge (2004) and Sanavia et al. (2006).

The finite element modelling software system OpenGeoSys[8] implements those specific formulations, as well as many others, a brief description is given in section 5.1. OpenGeoSys is used and developed as necessary for this project. The description of the setup of the VE as a problem to be solved using OpenGeoSys is described in section 6.1 and the results are presented in section 6.1.5.

The VE may be represented as the application of the governing balance equations within a *problem domain* in time and space. A solution to a *boundary value problem* satisfies a differential equation at all points in a domain and satisfies conditions defined along the boundary of the domain. A solution to an *initial value problem* satisfies a differential equation at all points given the initial values at all points in the domain. The problems posed by the VE are combined — *initial-boundary-value* problems.

Coupling schemes are explained later in section 4.3.2. The method of finding a solution for one quantity (e.g. hydraulic head) over the whole problem domain is:

1. formulate a *weak (integral) form*[9] of the governing differential equation,
2. discretise the weak form across the spatial part of the problem domain,
3. assemble the resulting equations, closed with constitutive equations and boundary conditions, into a *global system matrix*,
4. discretise the global system matrix across the temporal (time) part of the problem domain, for each time interval,
5. solve the system of equations.

For discretising the PDE, the real rock is represented by a computational mesh consisting of nodes and elements. The main advantage of the FEM is that the element shapes (e.g. triangles) are suitable for representing complex physical geometries such as geological structures.

To discretise the matrix formulations in time the *finite difference method* (FDM) is used because it is simpler and results in a faster computation.

For simplicity, most of this chapter assumes that a solution is sought for one unknown field variable of function $u$, or vector of unknown functions $\mathbf{u}$.

[8] http://www.opengeosys.net

[9] Weak formulations are guaranteed to hold only for certain *test functions* i.e. across a certain domain —they are less smooth.

### 4.3.1 The Finite Element Method

#### The Definition of the problem

A (spatial) domain $\Omega$ to which the differential equation can be associated is a subset of real numbers (i.e. $\Omega \subset \mathbb{R}^{\mathtt{n_{sd}}}$, where $\mathtt{n_{sd}}$ is the number of space dimensions: e.g. 1, 2 or 3), enclosed by a piecewise[10] smooth boundary $\Gamma$, so forming closure $\bar{\Omega}$ so that $\bar{\Omega} = \Omega \cup \Gamma$. For each point of the domain a function of that point is a real-valued function (i.e. $x \in \bar{\Omega}, f(x) \in \mathbb{R}$) (from Donea and Huerta, 2003, Pg. 19).

On portions of $\Gamma$, *Dirichlet* boundary conditions prescribe the value of the unknown function:

$$u = u_D \quad \text{on } \Gamma_{\mathtt{D}}\,,$$

and *Neumann* boundary conditions prescribe the normal derivative[11] of the unknown function:

$$\frac{\partial u}{\partial n} \quad \text{on } \Gamma_{\mathtt{N}}\,.$$

(*Robin* boundary conditions prescribe a mixture of the two (Donea and Huerta, 2003, Pg. 19).) On $\Gamma$, $\Gamma_{\mathtt{D}}$ and $\Gamma_{\mathtt{N}}$ do not coincide.

The result wanted from the solution of the problem is unknown function $\mathbf{u}$ that satisfies the sets[12] of differential equations $\boldsymbol{\mathcal{A}}$ in $\Omega$ and boundary conditions $\boldsymbol{\mathcal{B}}$ on $\Gamma$ such that $\boldsymbol{\mathcal{A}}\mathbf{u} = \boldsymbol{\mathcal{B}}$, where (after Zienkiewicz et al., 2005, Pg. 54):

$$\boldsymbol{\mathcal{A}}(\mathbf{u}) = \left\{ \begin{array}{c} A_1(\mathbf{u}) \\ A_2(\mathbf{u}) \\ \vdots \end{array} \right\} = \mathbf{0} \tag{4.31a}$$

$$\boldsymbol{\mathcal{B}}(\mathbf{u}) = \left\{ \begin{array}{c} B_1(\mathbf{u}) \\ B_2(\mathbf{u}) \\ \vdots \end{array} \right\} = \mathbf{0}\,. \tag{4.31b}$$

Assuming that the unknown functions are approximated by trial solutions based on nodal values and interpolation functions, the solution will be of the form

$$\mathbf{u} \approx \hat{\mathbf{u}} = \sum_{a=1}^{n} \mathbf{N}_a \tilde{\mathbf{u}}_a := \mathbf{N}\tilde{\mathbf{u}} \tag{4.32}$$

where $\mathbf{N}$ are shape functions prescribed in terms of independent variables (such as the coordinates $x, y, z$ etc), $\tilde{\mathbf{u}}$ is the solution in finite element space and all or most of the parameters are unknown.

The temporal part of the problem domain is embedded in time dependent boundary conditions already defined and the total duration of the problem ($t_{\mathtt{max}}$).

[10] *Piecewise* — defined for each piece of the domain and not necessarily for the whole domain.

[11] *Normal derivative* — the gradient orthogonal to the boundary $\Gamma$.

[12] The problem of unsaturated flow in the VE is non-linear, because the coefficient of flow depends on the flow, the entries of $\boldsymbol{\mathcal{A}}$ are functions of the unknowns. When the matrices are written with the notation used here, the problem can be linear or non-linear and the explanation is the same.

**Discretising the problem in space**

This process finds approximate integral forms of the PDEs and then approximates them, by the following steps:

- find a weak, or variational, form of the boundary value problem,
- discretise the weak form over a spatial domain.

Of the many different procedures used to approximate the governing equations, perhaps the most commonly used are based on the two approaches:

- *method of weighted residual* forces the error due to approximation to equal zero,
- *variational process* minimises the variation of $\mathbf{u}$ over $\hat{\Omega}$, (not discussed further here).

**Method of Weighted Residuals** The following is taken almost verbatim from Istok (1989, from pg. 30).

An *approximate solution* to the initial value/boundary problem is defined and substituted into the governing equation to produce a *residual* at all points in the domain. This residual error is then forced to equal zero:

$$L(u(x,y,z)) - F(x,y,z) = 0 \tag{4.33}$$

where $L$ is the differential operator, $u$ is the field variable and $F$ is a known function. An approximate solution $\hat{u}$ to this function is

$$\hat{u}(x,y,z) = \sum_{i=1}^{m} N_i(x,y,z)u_i \tag{4.34}$$

where $i$ are *interpolation functions*, $u_i$ are the (unknown) values of the field variable at the nodes and $m$ is the number of nodes in the mesh. Substituting the approximate solution into the exact solution (4.34 into 4.33) gives

$$L(\hat{u}(x,y,z)) - F(x,y,z) = R(x,y,z) \neq 0 \tag{4.35}$$

where $R$ is the *residual* due to the approximation. Now, the residual at an individual point cannot be forced to equal zero because the residual may increase at another point. Instead the *weighted average* of the residuals is forced to equal zero

$$\int_{\Omega} W(x,y,z)R(x,y,z)\, d\Omega = 0 \tag{4.36}$$

where $W(x,y,z)$ is a weighting function. Substituting (4.35) into (4.36)

$$\iiint_{\Omega} W(x,y,z)\left[L(\hat{u}(x,y,z)) - F(x,y,z)\right] d\Omega = 0\,. \tag{4.37}$$

Now, if $\Omega$ is partitioned into $\mathtt{n_{el}}$ number of elements (convex subdomains), such that

$$\bar{\Omega} = \bigcup_{e=1}^{\mathtt{n_{el}}} \bar{\Omega}^e \quad \text{and} \quad \Omega^e \cap \Omega^f = \emptyset \quad \text{for } e \neq f\,, \tag{4.38}$$

then for any element $e$

$$\hat{u}^{(e)}(x,y,z) = \sum_{i=1}^{n} N_i^{(e)} u_i \tag{4.39}$$

where $N^{(e)}$ are the *interpolation functions* for the element, one per node, $n$ being the number of nodes. The interpolation functions are (usually simple) geometric relations. At its simplest, for a one dimensional element $e$ with two nodes $j$ and $k$ it would be the average of $u$:

$$N_k^{(e)}(x) = \frac{x_j^{(e)} - x}{x_j^{(e)} - x_k^{(e)}} \quad \text{and} \quad N_j^{(e)}(x) = \frac{x - x_k^{(e)}}{x_j^{(e)} - x_k^{(e)}} \,.$$

The choice of weighting function $W$ (in equation 4.36) distinguishes the different methods of weighted residuals, that of the *Galerkin Method* is most common[13] and in which case, as it happens, $W$ is the same as the interpolation function:

$$W_k(x) = \frac{x_j^{(e)} - x}{x_j^{(e)} - x_k^{(e)}} \text{ for } x \geq x_k \,, \text{ and } W_j(x) = \frac{x - x_k^{(e)}}{x_j^{(e)} - x_k^{(e)}} \text{ for } x \geq x_k \,.$$

**Assembling the global system of equations**

All that is required to form the system and boundary matrices (of equation 4.31, for the whole domain) is to sum all of the element matrices:

$$\boldsymbol{\mathcal{A}}(\mathbf{u}) = \sum_{e=1}^{\mathtt{n_{el}}} A_{(e)}(\mathbf{u}) \tag{4.40a}$$

$$\boldsymbol{\mathcal{B}}(\mathbf{u}) = \sum_{e=1}^{\mathtt{n_{el}}} B_{(e)}(\mathbf{u}) \,. \tag{4.40b}$$

**Discretising the problem in time**

The time derivative of a function $u$ can be found at an instantaneous time $t_{\mathtt{i}}$ to be

$$\left.\frac{\partial u}{\partial t}\right|_{t=t_{\mathtt{i}}} = \frac{u(t+\Delta t) - u(t)}{\Delta t} \iff u(t_{\mathtt{i}}) = u(t) + (t_{\mathtt{i}} - t)\left.\frac{\partial u}{\partial t}\right|_{t=t_{\mathtt{i}}} . \tag{4.41}$$

Substituting $\omega = \frac{t_{\mathtt{i}} - t}{\Delta t}$ and noting that $0 \leq \omega \leq 1$ gives

$$\mathbf{u} = (1-\omega)\mathbf{u}_t + \omega \mathbf{u}_{(t+\Delta t)} \,, \tag{4.42a}$$

$$\boldsymbol{\mathcal{B}} = (1-\omega)\boldsymbol{\mathcal{B}}_t + \omega \boldsymbol{\mathcal{B}}_{(t+\Delta t)} \,. \tag{4.42b}$$

The ideal time step scheme reaches a solution for the whole problem duration ($t_{\mathtt{max}} - t_0$) in the quickest possible (wall clock) time $t_{\mathtt{wc}}$, within a certain accuracy. The $t_{\mathtt{wc}}$ is minimised by maximising the time step size $\Delta t_{(\mathtt{t})}$ at every time step and therefore minimising the number of time steps over which the problem time is discretised.

An automatic time stepping scheme is used[14] that chooses an appropriate time step length at the current time $\Delta t_{(\mathtt{t})}$ based on the last successful time step length $\Delta t_{(\mathtt{t\text{-}1})}$. If the accuracy

[13] The Galerkin Method produces a symmetrical system matrix which is computationally advantageous for solving.

[14] In OpenGeoSys the keyword to use is `PI_AUTO_STEP_SIZE`.

of the calculation is outwith specified bounds then the solution is rejected for that step. The advantage over specifying the lengths of each time step is that if the solution is rejected then OpenGeoSys will try again with a smaller time step rather than aborting. This is particularly useful for the long running models so that they do not abort because of one failed time step after a day or so of computations[15]. A disadvantage of using this scheme is that where relatively dynamic episodes in the rock follow periods of fairly constant conditions (i.e. at the start of a desaturation period) several iterations of *the same time step*, with progressively smaller estimates of $\Delta t_{(\mathtt{t})}$, will be made[16] before the solution is acceptable.

### 4.3.2 Coupling schemes

The dependence (i.e. *coupling*) of process $i$ on process $j$ where the system matrix $\mathbf{A}$, time $t$, coordinates $\mathbf{x}$, solution vector $\mathbf{u}_i$, boundary conditions vector $\mathbf{B}_i$ is shown by (Kolditz and De Jonge, 2004, Eq. 46):

$$\mathbf{A}_i(t, \mathbf{x}, \mathbf{u}_i, \mathbf{u}_j)\mathbf{u}_i = \mathbf{B}_i(t, \mathbf{x}, \mathbf{u}_i, \mathbf{u}_j)\,.$$

The individual processes that make up a coupled system may be calculated on separate finite element meshes, or across different time steps or in otherwise separate domains linked by boundary conditions. These techniques are useful where numerical stability criteria limit the contrasts possible in defining material properties (C. McDermott et al., 2008). Where a more complex coupling scheme is used, most of the computation time may be taken up assembling equations. The following discussion assumes that the processes use the same mesh and time discretisation and are coupled simply through shared parameters in the governing equations.

**Monolithic Algorithm** The solution of all equations in a single step. Kolditz and De Jonge (2004) found the monolithic scheme to be more correct and precise for calculating gas pressure and that incorporating swelling effects makes a big difference in saturation profile. This scheme is favourable for the stability of the calculation because the mutual influence of the processes can be taken into account directly (Degroote et al., 2009, Pg. 793).

**Partitioned Algorithm** The processes each have a system matrix and the systems of equations are solved sequentially and iteratively within the same time step (Kolditz and De Jonge, 2004).

### 4.3.3 Solving systems of equations

The system of equations (arising from the matrix-vector multiplication $\boldsymbol{\mathcal{A}}\mathbf{u}$) is solved to an acceptable accuracy by an iterative method. The acceptable accuracy is determined by confirming that the absolute difference between the solutions of two (or more) iterations, is less than a pre-defined parameter $\epsilon$. During a typical model run, most computational time will be spent in the solver. Two such methods are given below.

**Picard Method** A system of non-linear equations can be solved by constructing a matrix of coefficients from an initial guess of the value of the unknown variables and forming a system of linear equations. This linear system is solved for the matrix of unknowns and the solution

[15] Though there is a method of restarting OpenGeoSys from the last successful time step.
[16] For reasons of numerical instability as shown in section 4.3.4.

becomes the new estimate for the next iteration. The residual between the estimate and the new estimate is stored and convergence at an overall solution is when the absolute value of the maximum residual value is less than $\epsilon$.

**Newton-Raphson Method** Used for systems of non linear equations. This is an iterative method used to determine the roots of a real-valued function $f(x)$ given its derivative $f'(x)$ and an initial guess $x_0$, a better approximation is given by:

$$x_1 \approx x_0 - \frac{f(x_0)}{f'(x_0)}$$

and so on for further iterations $x_2, ...x_n$ until $x_n \approx x$ at the required precision (i.e. $|x_n - x| < \epsilon$).

**Single precision biconjugate gradient stabilised (SpBiCGStab)** This method is used for linear and non-linear problems in OpenGeoSys and is described in Meijerink and Vorst (1977).

### 4.3.4 Numerical instability

The Galerkin method can lead to oscillations in problems where convection dominates requiring mesh refinement or time step refinement unless a stabilisation technique is used during the discretisation. Many different stabilisation techniques are available.

The approximate solution reached at the end of a time step will have an error (or residual) compared with the exact solution. If the error grows over successive time steps then the calculation has become unstable.

There are several criteria that constrain the maximum time step size and element size (mesh spacing) in order to assure a stable solution. The criteria are generally applied to linear flow problems however they do depend on the particular equations being solved so may not be directly transferable.

A simulation may be stabilised by:

- increasing the diffusive component, or
- decreasing the time step duration $\Delta t$.

Where $v$ is the velocity of a substance across a domain, and $\Delta x$ is distance in the same domain the following criteria can be described (e.g. El-Kadi and Ling, 1993).

**Courant Number** Relating to convection and expressed as

$$Co = \frac{v\Delta t}{\Delta x}\,, \tag{4.43}$$

unless $Co \leq 1$, the substance is moving fast enough across the mesh to skip elements. A corollary of this is that if the mesh spacing is reduced then the time step will probably need to be reduced.

**von Neumann Criterion** The quantity can only diffuse at most half a cell at a time:

$$\frac{\Delta D}{\Delta x^2} \leq \tfrac{1}{2}\,.$$

**Péclet Number** Describes the relative importance of advection and dispersion:

$$Pe = \frac{\text{diffusive flux}}{\text{advective flux}} = \frac{v}{D}\Delta x\,,$$

a suitable criteria may be $Pe \leq 2$.

**Fourier Number** Not as widely used as the others, defined as:

$$Fn = \frac{Co}{Pe} = \frac{D\Delta t}{\Delta x^2}\,,$$

e.g. $Fn < 0.5$ (El-Kadi and Ling, 1993).

### Pore network models

As well as the $P_c(S)$ functions described in section 4.2.2, numerical models representing the porous medium as a network of pores may be used to describe a retention curve. Typically, the pore network is represented as a lattice of pore bodies (*sites*) connected through their pore throats (*bonds*) (Fischer and Celia, 1999).

There are two basic approaches (Blunt, 2001):

1. tune the parameters to fit experimental data,
2. model the random topology of the pore space directly[17]

The advantages of numerical over analytical methods are that (Fischer and Celia, 1999):

- analytical methods for $P_c, S$ relationships often do not predict (absolute) permeability well and so experimental determination of the 'matching point' ($K_o$ in equation 4.9 and 4.10) is required,
- analytical prediction of $k_{rel}$ requires a parameter accounting for connectivity and tortuosity[18] that cannot be determined by curve fitting,
- analytical methods typically allow a discontinuous non-wetting phase (e.g. gas pressure) that becomes undefined when (the solid phase porosity is) saturated with water[19],
- numerical models use parameters with real meanings in the pore-network context.

Pore network models were not used in this project however they may deserve some attention in further work because of the advantages outlined above.

[17] E.g. by particle size density (PSD) curves for sedimentary rocks, statistical methods for carbonates or computer tomography (CT).

[18] *Tortuosity* — the ratio of the length of a flowpath to the distance between its end points (Fetter, 1994, Pg. 454).

[19] The Modified Mualem-van Genuchten function of Schaap and Genuchten (2005), described in section 4.2.2 (e.g. equation 4.10), may be describing a continuous wetting phase (further investigation necessary).

Chapter 5

# COMPUTATIONAL METHODS

## 5.1 OpenGeoSys implementation

An OpenGeoSys model is specified in various ASCII format files as per table 5.1. OpenGeoSys is of *Object Oriented Design*[1] that allows generic methods to be easily applied to different types of problems. For example, the scheme for solving coupled multiphase flow process equations has been programmed by the various contributors and is applied by assigning to the variable `$PCS_TYPE` the keyword `MULTI_PHASE_FLOW` in the process setup file. The mesh, geometry, boundary conditions etc. are autonomous.

Table 5.1: OpenGeoSys files. *(After Kolditz, Beinhorn, et al., 2008).*

| Object | File extension |
|---|---|
| Processes | pcs |
| Initial conditions | ic |
| Boundary conditions | bc |
| Source/sink terms | st |
| Fluid properties | mfp |
| Solid properties | msp |
| Medium properties | mmp |
| Lookup values | rfd |
| Component properties | mcp |
| Time discretisation | tim |
| Numerical solver | num |
| Output specification | out |
| Geometric data | gli |
| Mesh data | msh |
| Restart data | rfr |
| Domain description | ddc |

When running a simulation some operations do not need to wait for the previous operation to complete before commencing. This enables parts of the code to be parallelised. Most notably, $\Omega$ may be partitioned (*decomposed*) into subdomains and each sent to a separate *compute node* for calculation. The principal behind High Performance Computing (HPC) is that the more compute nodes available to run the simulation on, the smaller $t_{\texttt{wc}}$. The general procedure for running a simulation on more than one compute node is shown in Algorithm 5.1.1.

A compute node could be a processing core of a multicore CPU[2], a single CPU, or a node on a graphics card (GPGPU[3]). The individual compute nodes may communicate by a protocol

[1] Object Oriented Design: *"A design method in which a system is modelled as a collection of cooperating objects..."*—Free On-Line Dictionary of Computing (http://foldoc.org/)

[2] Central processing unit.

[3] General purpose graphics processing unit.

**On the master node:**
Partition mesh into $\mathtt{n}_{\mathtt{cpu}}$ subdomains
Run OpenGeoSys on model files
**for all** $\Omega_{\mathtt{sub}}$ in $\bar{\Omega}$ **do**
- read mesh
- compute local finite element topology
- compute local $\mapsto \boldsymbol{\mathcal{A}}$

**end for**
**On all the compute nodes concurrently:**
**for all** process in file `'.pcs'` **do**
Create objects of type Process
- allocate memory,
- add to process list (`PCSlist`)

**end for**
**for all** process in `PCSlist` **do**
Configure object vectors
**end for**
**while** $t < t_{\mathtt{max}}$ **do**
**for all** process **do**
- calculate new time step based on numerical stability criteria
- adjust time-dependent boundary conditions and source terms
- calculate finite element matrices
- assemble equation system
- solve equation system
- calculate resultants such as fluxes or secondary variables using constitutive equations
- save time step results

**end for**
- calculate process interactions
- calculate subdomain interactions

**end while**

Algorithm 5.1.1: OpenGeoSys scheme for solving coupled process models in parallel. (Kalbacher, Wang, et al., 2008)

that provides a *message passing interface* (MPI) however inter-node traffic has an overhead and is sought to be minimised. MPI is only required by the linear solver where calculations involve border nodes shared by sub-domains (Wang, Kosakowski, et al., 2009)[4]. Since 2006 the potential of GPGPUs to outperform CPUs for this kind of application has begun to be exploited.

## 5.2 Workflow for the development of OpenGeoSys models

Different workers who use OpenGeoSys also use different tools for preparing files for input to OpenGeoSys and for postprocessing and presenting results. Historically, the *de facto* standard tool for postprocesing has been Tecplot, however it has probably now been superseded in popularity by Paraview. Tecplot is proprietary, about £1000 for a licence, Paraview is Open Source (free) and the output format of both, even in plain text format, is not easily processed by a human. Before the Paraview output format had been programmed in OpenGeoSys (circa 2009), and when developing very simple models to test discrete features of OpenGeoSys, a simple human-readable format was required and so a plain text, list type, output format was

[4]GPGPUs cannot use MPI and instead use a different algorithm — OpenMP.

developed and contributed[5] to the main OpenGeoSys Subversion repository.

Visualising the results of these small 1D and 2D models is achieved using the R Statistical Language[6].

To manage the changes in the versions of OpenGeoSys, the versions of the model and the results, metadata was imported into a PostgreSQL[7] relational database along with the results. Plots were generated using R scripts that connected to the database to retrieve results.

Three main custom components that were developed to achieve this were:

- a shell script to collect metadata about versions by querying the Git repositories of both the local OpenGeoSys source code and local model input files
- a shell script to import the results files and the metadata into the database
- the database schema itself
- plotting scripts in R.

This system was developed to speed up the cycle from changing a geological parameter value to viewing the results, while being able to replace the version of OpenGeoSys used with a more recent one. Working with the trunk of the OpenGeoSys repository was a significant challenge because there were many changes over the period that this work was taking place.

Of particular interest in this regard is the system of tables that make up the schema for managing provenance and reproducibility data, `prov`, to facilitate the reproduction of a particular set of results (see figure 5.1 and section 5.2.1). The scientific process requires that results are reproducible and so the benefits of this approach are obvious. In summary, two types of information are required for an entity (piece of software, collection of data, etc.) in order to achieve this; 1) information used to reproduce it and 2) information used to identify that it has been successfully recreated. Perhaps the most difficult issue is defining the minimum amount of information needed for reproducibility. For this project it has been assumed that anyone with access to the local git repository containing modified OpenGeoSys source code (included in Appendix B.2) and an Open Source software stack (for example GNU/Linux) would be able to reproduce the results just by knowing the git commit id, compiler arguments, and the version of the model files, which is another git commit id. Once the binary has been compiled and linked then it can be checked by comparing its cryptographic hash with the one for the original binary. In practise, a different version of the compiler may cause the hashes to differ and so the compiler version, or the operating system state should be stored.

[5] Later stripped out by the OpenGeoSys developers at UFZ.

[6] R Core Team (2012). *R: A Language and Environment for Statistical Computing*. ISBN 3-900051-07-0. R Foundation for Statistical Computing. Vienna, Austria.

[7] PostgreSQL Global Development Group (2012). *PostgreSQL: The world's most advanced open source database*. PostgreSQL.

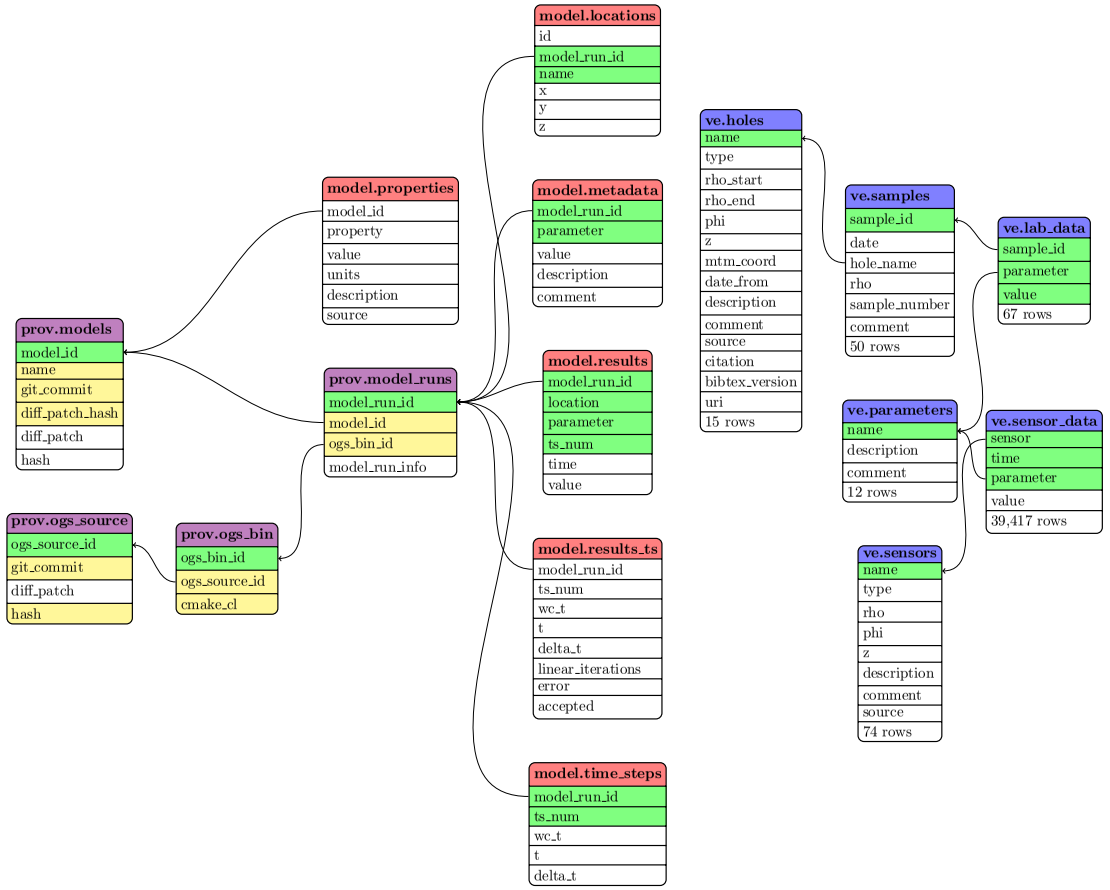


Figure 5.1: Database schemas (abbreviated), showing the database tables of the `'prov.'`, `'model.'` and `'ve.'` schemas (with purple, red and blue table names, respectively). The green rows are primary key fields and the yellow fields are indexed for speed. Although the schemas are all in the same database, the `model` and `ve` schemas are largely separate. Not shown are auxiliary tables, queries and functions that combine data from more than one schema to yield data for the plots of residuals vs targets, compute the boundary condition or postprocess results.

### 5.2.1 Table definition of the schema for managing provenance data (prov)

```
CREATE SCHEMA prov; -- to keep provenance data in

  CREATE TABLE prov.ogs_source (
  -- OpenGeoSys source code definition
  ogs_source_id SERIAL PRIMARY KEY,
  git_commit varchar(40),        -- as per git log
  diff_patch text NOT NULL,      -- default is 'none'
  hash char(32),                 -- sha1sum, 44 with the  - , 32 without
  UNIQUE ( git_commit, hash )    -- defines source
  );

  CREATE TABLE prov.ogs_bin (
  -- OpenGeoSys binary executable definition
  ogs_bin_id SERIAL PRIMARY KEY,
  ogs_source_id integer REFERENCES prov.ogs_source ON DELETE CASCADE,
  cmake_cl text NOT NULL,    -- default 'none' the cmake command line
  UNIQUE ( ogs_source_id, cmake_cl ) -- defines executable
  );

  CREATE TABLE prov.models (
  -- OpenGeoSys model file set defnition
  model_id SERIAL PRIMARY KEY,
  name char(40),             -- more than one model may share a git repo
  git_commit char(40),       -- as per git log
  diff_patch_hash char(44), -- md5sum hash of patch
  diff_patch text NOT NULL, -- default 'none', for array model gives the
                             -- actual difference (e.g.\space porosity)
  hash char(44),             -- sha1sum, 44 with the  - , 40 without
  UNIQUE ( name, git_commit, diff_patch_hash ) -- defines a model
  );

  CREATE TABLE prov.model_runs (
  -- Combines OpenGeoSys binary executable and model files
  model_run_id SERIAL PRIMARY KEY,
  model_id integer REFERENCES prov.models ON DELETE CASCADE,
  ogs_bin_id integer REFERENCES prov.ogs_bin ON DELETE CASCADE,
  model_run_info varchar(100),    -- a phrase associated with this model run
  UNIQUE ( model_id, ogs_bin_id ) -- defines a model run
  );
```

## 5.3 Model evolution

A description of models of the Ventilation Experiment (VE) for Task A of the DECOVALEX-2011 project using the Finite Element Method and OpenGeoSys (OGS).

### 5.3.1 Design principals

The development has largely followed these principals:

- the upper limit of the sophistication of a model of the VE, is set by the VE results dataset
- start with the simplest model that will yield the required results
- take small development steps where practical, testing after each change
- take larger development steps if it may be expected reasonably to be successful and save significant time (as necessary to meet a reporting deadline) compared with the sum of the constituent smaller steps, upon failure work backwards
- avoid repeating error prone procedures (e.g. model geometry changes requiring remeshing)
- where possible, write automated functional tests to confirm that a feature is working as expected between software changes.

Model output is required for a set of points, times and physical parameters to enable comparisons between teams (figure 6.4, table 6.7), meshes are generated so that these points coincide with mesh nodes.

Other major factors influencing model evolution have been the fixed DECOVALEX reporting schedule and OGS development.

Minimalistic models that test very basic functionality and have been incoporated into the OGS build system are not reported here. Such models have become known as *mini benchmark tests* and may consist of just two elements. On running the test suite the models are run and if the output matches the expected output then the tests pass. Individual models are now described according to various criteria (purpose, rationale, etc.).

### 5.3.2 Rock Models

All of the models are axisymmetric about a point (1D), vertical line (2D) or vertical plane (3D) through the centre of the tunnel; only half of the real domain needs to be considered. All of the models use the same material properties as the Step 0 model because there has been no reason to change them.

#### 3D Heat Transport

**Purpose:** to get the first OGS model files set up and running; an overview of the modelling process (or 'workflow')

**Rationale:** heat transport is the best established process in OGS and numerically stable. There is a relative humidity gradient down the tunnel and so it was recognised that a 3D model is necessary to represent this. 3D data is available from the VE.

**Model domain:** 3D slice (figure 5.2a), the slice is arbitrarily thin to reduce the size of the domain whilst retaining the basic behaviour of a larger model that may be developed in future

**Element type:** tetrahedrons

**Problems:** none

#### 3D Multiphase flow with flux

**Purpose:** to model multiphase (gas and liquid) flow processes (advection and dispersion) in multicomponents (dry air and water)

**Rationale:** substituting heat transport for multiphase flow, following on from section 5.3.2

**Model domain:** figure 5.2a

**Element type:** tetrahedrons

**Problems:** Applying the tunnel boundary condition was inconsistent, various different orientations were attempted (figure 5.2). Time stepping using the basic scheme (specified time steps) was also inconsistent causing some output times to be skipped. Very long runtime and numerical instability were encountered especially during rapidly changing boundary conditions. Bugs were found and reported. There is no formal bug handling or discussion for the OGS project. The scheme was changed from `TWO_PHASE_FLOW` to `MULTI_PHASE_FLOW` on advice from UFZ Leipzig. There are no benchmarks using `TWO_PHASE_FLOW`. Parallel processing was attempted in order to help with the long runtime. Further problems were encountered and discussed with UFZ Leipzig and there was uncertainty over whether multiphase flow models could be expected to run in parallel or not; they do not. Some new code to calculate the flux caused memory to fill up and this was resolved. Problems were also encountered due to the trunk of the source code failing to compile, inconsistencies in line endings in the Subversion repository and failing benchmark tests.

It was recognised that for large models the thinness of the slice combined with tetrahedrons lead to unfavourable shapes at the outer domain boundary where the mesh was very coarse but the slice was very thin — the elements were blade shaped. Prism elements would solve this problem but, as discussed in section 5.3.4, this lead to other problems.

#### 2D Multiphase flow

A 2D model was constructed with a mesh of triangles (figure 5.4) because the 3D model suffered from very long run time and solver instability.

It was suggested that the curved outer model boundary caused problems with solver stability due to boundary effects and also with the application of boundary conditions. A rectangular domain was constructed (figure 5.5). From this, a cuboid domain with subrectangular cross section was constructed (figure 5.10). Problems persisted and so the scheme was changed to Richards' Flow and 1D.

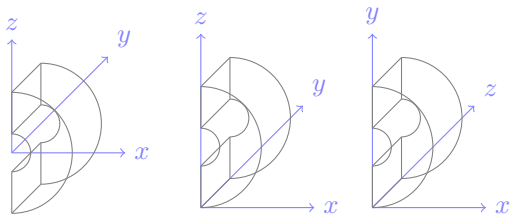


(a) (b) (c)

Figure 5.2: 3D slices with different orientations. To investigate problems the origin and orientation of the axes was changed.

### 1D Richards flow (and mechanical deformation)

**Purpose:** to start again with the simplest possible model

**Rationale:** 1D results would be sufficient and, once running, the mesh spacing can be applied to models of higher dimensions. A 1D model will not encounter as many bugs related to geometrical operations.

**Model domain:** linear

**Element type:** line

**Problems:** mechanical deformation did not work

After running for the duration of the VE with the applied boundary condition, analyses were made of the sensitivity of water pressure to changes in intrinsic permeability and porosity.

Intrinsic permeability (in $m^2$) was varied through $2.60 \times 10^{-19}$, $1.52 \times 10^{-19}$, $1.22 \times 10^{-19}$, $9.20 \times 10^{-20}$, $6.20 \times 10^{-20}$, $3.20 \times 10^{-20}$, $2.00 \times 10^{-21}$, while keeping porosity at 0.19. The first two values and $6.20 \times 10^{-20}$ did not run well. When the solver has difficulty the automatic time stepper reduces the time step to be very small and so the model run is then stopped manually. The reason why the value, in the middle of the range, caused the model to run with difficulty is because when the tunnel wall desaturates and resaturates a wave of desaturation travels into the rock causing an elbow in the saturation against distance curve. This elbow is sharper for low permeabiliteis and occurs further into the rock for higher permeabilities. This particular value causes the elbow to occur far enough into the rock where the mesh is more coarse and yet the elbow is still fairly sharp (indicating higher rate of change of saturation).

Porosity was varied from 0.14 to 0.20 while keeping intrinsic permeability constant at $3.2 \times 10^{-20}$ $m^2$. The values 0.15 and 0.17 did not run well, assumed to be for reasons described above. The results are shown on figure 5.6.

### 2D Richards flow

Using the parameters from the 1D model, a 2D rectangular domain was set up with a mesh using triangular elements (figure 5.5). The model is full size (figure 5.7). This model worked well, similarly to the 1D model.

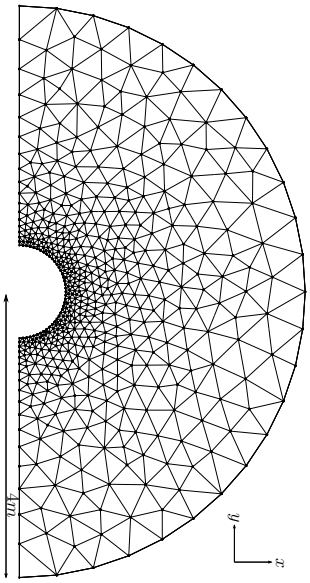


(a)

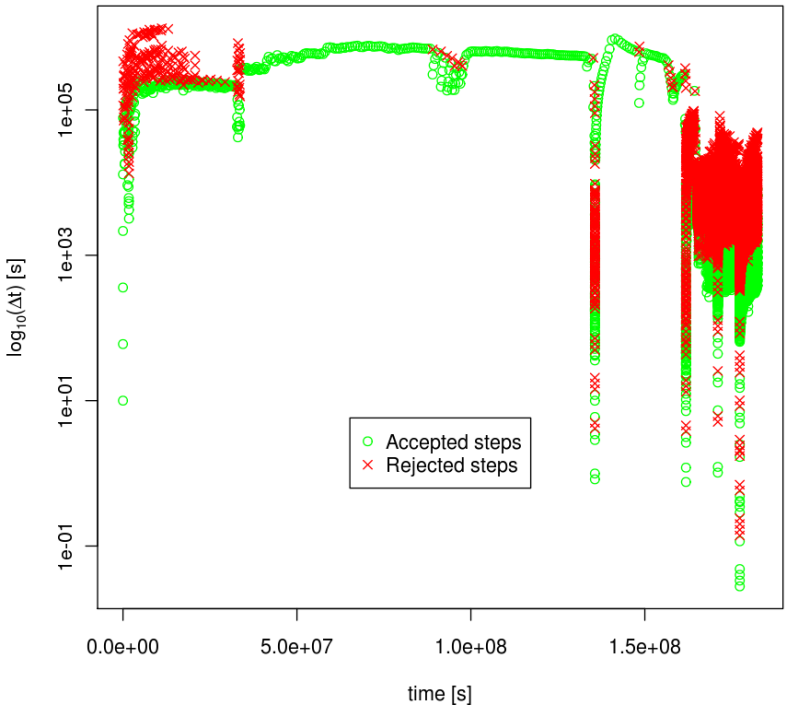


(b)

Figure 5.3: 2D multiphase flow: mesh and time stepping. (a) Mesh of triangle elements for the 2D multiphase flow model of 4m radius. (b) Instability shows up during the more rapid relative humidity (capillary pressure) changes at the boundary, as long runtime. A time control is used that calculates the time step length automatically.

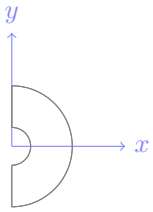


Figure 5.4: 2D circular domain.

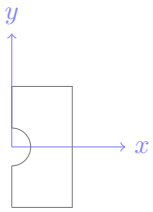


Figure 5.5: 2D rectangular domain.

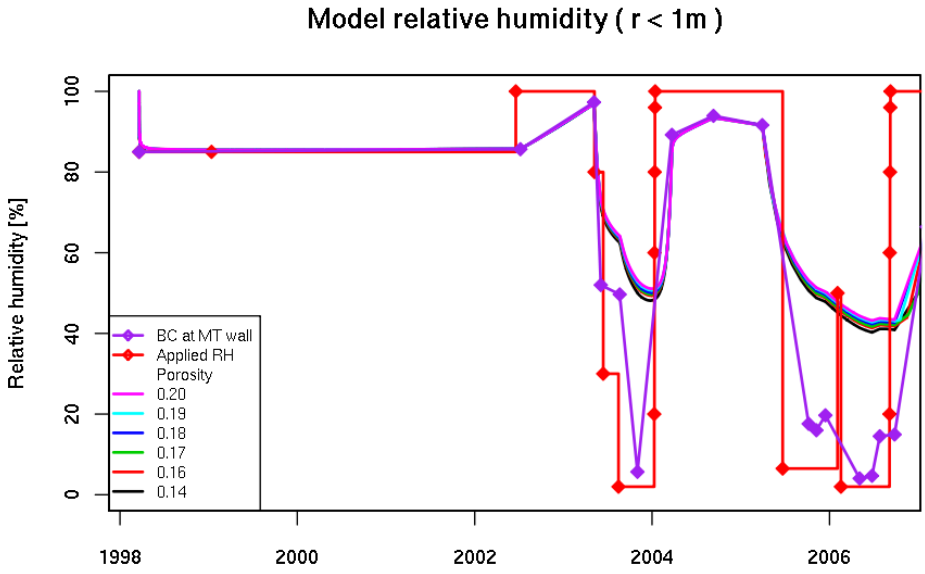


Figure 5.6: Sensitivity of relative humidity to variation in porosity for regions close to the tunnel wall. The results are influenced strongly by the boundary condition and less strongly by porosity.

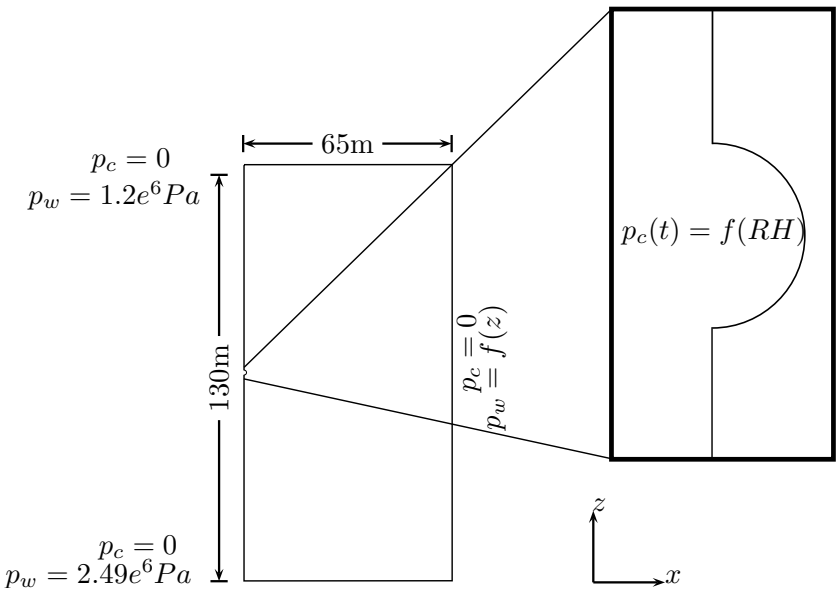


Figure 5.7: Boundary conditions and domain geometry represented by the 2D rectangular Richards Flow model. $p_C$ is capillary pressure, $p_w$ is water pressure, $RH$ is relative humidity. The $z$ axis points vertically upwards.

#### 3D Richards flow

A 3D model was set up based on the 2D model (figure 5.10). The mesh was made by extruding the 2D mesh along the length of the tunnel, using Gmsh, thus creating prism elements figure 5.8. The 3D model was tested using the same homogeneous (along the tunnel axis) boundary condition as used for the 2D and 1D Richards models (figure 5.9) and indeed all previous successful and unsuccessful models. The results of this and the 2D model are, not unsurprisingly similar to that of the 1D model and conceptually offer no advantages over it yet.

### 5.3.3 Tunnel models

The Richards Flow models of the rock described so far all show that the response of the rock to the applied capillary pressure boundary condition at the tunnel wall follows closely the shape of the boundary condition. A model of the tunnel has been included because:

- the varying boundary conditions of the VE were the air inflow and outflow of the tunnel
- the boundary conditions of a real repository would be the ambient air conditions measured at several points
- the current model results so far reflect the particular statistic used for estimating the relative humidity at the boundary condition rather than measured values
- including a model of the tunnel was identified at the DECOVALEX meeting in Prague in 2009 as being a major objective for all teams who had not yet done so.

#### 3D Tunnel model — groundwater flow, prisms

As the first tunnel model to be developed, it approximates the flow of moist air in the tunnel using the groundwater flow scheme of OGS with the porosity set to 0.99 and fluid and material

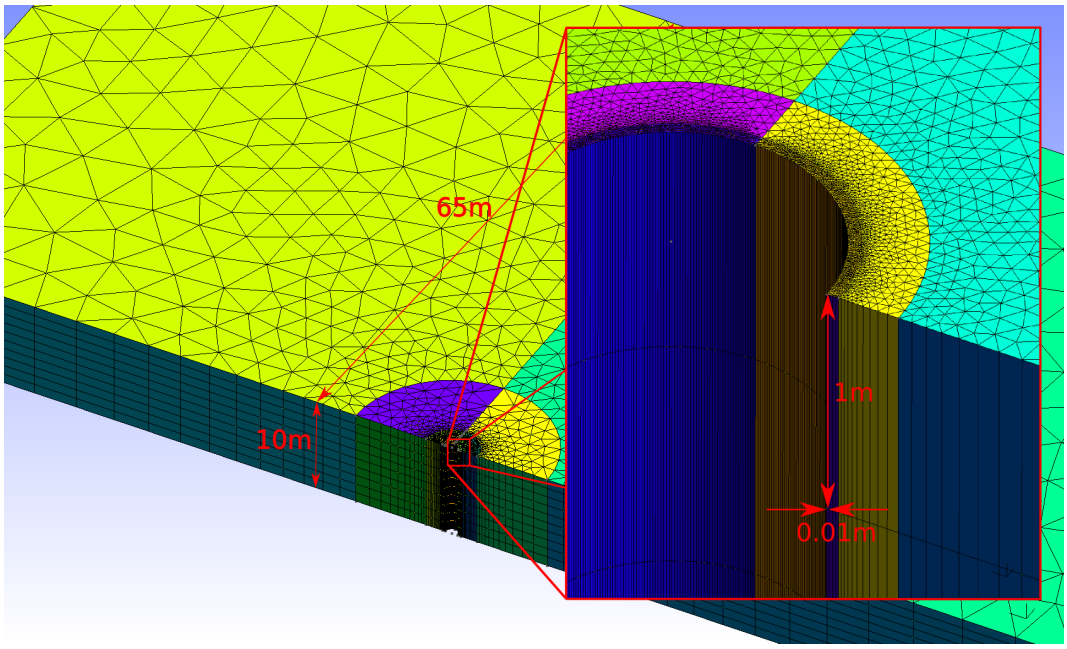


Figure 5.8: 3D prismatic mesh, rock model. This first attempt at a prism mesh shows a full scale rock model (10m long), discretised into 1m long prisms. Further discretisation along the tunnel wall would cause flattening of the elements deeper into the rock where the prisms are of greater volumes.

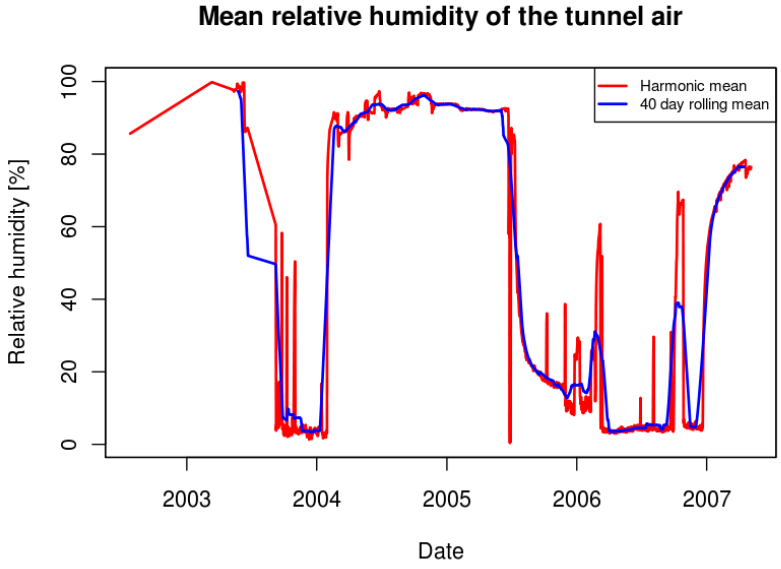


Figure 5.9: Tunnel wall boundary condition calculated using the 40 day rolling geometric mean of four sensors.

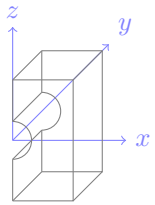


Figure 5.10: 3D cuboid domain.

properties are adjusted so that the fluid phase is air rather than water. Water is transported as a conservative species. The flow rates through the tunnel are controlled by equivalent hydraulic gradient imposed by head boundaries at the inlet and outflow. The relative humidity is calculated as the equivalent concentration of water in the air. The inlet is located 2 m into the 10 m tunnel.

The linked nodes method, described next in section 5.3.4, was developed as a simple first attempt at incorporating the tunnel in the VE model.

### 5.3.4 Linked nodes method

#### Description

Two models (e.g. rock and tunnel) may be linked together along shared physical boundaries even though they use different variables by converting between the variable types at the nodes for every timestep (`fig:linkedNodes`). Source terms handle inputs and outputs within the model domain (typically recharge, wells, leakance). Although the shared nodes (for the particular models described) are actually at the boundary of the domains, the most convenient place to implement this scheme, in OpenGeoSys, is as source terms. The source code is included in Appendix B.3.

The development is at a stage where a user could probably setup and run a model without knowing anything about the implementation. This is not because a lot of time has been spent on development but because the implementation uses little extra code.

#### Concept

One model runs for one timestep and writes the new node values, the second model then reads a subset of these node values, converts them to another state variable as necessary, runs for one timestep and writes the node values back again. Various time stepping schemes would be possible but the one implemented here is that the second model never runs ahead of the first.

#### Model setup for OGS

The following concerns a model of the rock named simply '`a`'. OGS expects all the input files for this model to be named '`a.*`' and to exist in the same directory.

If model '`a`' is linked with model '`b`' then the two sets of input files must all exist in the same directory[8].

The mesh nodes to be linked are specified in the file '`a.lnk`'. The format of this file is:

[8] OGS is not directory-aware on any level, (e.g. model results are put in the same directory as the model files) so although it would be preferable to keep the two models separate (because they are almost agnostic of one another) it is not possible to say *'run* OGS *using the model files in path/to/directory'*.

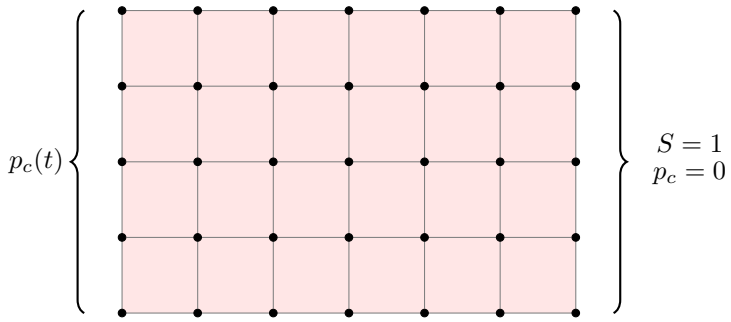


(a) Rock model finite element mesh.

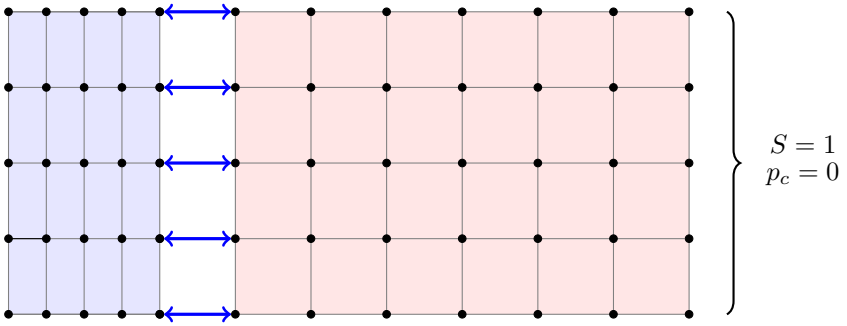


(b) Linked rock and tunnel models.

Figure 5.11: The uniform boundary condition of the rock model (a) is replaced with source terms by linking mesh nodes with those of the tunnel model (the blue rectangle) (b). (Rectangular elements are shown for clarity.)

```
process_name
initial_value
for each node in linked_nodes:
    node_id [whitespace] variable_name
```

For example:

```
RICHARDS FLOW
0.0108465
1     PRESSURE1
2     PRESSURE1
62    PRESSURE1
104   PRESSURE1
```

To get the `node_id` the model must be run initially with the existing OGS keyword `$BOUNDARY_CONDITION_OUTPUT` under the appropriate `$PCS_TYPE` in the '`.pcs`' file.

```
#PROCESS
 $PCS_TYPE
   RICHARDS_FLOW
 $BOUNDARY_CONDITION_OUTPUT
#STOP
```

...which outputs `node_id` for *all* boundary conditions in `a.bc`, so, after disabling all boundary conditions that are not to be linked and running the model for a couple of seconds, the result is the following contents (abbr.) for file `a_RICHARDS_FLOW_BC_ST.asc`:

```
#Dirchilet BC (from a_RICHARDS_FLOW_BC_ST.asc.bc file)
#Total BC nodes 2244
#Node index, name, x, y, z, value:
1 PRESSURE1 0.0000000e+00 0.0000000e+00 6.4350000e+01 -1.0000000e+00
2 PRESSURE1 6.5000000e-01 0.0000000e+00 6.5000000e+01 -1.0000000e+00
62 PRESSURE1 6.5000000e-01 1.0000000e+01 6.5000000e+01 -1.0000000e+00
104 PRESSURE1 0.0000000e+00 1.0000000e+01 6.4350000e+01 -1.0000000e+00
110 PRESSURE1 1.0009580e-02 0.0000000e+00 6.4350077e+01 -1.0000000e+00
111 PRESSURE1 2.0016788e-02 0.0000000e+00 6.4350308e+01 -1.0000000e+00
112 PRESSURE1 3.0019248e-02 0.0000000e+00 6.4350693e+01 -1.0000000e+00
113 PRESSURE1 4.0014588e-02 0.0000000e+00 6.4351232e+01 -1.0000000e+00
...etc.
```

...from which the file '`a.lnk`' can be made.

'`b.lnk`' is set up similarly. The only requirement is that the number of linked nodes must be the same as in '`a.lnk`'.

To check that the initial list of nodes output is probably correct, the meshes of the two models are constructed using boundary nodes with exactly the same locations and then the two `.asc` files are read into a database so that it can be checked that $\forall n_a \in N_a, \exists! n_b \in N_b : n_a(x,y,z) \equiv n_b(x,y,z)$, in other words, all nodes are accounted for. Apart from being able to do that test, there is no other requirement for each pair of linked nodes to occupy the same location.

Recent developments of the OGS geometry library and a little extra reliability (e.g. for finding the nodes on the surface of a TIN[9]) together with more separation between reading model files and initialising objects, would make it possible to specify the name of the geometrical object representing the shared boundary instead of having to list the node numbers.

Source terms are set up for each model. The file '`a.st`' contains:

```
#SOURCE_TERM
 $PCS_TYPE
  RICHARDS_FLOW
 $PRIMARY_VARIABLE
  PRESSURE1
 $GEO_TYPE
  LINKED_NODES
 $DIS_TYPE
  LINKED H2OtoPc
#STOP
```

The `LINKED_NODES` directs that the nodes to which this source applies are defined in the '`a.lnk`' file and the `H2OtoPc` identifies a function to use when converting from the value of the shared node to the source term value to apply at the nodes. This function is the only information in the model files for model `a` that relates to model `b` so at this stage the computational scheme implements a very clean interface. At runtime some other information is shared between the models.

[9] Triangular Irregular Network

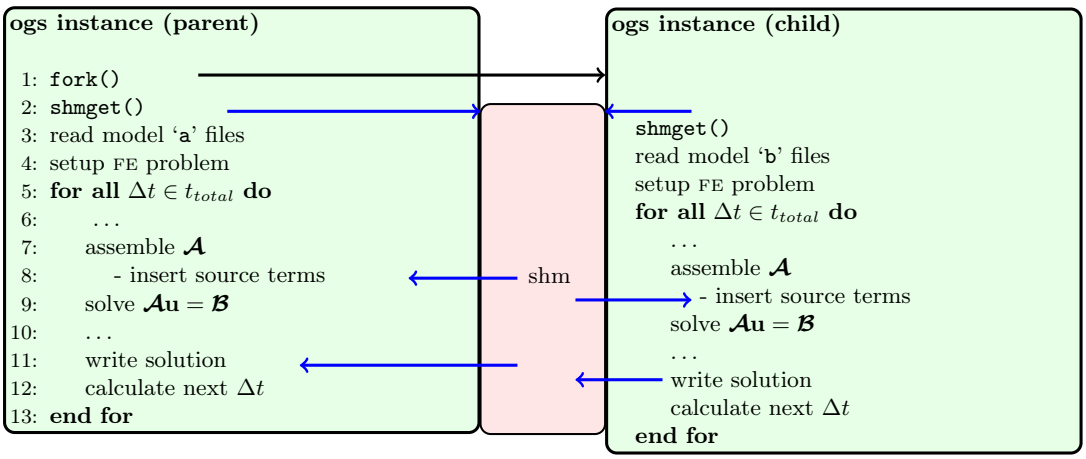


Figure 5.12: Abbreviated excecution scheme of linked models showing separate memory address spaces and interaction via a third — the shared memory segment (labelled *shm*). The call to `fork()` copies the `ogs` process to a separate memory space. The calls to `shmget()` create, or attach to, a shared memory segment. Blue arrows indicate read or write operations depending on direction.

To run the two linked models the model `a` is run in the usual way from the command line:

```
$ ogs a
```

and the name of the linked model, `b`, is hard coded.

### Implementation in OGS

Briefly, when OGS is run it does some initialisation and very soon calls `fork()`. This causes the operating system to make an exact copy of the running OGS process but in a *separate address space*. The two processes are known as the *parent* and *child* respectively and are now totally independent and running concurrently (i.e. in parallel). Each process can tell whether they are the parent or the child by checking their own process id.

The parent loads the '`a.*`' model files and the child loads the '`b.*`' model files.

Each process then requests a *shared memory segment* from the operating system. If it already exists, because the other process got there first, then it connects to it. The shared node data, and some other things, are kept in this shared memory segment. figure 5.12 shows this.

Semaphores are used to control access to this memory segment; when one process accesses the segment the semaphore is locked, and the other waits until it is released[10].

These semaphores also implement the time control for the linked models. The scheme used at the moment is that the parent runs for one time step, though not exceeding the first critical time[11] of the child model. When it comes to incorporating the linked source terms into the system matrix it uses the function specified in the '`.lnk`' file to convert the values it finds there. For the first time step it uses the `initial_value`[12] as the shared node value. Then the child

[10] So, in the main loop the two processes effectively do not run in parallel since one is always waiting for the other.

[11] *Critical time* — A required output time (or, with a patch, a point on a time series boundary condition) may cause times into the time control to force it to 'step on' that particular time.

[12] This `initial_value` must be back calculated from the value that the model would want to end up with, and then applying the inverse of the read function.

runs for one timestep not exceeding the time of the parent. To implement this, obviously the shared memory segment is also used to pass the critical times and the current time.

It was thought that it may be better to have the values of the linked nodes stored as relative humidity so that the rock model converted to and from capillary pressure and the tunnel model converted to and from concentration of water vapour however this would have required twice as many parameter conversions.

#### 3D Richards rock model — prisms

The 3D Richards model with prism elements described in section 5.3.2 was run linked to the tunnel model that also used prism elements (section 5.3.3).

The results in the screenshots figure 5.14 and figure 5.15, show that the linked method works as intended. It is assumed that increasing the number of shared nodes along the length of the tunnel would reduce the instability caused by sudden changes in the node values. The tunnel seemed to be able to cope with the sudden changes but the rock could not. Given the work done investigating different mesh spacings using the 1D Richards model, this was not unexpected of such a coarse mesh.

A problem with the prismatic 3D model is that the elements are the same length at the tunnel wall as they are at the outer boundary (deep in the rock) with the effect that refinement at the tunnel wall causes refinement throughout the rock — increasing runtime.

#### 3D Richards rock model — tetrahedrons

The mesh of the prismatic model was converted to use tetrahedrons by using a more complicated alternative to extruding a surface of triangles in Gmsh. The mesh spacing used is based on that determined for the 1D and 2D radial models. The final mesh of the geometry took a long time to compute and then it was realised that the ensuing size of the FE problem would require a very long runtime or/and parallelisation and so a prudent intermediate step is to make a 2D axial model first.

#### 2D axial Richards rock model

This model (figure 5.13) is expected to provide all the features of a 3D model apart from 3D mechanical response (when added). It will enable the linked behaviour of the tunnel and the rock to be investigated on a much smaller scale than the full 3D models.

The current state of the work is:

- the model has been run using the usual uniform tunnel boundary condition — it takes quite a long time,
- for speed, the mesh has been partitioned into subdomains and appears to run in parallel on 4 compute nodes of adder.geos.ed.ac.uk,
- the corresponding tunnel mesh is almost complete and lacking the correct refinement around the inlet pipe.

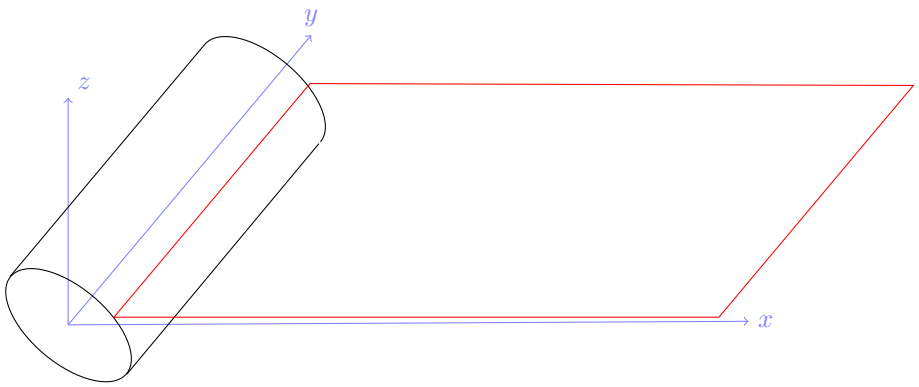


Figure 5.13: 2D axial rock model.

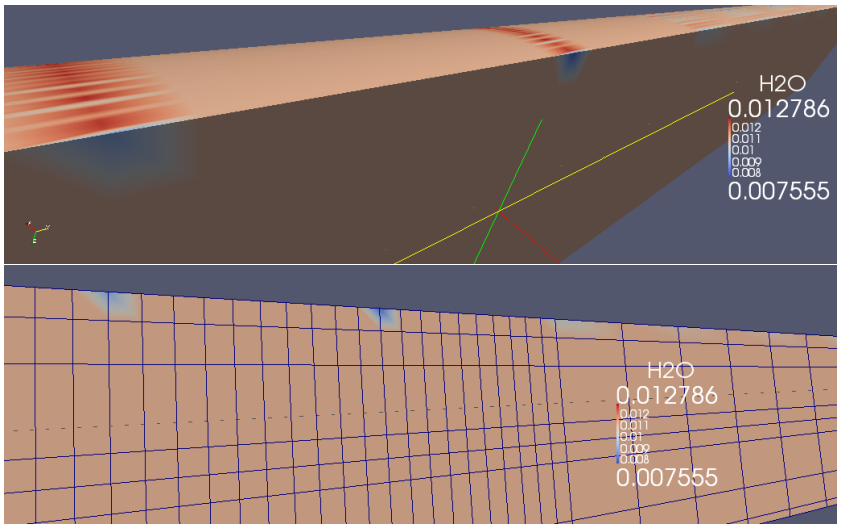


Figure 5.14: Linked 3D tunnel model — closeup views. The top image shows two surfaces: blue on the vertical plane through the tunnel axis, and red on the curved tunnel wall. This shows the tunnel model with prism elements — the smallest is approximately 0.2 m long. The colours are the concentration of a conservative species (water) transported by advection and diffusion in a fluid (air). This model ran for a few seconds of model time but needed a few hours of real time.

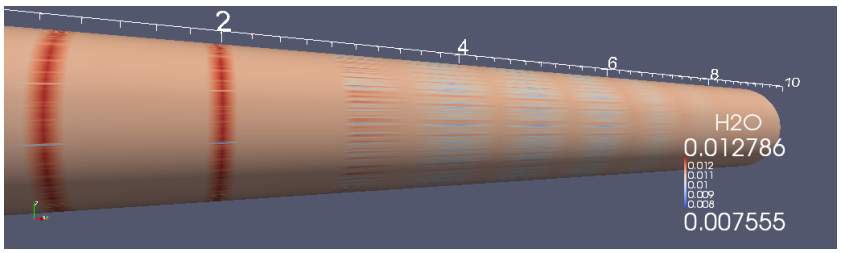


Figure 5.15: Linked 3D tunnel model — overview. The numbers are in metres down the tunnel. The two red lines show higher concentration of water vapour because they are *upstream* of the inlet pipe which is located at 2 m down the tunnel and so only effected by diffusion. The blue areas shown that more dispersion has occurred because advection is acting in these regions.

| Dimension | Domain shape | Domain size | Element type | Process type |
|---|---|---|---|---|
| 3D | cylindrical | 10m | tetrahedrons | H |
| 3D | cylindrical | 4,10,20,60m | tetrahedrons | MPF |
| 2D | circular | 4,10,20,60m | triangles | MPF |
| 1D | linear | 10,60m | line | RF & M |
| 2D | rectangular | 60m | triangles | RF |
| 2D | rectangular | 60m | triangles | RF & M |
| 3D | cuboid | 60m | prisms | RF |
| 3D | cuboid | 60m | tetrahedrons | RF |

(a) Rock models

| Dimension | Domain shape | Element type | Process type |
|---|---|---|---|
| 3D | cylindrical | prisms | GF and mass transport |
| 3D | cylindrical | tetrahedrons | GF and mass transport |
| 2D | rectangular | tetrahedrons | GF and mass transport |

(b) Tunnel models

Table 5.2: Summary of VE models developed. The 'Domain size' is the distance from the tunnel to the outer boundary. (Abbreviations used: H = heat transport, MPF = multiphase flow, RF = Richards flow, M = mechanical deformation, GF = Groundwater flow.). All of them represent the whole tunnel (i.e. 10 m long and 0.65 m radius).

### 5.3.5 Conclusions

Many models have been in use and have shown up limitations, difficulties and simplifications. The most appropriate ones are the Richards' Flow models and there has been rapid progress with these has been since the Step 1 report in spring 2010.

At this point, to fully explore the VE, the following objectives were identified:

- **include the tunnel**, using 2D axial linked models and then 3D tetrahedral linked models,
- **include conservative mass transport** of chloride, with test models then Task A models: 1D, 2D rectangular, 2D axial linked,
- **include mechanical deformation** processes using test models then the Task A models: 1D then 3D tetrahedral linked models, possibly reverting to 2D rectangular then 3D cuboid then 2D axial linked models.

However, the final models of the VE are 1D linear and axisymmetric models with inferred mechanical deformation and conservative mass transport, described next in section 6.1.

Chapter 6

# APPLICATIONS

## 6.1 Modelling the Ventilation Experiment

### 6.1.1 Introduction

The Ventilation Experiment (VE) at Mont Terri is a field experiment investigating the desaturation of the Opalinus Clay during the operational period of the construction of a radioactive waste repository. Groundwater flow is modelled by unsaturated viscous flow (using Richards' Equation) and mass transport processes using the Finite Element Method in OpenGeoSys. Results for this work are presented here for a 1D axisymmetric model and comparison is made with a 1D linear model. An additional 2D model is in development and links to a 2D model of the tunnel. A description of this developing model has been provided in section 5.3.4.

The Steps of Task A are shown in table 6.1. Step 4 was extra for all Task participants. Three physical models are required to achieve these steps; hydrodynamical, mechanical and mass transport models.

Table 6.1: Summary of the Steps of Task A

| Step | Name | Status |
|---|---|---|
| Step 0: | Drying Test | Completed |
| Step 1: | VE Phase 1 | Hydraulics completed, inferred mechanics |
| Step 2: | VE Phase 2 | Completed, inferred mechanics, tunnel attempted |
| Step 3: | Chloride Calculations | Completed |
| Step 4: | Sulphate Calculations | Not attempted |

#### Hydrodynamic model

Decreasing relative humidity in the tunnel causes drying of the rock by evaporation from the tunnel wall. Over time, the drying front progresses into the rock as liquid water is induced to flow towards the tunnel wall, from the deeper rock, by pressure induced viscous liquid flow and vapour diffusion.

Observations indicate the flow of the liquid water through the rock is as through an homogeneous isotropic porous medium, and so may be described using Darcy's Law; the flux being proportional to the pressure gradient through the rock and a permeability constant. By extending this Law to the unsaturated case, this constant is replaced by scaling the intrinsic permeability with a function of saturation.

At the boundary of the rock domain with the tunnel there are three alternative methods in use for representing the boundary condition:

- specifying the capillary pressure as a function of relative humidity in the tunnel
- specifying the evaporation rate (a Neumann type condition), derived from empirical results of evaporation rate with changing relative humidity
- allowing a model of the air flow in the tunnel to determine the boundary condition for the rock, and *vice versa*.

In the context of the repository concept, modelling the third scenario is preferable because the measurements of the driving parameters, air flowing into and out of the tunnel, become the boundary conditions of the problem, rather than using an average of the measured response, as for the first method.

#### Conservative mass transport model

Chloride forms ions in solution with pore water in the rock and is considered conservative in that it does not decay, form compounds with other elements or adsorb to solid material.

Chloride is transported by advection and by molecular diffusion processes. Mass is transported by advection in proportion to the velocity of the solute, and by diffusion proportional to its concentration.

Two effects modify the application of these transport processes, one at the boundary and another in the domain. At the tunnel wall, whereas water vapour can exchange with the air in the tunnel, chloride cannot exist in the gaseous phase and is barred from crossing. During desaturation the chloride concentration progressively increases and during resaturation it is diluted. The second effect arises from various convoluted processes that manifest themselves as a reduction in the porosity available for the transport of chloride. These processes include exclusion of chloride ions from pore spaces that are physically smaller and because of anion exclusion because of the clay's diffuse double layer.

### 6.1.2 Porous media mathematical model

#### The Richards Equation

Groundwater flow through an unsaturated porous medium may be described by Richards' Equation, as derived in section 4.2.4. Writing equation 4.30 here for convenience:

$$C\frac{\partial\psi}{\partial t} - \nabla\cdot(\mathbf{K}\nabla(\psi + z)) = f\,.$$

Assuming the porous medium is homogeneous and isotropic, the hydraulic conductivity tensor $\mathbf{K}$ becomes a scalar K in the three directions of the identity matrix $\mathrm{K} = \mathbf{KI}$. Assuming there are no sources or sinks in the domain and that the divergence of the elevation head is negligible, for example, because the domain is in the horizontal plane, so the component of elevation head is the same everywhere, it becomes:

$$C\frac{\partial\psi}{\partial t} - \nabla\cdot(\mathrm{K}\nabla\psi) = 0 \text{ on } \Omega\,.$$

Assuming that the fluid (water) is isothermal and isopycnic, the equation can be multiplied by $\mu/\rho g$ to replace pressure head with water pressure as the primary variable and so the hydraulic conductivity is replaced by the (scalar) intrinsic permeability:

$$C\frac{\partial \Psi}{\partial t} - \nabla\cdot(\mathrm{k}\nabla\Psi) = 0 \text{ on } \Omega\,.$$

Defining the reference, background pressure in the rock ($p_0$) as 0 Pa, and writing the boundary value problem in terms of the unknown $u :\rightarrow \psi$. Where $\Gamma_1 \cup \Gamma_2$ is a partition of $\partial\Omega$ the boundary conditions of the Ventilation Experiment are:

$$C\frac{\partial u}{\partial t} - \nabla\cdot(\mathrm{k}\nabla u) = 0 \text{ in } \Omega \times t_{stop}\,, \tag{6.1}$$

$$u = u_0(t) \text{ on } \Gamma_0\,, \tag{6.2}$$

$$\frac{\partial u}{\partial n} = 0 \text{ on } \partial\Omega \setminus \Gamma_0\,, \tag{6.3}$$

$$u = u_R \text{ at } t = 0\,. \tag{6.4}$$

The partition $\Gamma_0$ is the tunnel wall and $\partial\Omega \setminus \Gamma_0$ is deep in the rock. The function that $RH \mapsto P_c(t)$ is:

$$u_0(t) = \ln(RH) \times \rho_w \frac{RT}{M_w}\,.$$

Richards' Equation assumes that the gas pressure remains constant at the reference pressure. This assumption implies that, given the capillary pressure relation $P_c = P_{air} - P_{water}$ then $P_{water} = -P_c$. Furthermore, although the gas pressure in the formulation remains constant, vapour is still considered to be mobile and its transport is accounted for by the relative permeability function.

### Discretisation and solving

The Richards Equation is formulated with capillary pressure as the primary variable and discretised in space using the Galerkin Finite Element Method, and in time by finite differences using the Crank-Nicolson weighting scheme. Mass lumping is used the aid stability of the solver. Picard iterations are used for the non linear iterations.

### Mechanical deformation

The mechanical behaviour of the rock may be inferred by post processing the water pressure and saturation results to infer a porosity change from the estimated rock compressibility. In one dimension, the linear displacement of all of the line elements may be calculated over each time step by summing the change in porosity that would have occurred if the rock strain state had achieved equilibrium with the water pressure and saturation conditions by the end of each time step. This calculation progresses as follows:

$$\begin{aligned}
\phi_{(N_i,t)} &= \phi_o \times exp\left[S_{(N_i,t)}\left(P_o - P_{(N_i,t)}\right) + \left(\frac{P_o\beta(1-S)}{\phi}\right)\right],\\
\varepsilon_{(N_i,t)} &= \phi_o\left(\left(\frac{{\phi_{(N_i,t)}}^{1/3}}{\phi_o^{1/3}}\right) - 1\right),\\
\frac{\mathrm{d}\varepsilon}{\mathrm{d}x_e} &= \left(\frac{\varepsilon_{N_i} - \varepsilon_{N_{(i+1)}}}{2}\right)\left(x_{N_{(i+1)}} - x_{N_i}\right),\\
\frac{\Delta s}{\Delta t} &= \sum^{\Omega}\frac{\mathrm{d}\varepsilon}{\mathrm{d}x_e},
\end{aligned}$$

where the subscript $_{(N_i,t)}$ means "at node $i$ and time $t$", $S$ is saturation, $P$ is pressure, $\beta$ is the compressibility [$\mathrm{Pa}^{-1}$], $\varepsilon$ is strain and $\phi_o$ is the initial porosity.

The compressibility is found from the Young's modulus ($Y$), Bulk modulus ($B$) and Poisson's ratio ($v$) in this relation, in 3D:

$$\beta = \frac{1}{B} = \frac{(3 \times (1 - 2 \times v))}{Y}\,. \tag{6.5}$$

The main limitation of this method is that it is a simple postprocessing step and so cannot be coupled with other processes or allow for changes in the stress field.

The calculation is suited to tabulated data and so was implemented directly in the database holding the model results. The database query is given in Appendix B.6.

#### Mass transport

Transport of chloride ions in the liquid phase as a solute is modelled by the conservative mass transport equations. Advection and diffusion of a conservative species in one dimension through an homogeneous and isotropic medium is described by Kolditz and Shao, 2010:

$$\frac{\partial C}{\partial t} + q \cdot \frac{\partial C}{\partial x} = D_{xx} \frac{\partial^2 C}{\partial x^2}$$

where $C$ is the concentration of the species in the solute [$\mathrm{kg\,m^{-3}}$], $q$ is the velocity of the solute through the pores in the x direction [$\mathrm{m\,s^{-1}}$] and $D_{xx}$ is the diffusion coefficient in the x direction [$\mathrm{m^2\,s^{-1}}$].

The chloride accessible porosity is defined to account for the observed discrepancy between concentrations of chloride measured by aqueous extract and measured by squeezing out of pore water. This parameter is usually discussed as being a proportion of the water loss porosity.

### 6.1.3 Model setup parameters boundary conditions

#### Changes from Step 0 parameters

The parameter set used in the final calibration for the Step 0 report (A. Bond, C. McDermott, et al., 2009) was used as a starting point. Subsequently the intrinsic permeability was changed to fit the mass balance estimation, and this became the base case against which sensitivity analyses were carried out, but no other parameters were changed substantially. Final material properties are given in table 6.6 where the chloride porosity given is the ratio of chloride porosity to water loss porosity.

#### Relative permeability function

For converting between volumetric water content and saturation equation 6.6 is used, with notation and parameter values defined below in table 6.2. Throughout the modelling, the rock remained saturated at depths greater than 14.8 m.

$$\theta = \frac{\phi S \times 1000}{\rho_{dry}} \times 100 \tag{6.6}$$

Table 6.2: Rock properties

| Parameter | Value | Units | Symbol | Source |
|---|---|---|---|---|
| porosity | 0.19 | - | $n$ | A. Bond, C. McDermott, et al. (2009) |
| bulk density | 2707 | $km^3$ | $\rho_{dry}$ | Fernández et al. (2007, p. 27) |
| water content, saturated | 8.67 | % | $\theta_s$ | equation 6.6 |
| water content, residual | 0.007 | % | $\theta_r$ | estimate |

Table 6.3: van Genuchten parameters

| Parameter | Value | Units | Source |
|---|---|---|---|
| $\alpha$ | 0.6 | - | Genuchten (1980) |
| $n$ | 2.5 | - | Genuchten (1980) |
| $m$ | 0.6 | - | $:= 1 - 1/n$ |

The van Genuchten equations use the water content rather than saturation, and so the porosity is needed in the calculation. A porosity of 0.19 was used and other parameters values of the van Genuchten function (equation 4.9) are shown in table 6.3.

The resulting curve used to determine relative permeability from saturation is shown in figure 6.1. Points on this curve were entered directly into an OpenGeoSys input file.

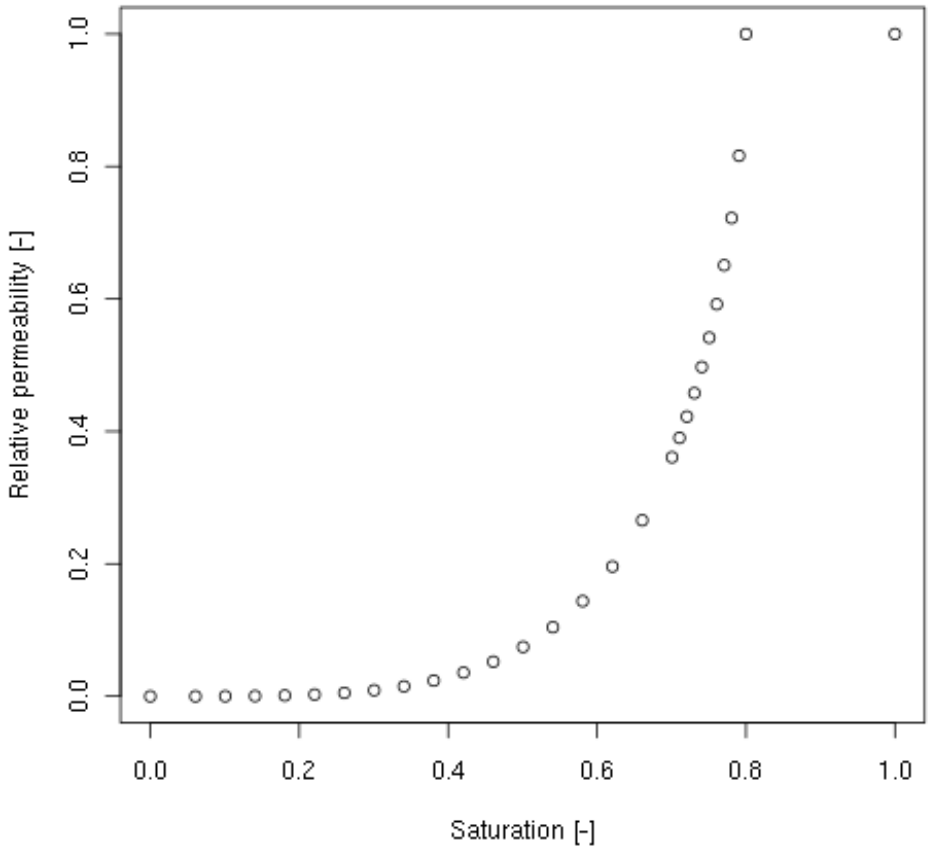


Figure 6.1: Relative permeability against saturation, following the van Genuchten method. A porosity of 0.19 was used to convert between volumetric water content and saturation.

### Boundary conditions

The boundary condition of the rock domain at the tunnel wall is modelled as being capillary pressure as a function of (an average value of) relative humidity of the tunnel air (i.e. using equation 4.6). Since relative humidity is a ratio of physical properties, the geometric mean is used. Gauges RH-HyV-In, RH-HyV-Out, TS-RH1, TS-RH2 are assumed to be representative of the RH in the tunnel. The resulting time series plot is noisy and so the 20 day rolling mean is taken with a forward aligned window, so that sensors lag events rather than predicting them; figure 6.2.

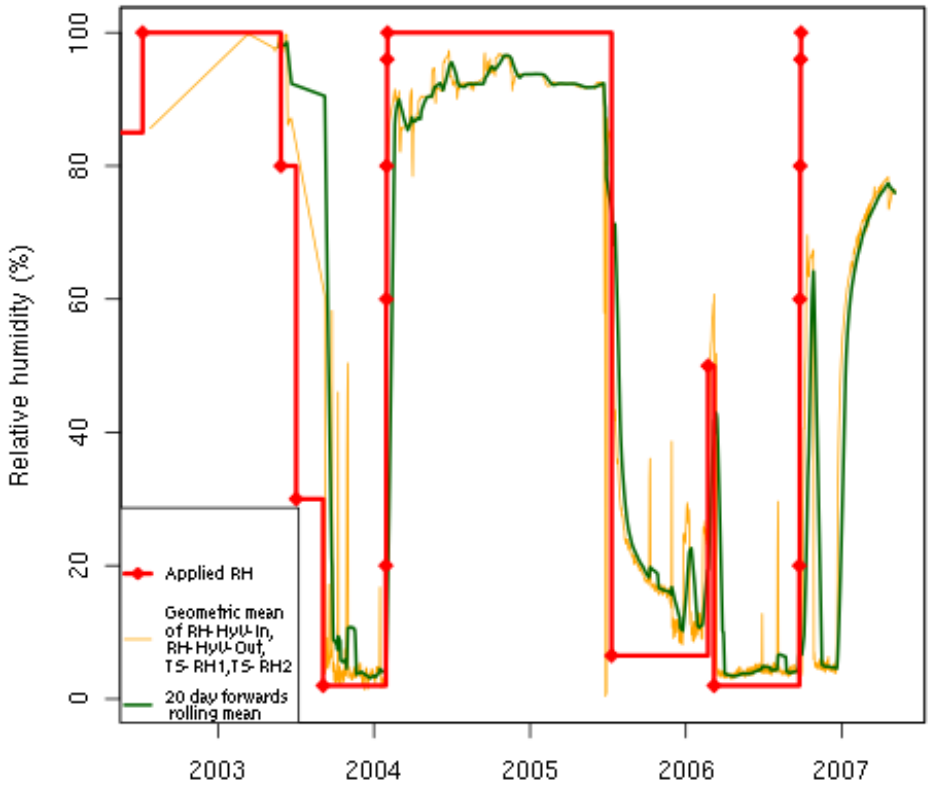


Figure 6.2: Applied relative humidity and selected gauges

Selecting enough points (fifty seven) to adequately capture the shape along the smoothed time series and drawing straight lines between them results in figure 6.3. The application of the psychrometric equation (equation 4.6) results in the capillary pressure boundary condition.

According to the conceptual model, a Neumann type boundary condition would be used to set the mass flux of chloride across the tunnel wall to zero (i.e. $dC/dx = 0$ ). This is expanded in section 6.1.4.

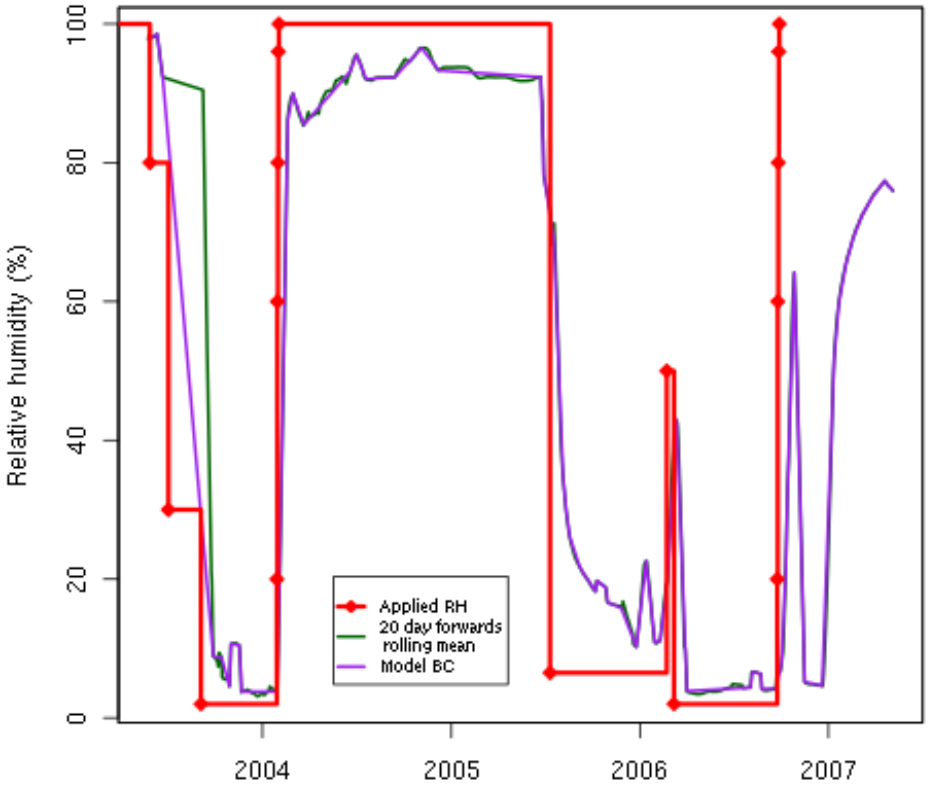


Figure 6.3: Tunnel wall boundary condition. Points are chosen along the rolling mean to become the boundary condition.

### Tables of parameters

The initial conditions, boundary conditions, material properties and output requirements are shown in table 6.4, table 6.5, table 6.6, table 6.7a.

Table 6.4: Initial conditions of the ventilation experiment model.

| Parameter | Value | Units | Source |
|---|---|---|---|
| chloride concentration | 6.05 | $km^3$ | Fernández et al. (2007) |
| saturation (water) | 1 | - | |
| pressure (water) | 1.85 | MPa | |

Table 6.5: Boundary conditions of the ventilation experiment model.

| Parameter | Location | f(t) | Value | Unit | Source |
|---|---|---|---|---|---|
| chloride mass | Deep rock | constant | 6.05 | $km^3$ | Fernández et al. (2007) |
| chloride mass | Tunnel wall | varies | 1 | - | |
| saturation | Deep rock | constant | 1 | - | |
| capillary pressure | Tunnel wall | varies | Eqn. 4.6 | Pa | Muñoz et al. (2003) |

Table 6.6: Material properties of the ventilation experiment model.

| Property | Value | Units | Symbol | Source |
|---|---|---|---|---|
| porosity | 0.19 | unitless | $\phi$ | Step 0, A. Bond, C. McDermott, et al. (2009) |
| intrinsic permeability | $6 \times 10^{-20}$ | $m^2$ | K | Calibrated |
| compressibility | $3.33 \times 10^{-6}$ | $Pa^{-1}$ | $\beta$ | Steps 2&3, A. Bond (2011) |
| dry grain density | 2700 | $km^3$ | | Fernández et al. (2007) |
| Young's modulus | 1 | GPa | $Y$ | Equation 6.5 |
| suction curve | | | | Muñoz et al. (2003) |
| diffusion coeff. of $Cl^-$ in free water | $2.03 \times 10^{-9}$ | $m^2\,s^{-1}$ | $D_w$ | Boudreau (1997) |
| chloride porosity | 0.56 | unitless | $n_{cl}/n$ | Fernández et al. (2007) |

| Time since start [days] |
|---|
| 1548 |
| 1571 |
| 1875 |
| 1974 |
| 2118 |
| 2579 |
| 2876 |
| 2890 |
| 3100 |

(a)

| Physical parameters |
|---|
| water balance |
| relative humidity |
| water pressure |
| water content |
| radial displacement |

(b)

Table 6.7: Required output times (a) and physical parameters (b) for the models for comparing results with other teams.

### 6.1.4 Implementation

#### OpenGeoSys

The model was implemented using OpenGeoSys. Several minor modifications were made to the source code for the purposes of usability, correction and output formatting. More involved modifications were made to implement the correct handling of chloride at the tunnel wall. Model

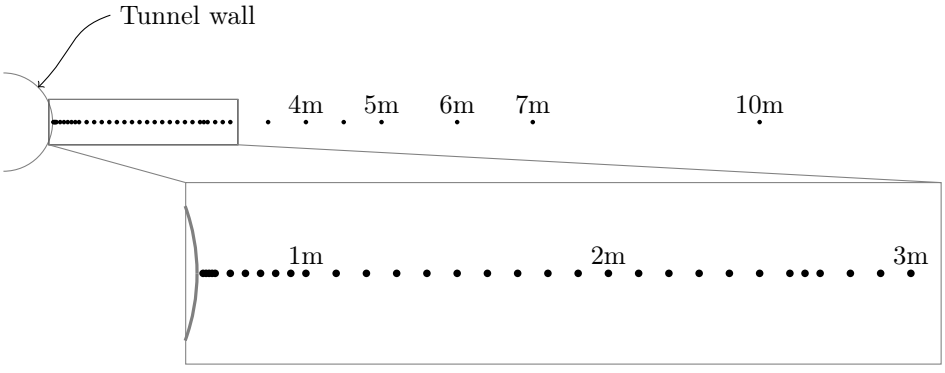


Figure 6.4: Observation points at which model results are required for comparison with other teams. Distances given at selected points are in metres from the centre of the tunnel (of radius 0.65 m). There are forty points in all and they are concentrated within the first 2.35 m of the rock.

results were imported into a PostgreSQL database for postprocessing. Analysis of results was done in a reproducible way and captured in a plain text file.

Relative permeability functions may be specified in OpenGeoSys either as an option or explicitly as points of saturation and relative permeability. The second option is simpler and more flexible and the saturation must be derived from the volumetric water content, which requires the porosity of the medium. When the porosity is changed, e.g. during sensitivity analysis, the retention curve must be recalculated and re-inserted into OpenGeoSys.

In order to implement the boundary to chloride at the tunnel wall, rather than intervening in the finite element assembly of the advection term, the mass was allowed to be transported out and was then added back in again via a source term in the next time step.

The source code can be found in Appendix B.2.

### Models developed

Various models have been developed using different shapes, number of dimensions, element types, domain sizes and axes orientations. A multiphase flow formulation has also been investigated. These unsuccessful models are described in section 5.3.

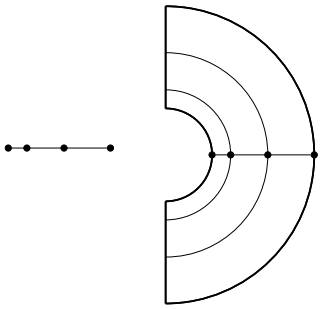

Figure 6.5: 1D model domain and mesh of line elements (left), and the axisymmetric variant (right) showing the increased element volumes associated with the line elements.

However, the main assumption of the conceptual model constrains the relevance of any results; that the boundary condition at the tunnel wall is prescribed as capillary pressure. Given this constraint, a 2D model was developed in the radial plane (figure 5.7) and subsequently, it was found that a 1D Richards' Flow model produces very similar results with the benefits of a shorter runtime and lower overall complexity. The basic 1D model used line elements and was subsequently converted to be an axisymmetric model that allows for increased volume with radius, as shown in figure 6.5.

All that was required to convert a 1D model to an axisymmetric model was to add the OpenGeoSys keyword `'AXISYMMETRY'` to the mesh file.

The 1D domain represents a horizontal portion of rock from the tunnel wall out to a distance (or depth) of 65 m. The finite element mesh is comprised of 297 line elements with lengths ranging from 1 mm to 1.2 m. Most elements are concentrated within the first 2 m of the tunnel wall (figure 6.6, figure 6.6). This simple model takes about 10 seconds to run.

The model files for use with OpenGeoSys can be found in Appendix B.1.

A start was made on reproducing the model using FEniCS (Logg et al., 2012). The model files for use with FEniCS can be found in Appendix B.7.

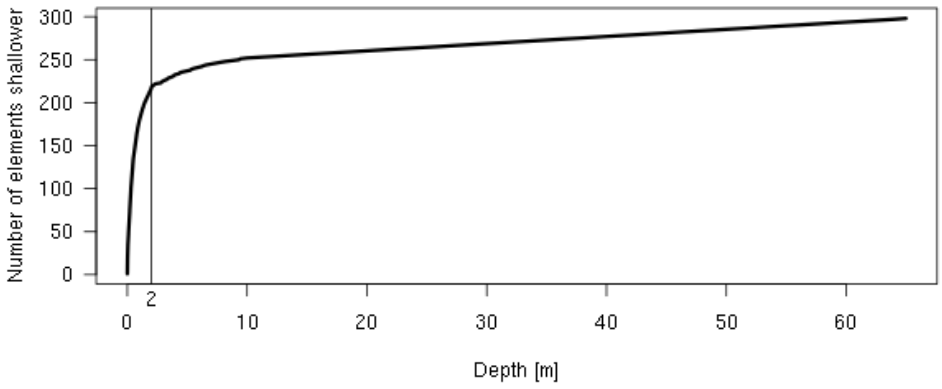


Figure 6.6: 1D mesh spacing. Most elements are within 2m of the tunnel wall.

### 6.1.5 Results

#### Relative humidity

Conversion from capillary pressure is by equation 4.6. There are sixteen gauges measuring relative humidity in the rock, five of these show responses that look as if they could be used in assessing the model results. Three of the five show time series that are very irregular and may not yield useful information after significant cleaning and interpretation. So there are only two remaining gauges (`HC-SB1`, `HC-SB2`) that are immediately useful and these are attached to the tunnel walls at a depth of one or two centimetres.

In the model the relative humidity profile is not sensitive to different porosities as shown in figure 6.8. It is however sensitive to small changes in depth; figure 6.9 shows comparison with rock 3 cm deeper than the true location of the gauge.

#### Water mass balance

The sensitivity of the model to varying porosity and intrinsic permeability was investigated and compared with the water mass balance calculated across the inlet and outlet of the tunnel.

Potential targets for comparison of mass balance results are shown on figure 6.10; there are three main curves, and two shorter lines. The question of with which curve it is most appropriate to compare results is discussed in section 6.1.6, the conclusion of which is that the blue line labelled "Qout:=Qin" and the two shorter lines labelled "RH-HyCnt-L" and "RH-HyCnt-R" will be considered in this section.

The porosity of 0.19 determined for the Drying Test (Step 0), shows a better fit to the water mass balance results (see Figures 6.11 and 6.12) than the lower porosities. The earlier part of the main desaturation event fits the results better than at later times.

Intrinsic permeability (shown in figure 6.13) is much less influential than porosity is.

#### Water content

The water contents of samples taken from boreholes before and after the second desaturation period by Traber (2004) and Fernández et al. (2007) are assessed against model results in

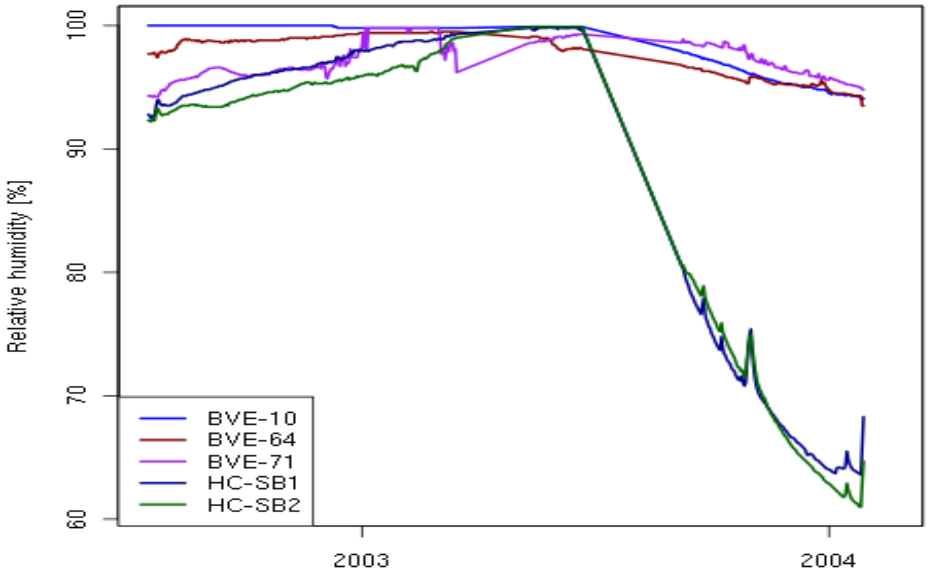


Figure 6.7: Available relative humidity results for the VE. Gauges `HC-SB1` and `HC-SB2` are very shallow.

figure 6.15 and figure 6.16 respectively. In both cases the water contents determined in the laboratory have been recalculated according to the porosity of the base case model (i.e. 0.19).

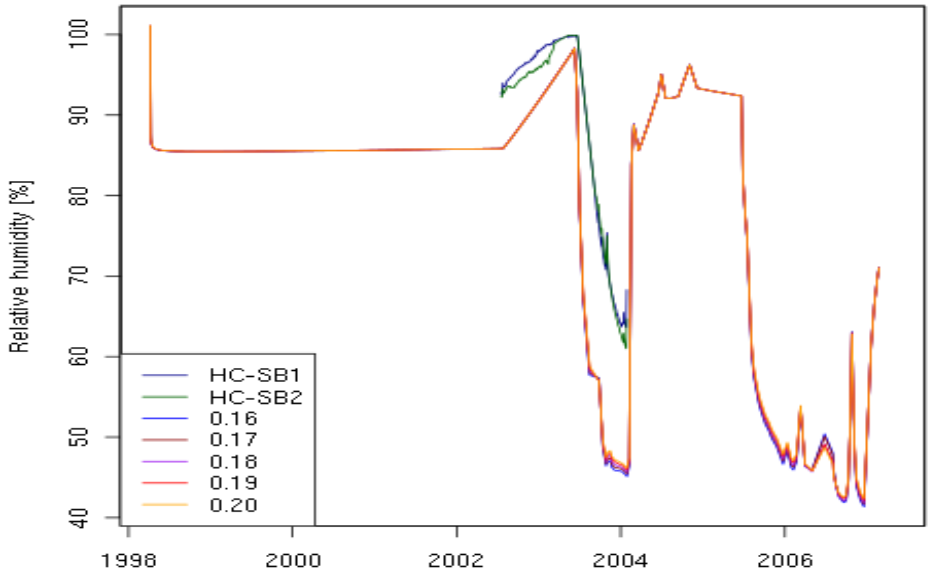


Figure 6.8: Sensitivity of relative humidity to variation in porosity, in comparison with VE gauges `HC-SB1` and `HC-SB2`.

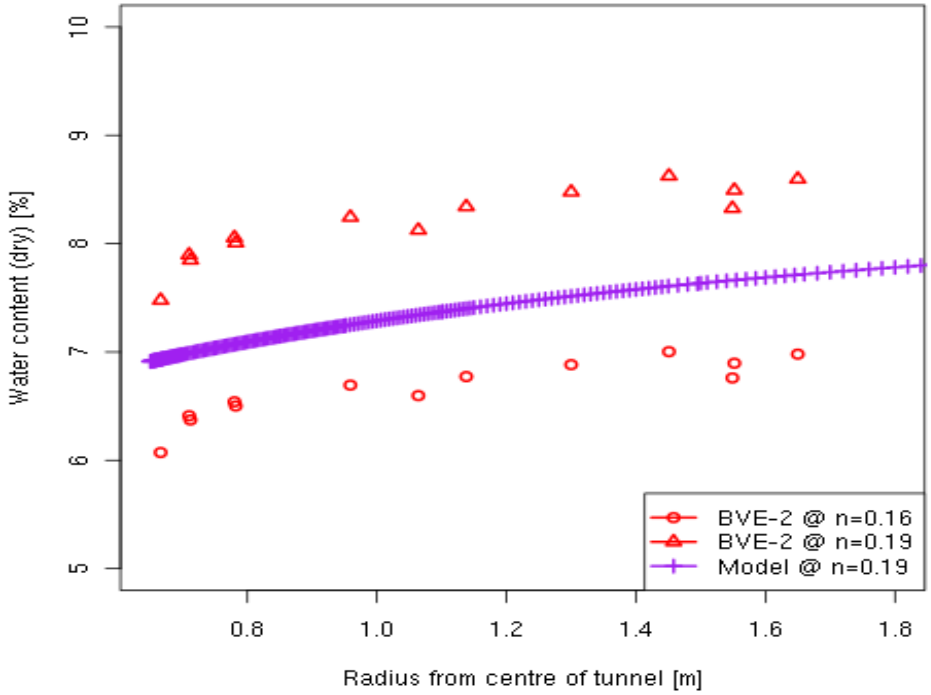


Figure 6.15: 'Initial' water content: at 2002-07-05.

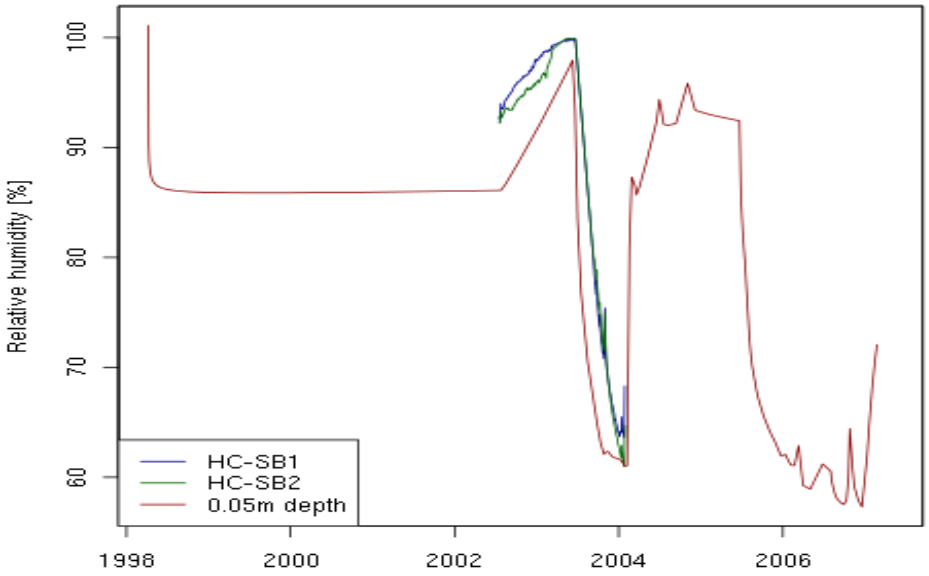


Figure 6.9: Relative humidity fit sensitivity with depth.

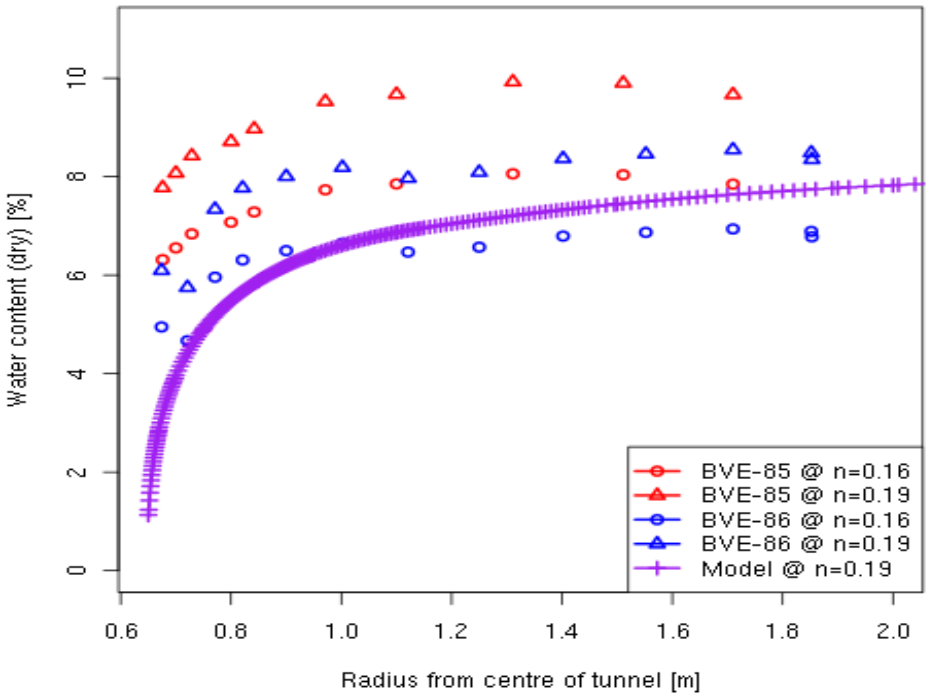


Figure 6.16: 'Final' water content: at 2004-01-26.

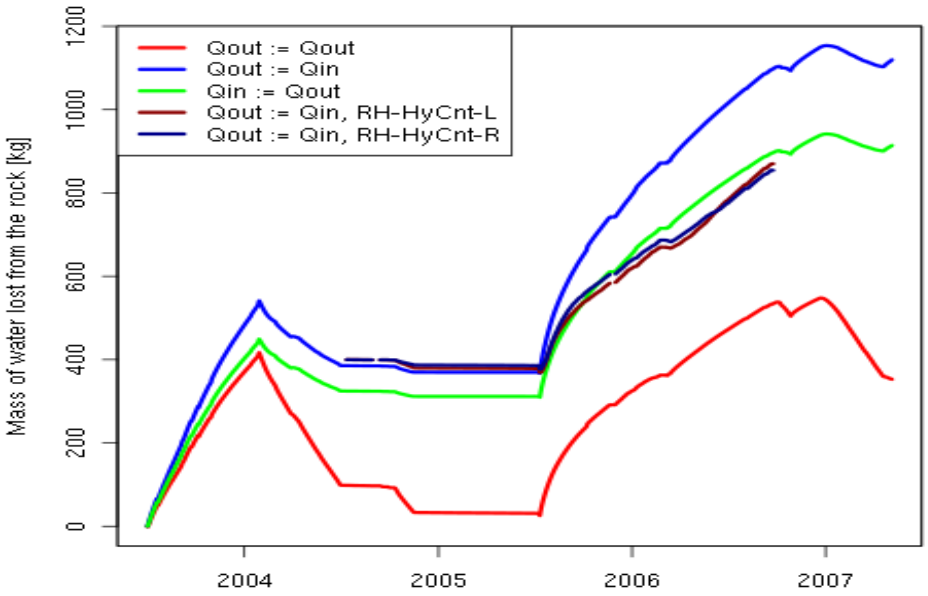


Figure 6.10: Comparison of mass balance calculations. The new lines have been shifted up to allow for easy comparison with the other lines.

### Water pressure

As part of the VE there are twenty eight gauges measuring water pressure, to a maximum depth of 2.13 m. The model becomes unsaturated beyond this depth by the time the VE results commence. Since $P_{water} = -P_c$, the model results are typically greater than 5 MPa, but the VE results are less than 0.9 MPa.

The VE water pressure results contain one group of ten gauges that show prominent peaks at 2002-11-05 (see figure 6.17). The ratios of the peaks to the values just before the peaks falls into two groups: either around eight times larger than the previous value, or less than four times. This correlates with radius from the centre of the tunnel, the division between the two groups being between 2.05 m and 2.15 m radius (i.e. 1.4 m to 1.5 m depth). The cause of the difference is not known.

### Mechanical deformation

Overall, the modelled mechanical response of the rock shows an averaging effect inherent in the mathematical method used. The response has a particularly good fit to the sensor in borehole `BVE-28`. The agreement is best with the subhorizontal holes (i.e. in cylindrical coordinates, with a phi of around 90° or 270°) listed in table 6.8 and a less good agreement with those at steeper angles from the horizontal.

The 1D model using linear elements showed an under response similar to that seen in the mass balance graphs due to the over simplified geometry of the 1D model.

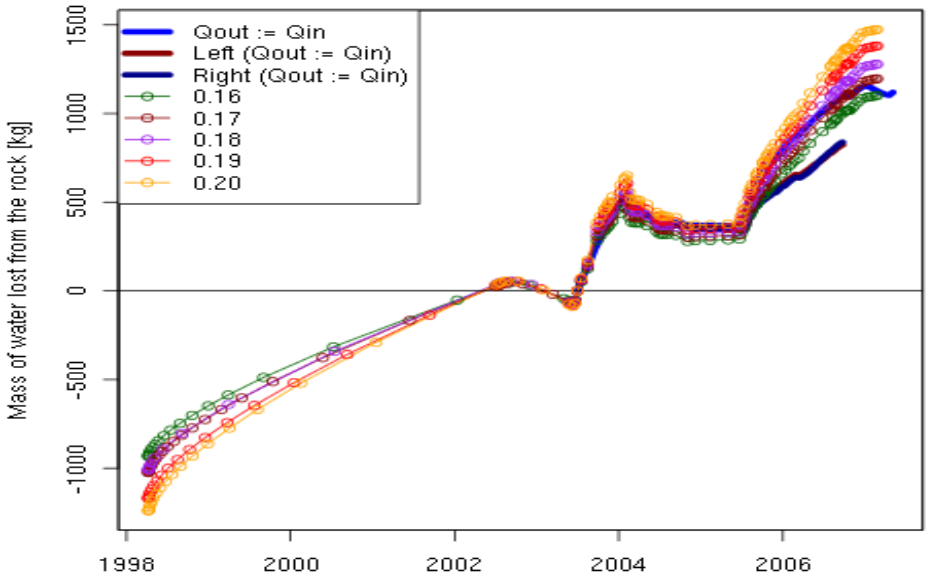


Figure 6.11: Sensitivity of water mass balance to porosity over the whole model time.

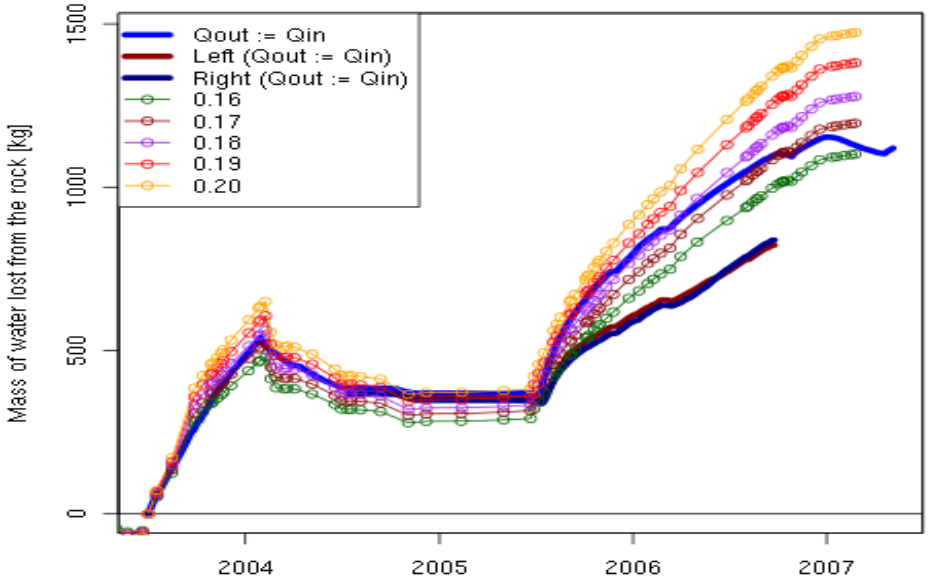


Figure 6.12: Sensitivity of water mass balance to porosity, during the VE.

### Chloride content

Modelled chloride results are in good agreement with the laboratory test results when presented as mass of chloride per mass of wet rock (Figure 6.19 to Figure 6.22).

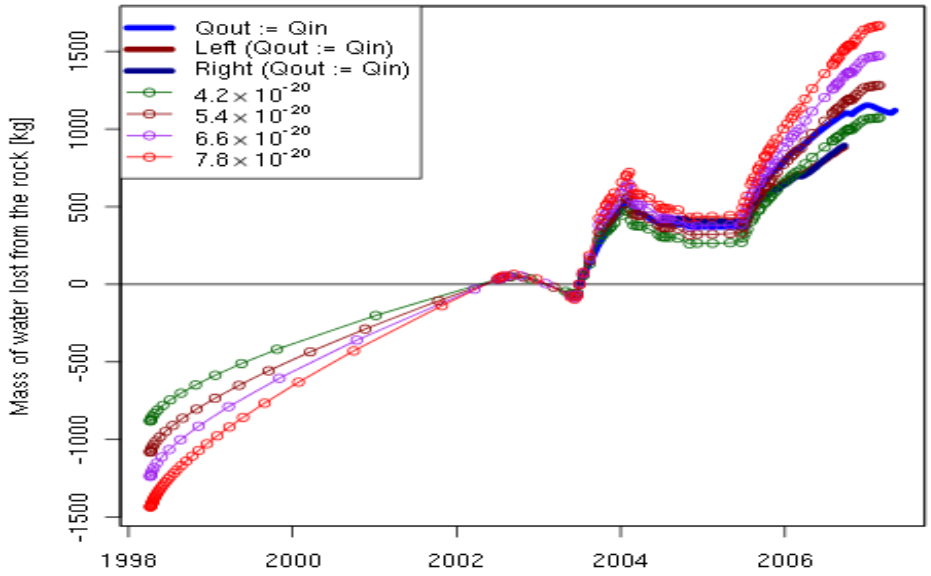


Figure 6.13: Sensitivity of water mass balance to intrinsic permeability ($m^2$) over the whole model time.

Table 6.8: Boreholes whose sensors are in good agreement with the mechanical response of the VE. Rho is radius from the centre of the tunnel, z is distance down the tunnel, phi is angle from horizontal.

| Borehole | rho [m] | phi [°] | z [m] |
|---|---|---|---|
| BVE-47 | 2.65 | 100 | 4.4 |
| BVE-49 | 2.65 | 260 | 4.4 |
| BVE-26 | 2.65 | 100 | 6.85 |
| BVE-28 | 2.65 | 260 | 6.85 |

### 6.1.6 Discussion

#### Water mass balance

Assessing model performance by comparison with a quantity that is cumulative in time, as is done here with the water mass balance, allows the possibility that the accuracy of later model behaviour may be obfuscated by earlier assumptions in calculating the target quantity. That is to say, assumptions made at certain times are also cumulative.

A mass balance calculation for the water in the rock and the tunnel was provided to all teams by the Task A organiser. There are several uncertainties inherent in it.

The main issue is the availability of continuous data at individual gauges at the air inlet and outlet of the tunnel. figure 6.23 shows that measurement of the outflow rate is available after the first drying phase (mid-2003) and then only for three and a half months. The corresponding RH measurement at the outlet (labelled 'RH out') is missing for half of this time.

Another uncertainty is that the calculation is based on averaged time series data though the calculation that produced these averages is not included and could be significant. For example,

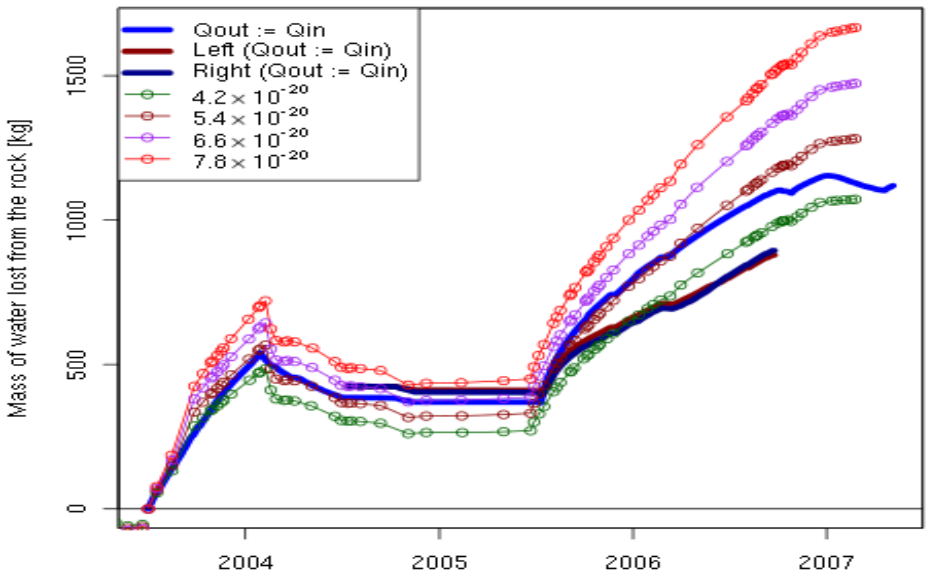


Figure 6.14: Sensitivity of water mass balance to intrinsic permeability (m{2}) during the VE.

from 2005-06-24 to 2005-11-28, the reported values for relative humidity at `RH-HyV-In`, appears to be the voltage of the battery multiplied by minus ten. It is not explicit whether this data is included in the mass balance or not.

The common way of assessing the flow rate in the tunnel is to accept that the outflow measurement is accurate, and that therefore air must be leaking, and that the leakage rate is constant after the last datum and for the remaining duration of the VE. To calculate the mass balance, a further assumption must then be made about what the RH of that leaking air may have been, based on where the leak may have been occurring. The mass balance can then be represented as three curves bounding the possible behaviour; depending on whether the outflow rate 1) is set to the inflow rate, or 2) set to a function of the outflow rate observed at earlier times, or 3) left uncorrected.

Given the data coverage described above, interpretation number 1) is thought to be the best option of the three although it still relies on the supplied averaged RH. In order to estimate the remaining uncertainty another estimation of the water mass balance is required.

Here we calculate a mass balance from the available data for comparison with the curve of option 1) using two RH gauges (`RH-HyCnt-L` and `RH-HyCnt-R`) located half way down the tunnel. The only additional assumptions made here are that:

- the first half of the tunnel will lose/gain as much water as the second half of the tunnel
- the rate of air flow at the outlet is the same as that measured at the inlet

The main difference in the mass balance calculated above in figure 6.24 is that no attempt has been made here to combine data from different gauges in order to fill missing values and so Phase 1 is not represented. This could be done to some extent, and would be necessary for comparison with other teams, but it is felt that the Phase 2 curve is informative enough

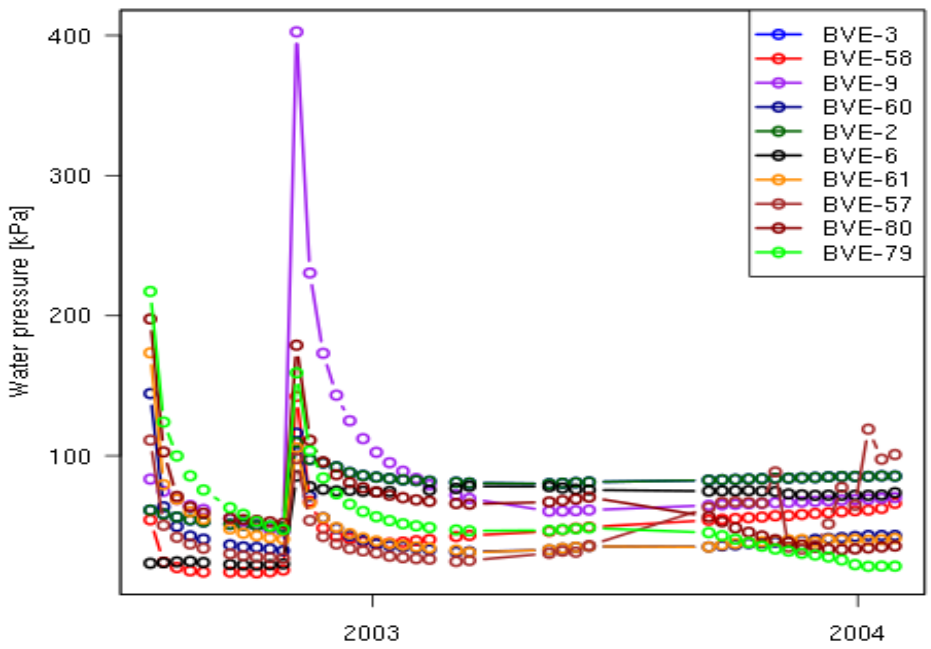


Figure 6.17: Water pressure VE results for gauges that show peaks

for the current purposes. The two new cumulative mass balance curves in the bottom plot in figure 6.24 are continuous, apart from the small isolated segments in late 2003 that are discarded henceforth, and so the *shape* is valid for use as a target for comparison with the model results.

Comparing the new and established mass balance calculations on one plot (figure 6.25 and figure 6.26) it can be seen that, in comparison with Qout:=Qin, less mass is lost according to the new calculation (the curve is positioned lower) and the rate of mass lost during the second desaturation period is also less (the curve is less steep).

It is now valid to assess the model results against this new mass balance. figure 6.27 shows the 1D model and shows less agreement than with any of the other curves because they have been calibrated for permeability and porosity against the other curves.

However, if the relative permeability curve is replaced with the one in figure 6.28, then the modelled and experimental results are in much better agreement as seen in figure 6.29, especially for higher porosities. In fact, this model uses exactly the same relative permeability curve and material properties as Step 0 (the Drying Test). The model does not continue steeply enough at later times and most of this is attributable to the 1D geometry; the axisymmetric model fits better over the same period (discussed later in section 6.1.6).

The effect of the steep drop off in relative permeability below saturations of about 0.8 is that the rock desaturates easily until below 0.8, but then ingress of water is much more difficult and does not penetrate to the full depth of the desaturation zone before the next desaturation period. This isolates a zone of rock near the tunnel that participates in the subsequent desaturation phase. The size of this isolated block determines the volume of water it can supply.

It is difficult to assess the precision of either of the mass balance estimations discussed above.

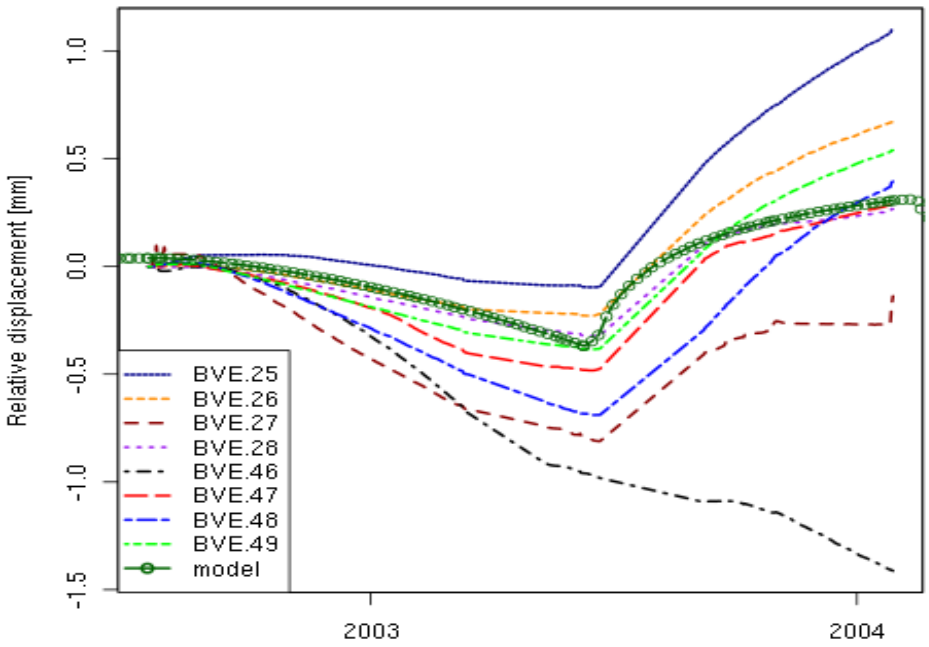


Figure 6.18: Mechanical deformation targets and model results. The model results show good agreement with BVE-47.

Error bars on the target plots would constrain the calibration.

The overall impression is that it is difficult to disentangle the influence of the relative permeability curve from the material properties and the geometry of the flow regime given the variation in mass balance targets. However, two interesting features that would help in the discrimination are that:

- the main effect of changing the relative permeability curve is the change in the size of the step down during the second desaturation period, and
- the main effect of changing the material property values is seen in the second resaturation curve.

This suggests that in future experiments a greater model sensitivity to variation in material properties, and therefore a greater resolution in calibration, may be achieved for *oscillating problems*, assuming the parameters of the relative permeability curve are well known.

If investigating anisotropy, it would be interesting to assume that the new curves are only representative of the second half of the tunnel and thereby calculate what the mass lost from the first half of the tunnel would need to be in order to arrive at the same "Qout:=Qin" curve.

### Domain geometry effects

As mentioned earlier, many different geometries and models have been attempted. It is typically not straightforward to directly compare and contrast between them, not least because many

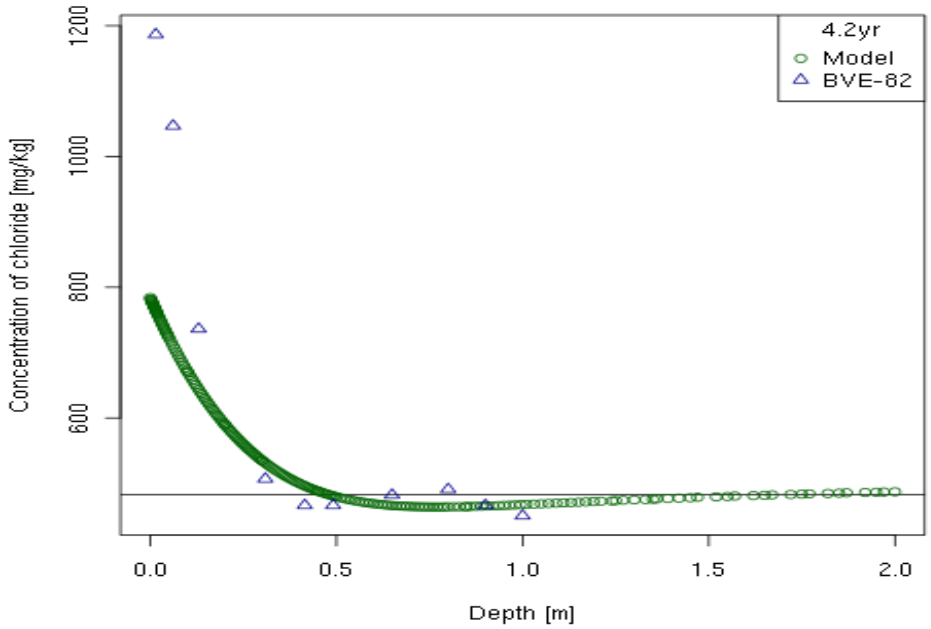


Figure 6.19: Chloride concentration: at 4.2 years.

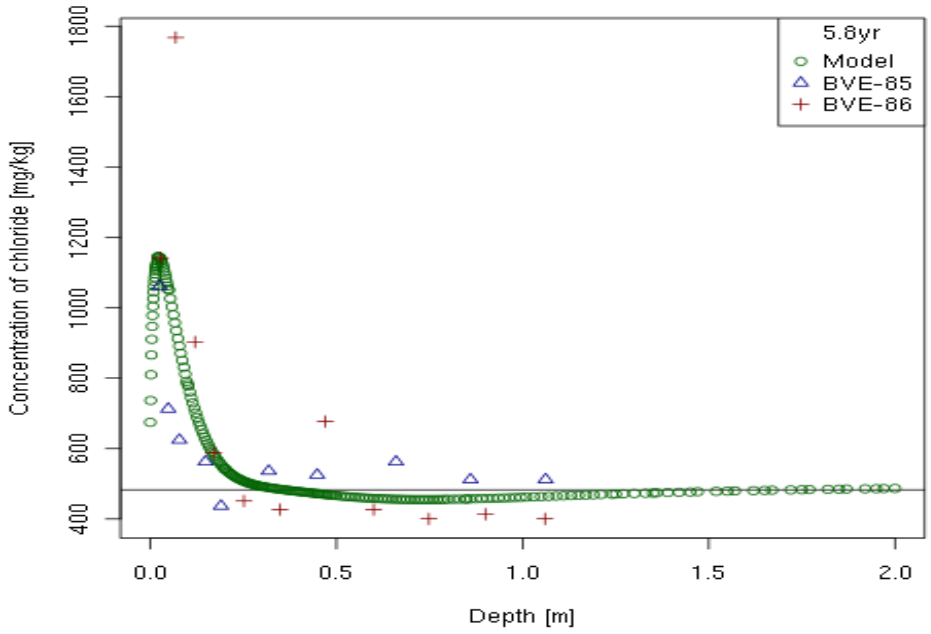


Figure 6.20: Chloride concentration: at 5.8 years.

have not been completely successful. However there are two that are readily comparable. A 1D model with line elements was later modified to be axisymmetric around the tunnel; each line element came to represent the rock between two radii rather than depths. This axisymmetric model is presented as the 'base case' in this thesis.

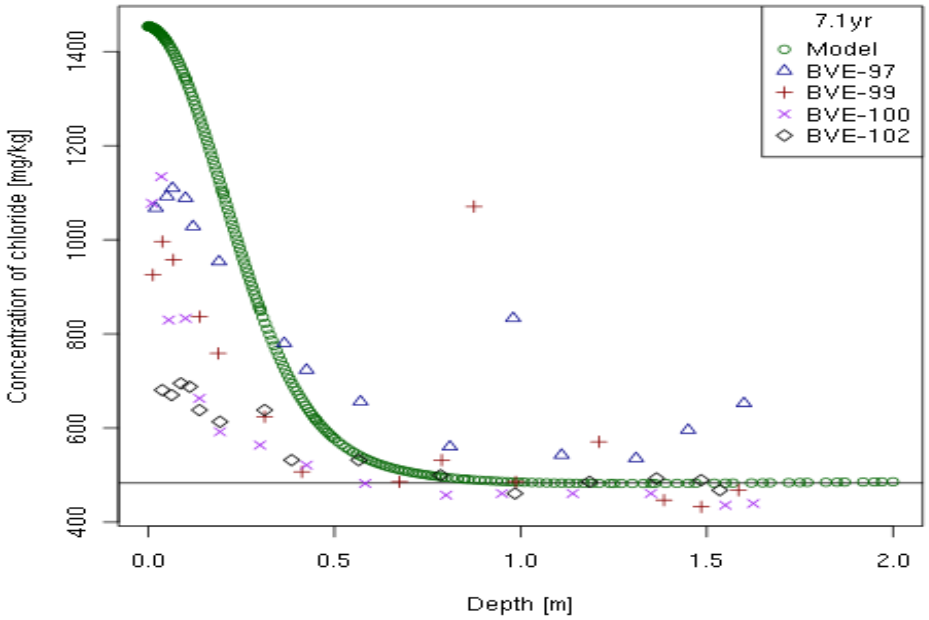


Figure 6.21: Chloride concentration: at 7.1 years.

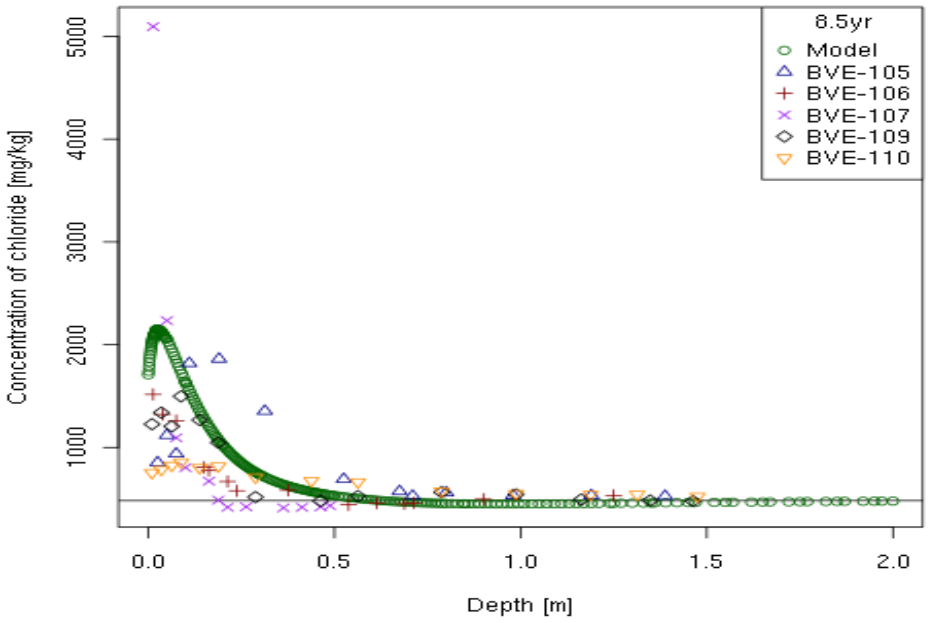


Figure 6.22: Chloride concentration: at 8.5 years.

A basic comparison between the two (figure 6.31) shows that the simple 1D geometry in general under represents water flux, because it under represents the area of rock perpendicular to the radial direction through which flow occurs towards, and away from, the tunnel wall.

The very last desaturation event shown on "Qout:=Qin", in 2007, is fitted better by the

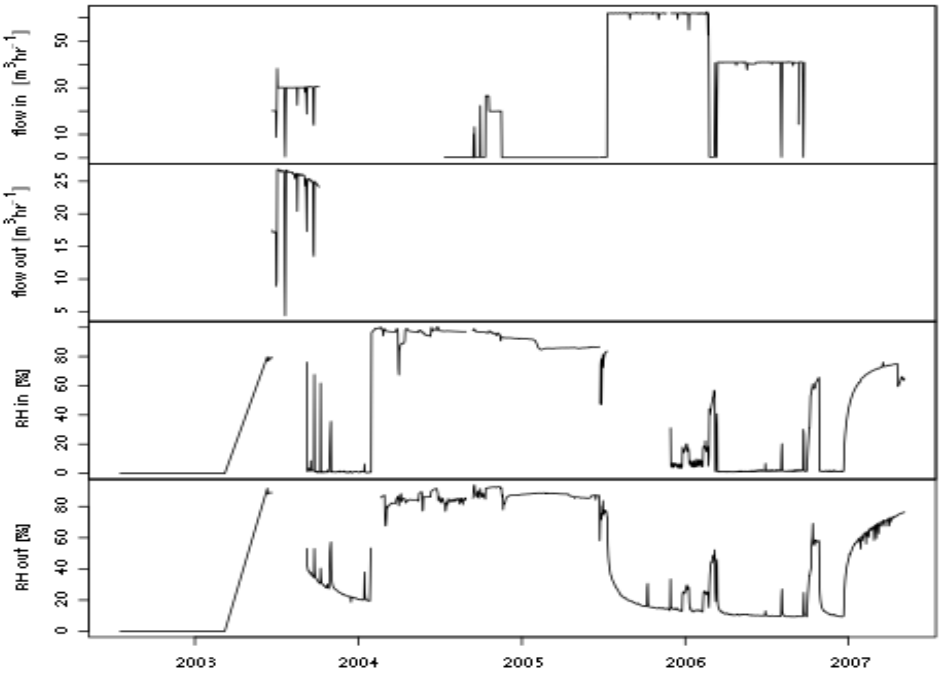


Figure 6.23: Data availability for water mass flux calculation at the inlet and outlet of the tunnel.

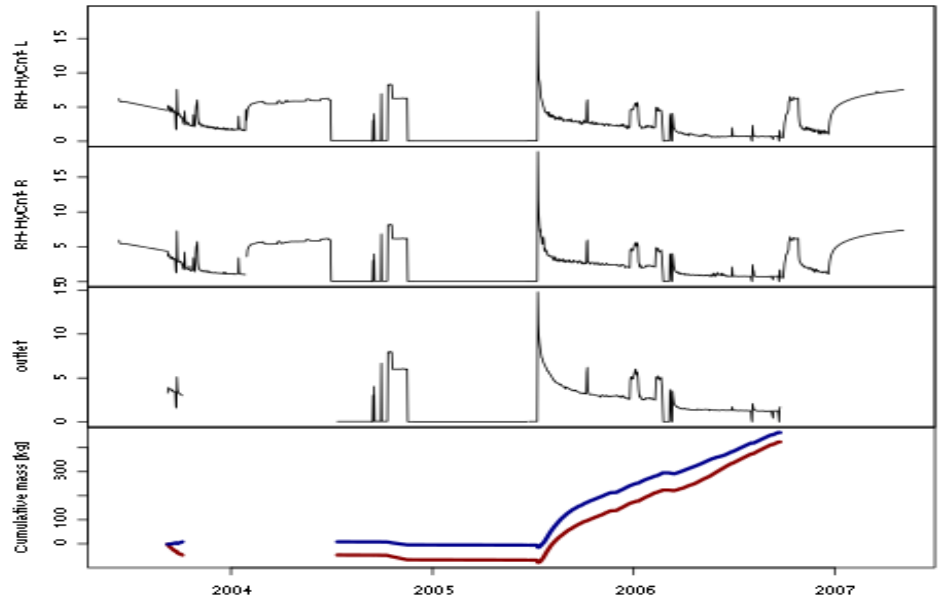


Figure 6.24: Water mass flux in the VE. The top three plots show the mass flux in (kg day$^{-1}$) at two gauges halfway down the tunnel (RH-HyCnt-L and RH-HyCnt-R) and at the outlet. The bottom plot shows the cumulative mass balance of water for the whole tunnel using gauges RH-HyCnt-L (red) and RH-HyCnt-R (blue).

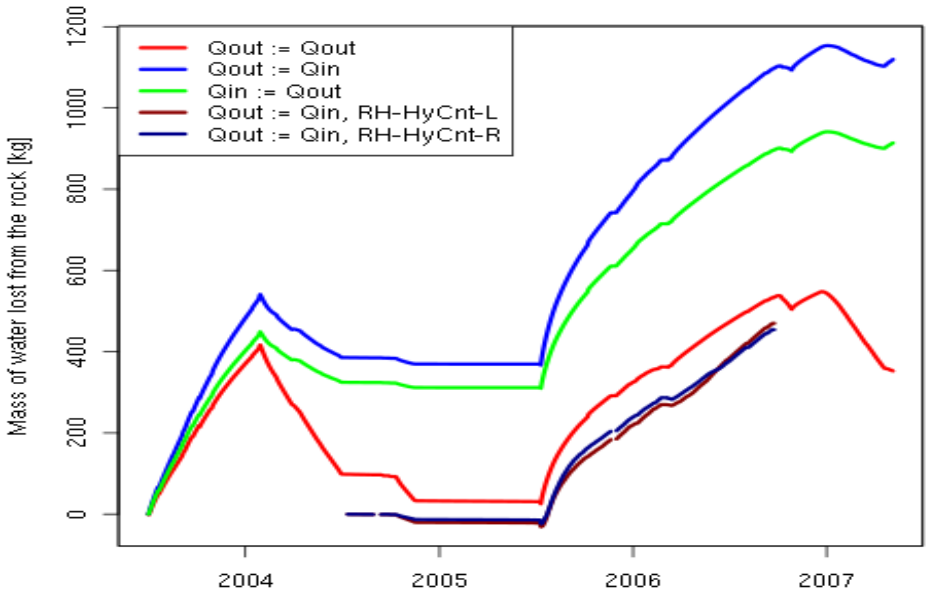


Figure 6.25: Comparison of mass balance calculations and model results. The two lower lines could be shifted up to allow for missing data around 2004.

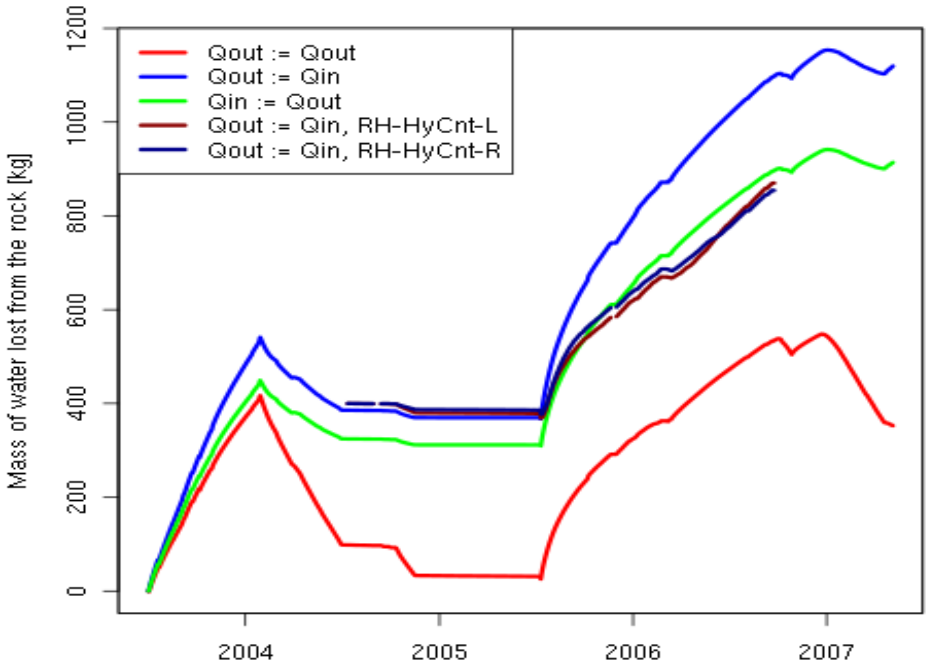


Figure 6.26: Comparison of mass balance calculations. The new lines have been shifted up to allow for easy comparison with the other lines.

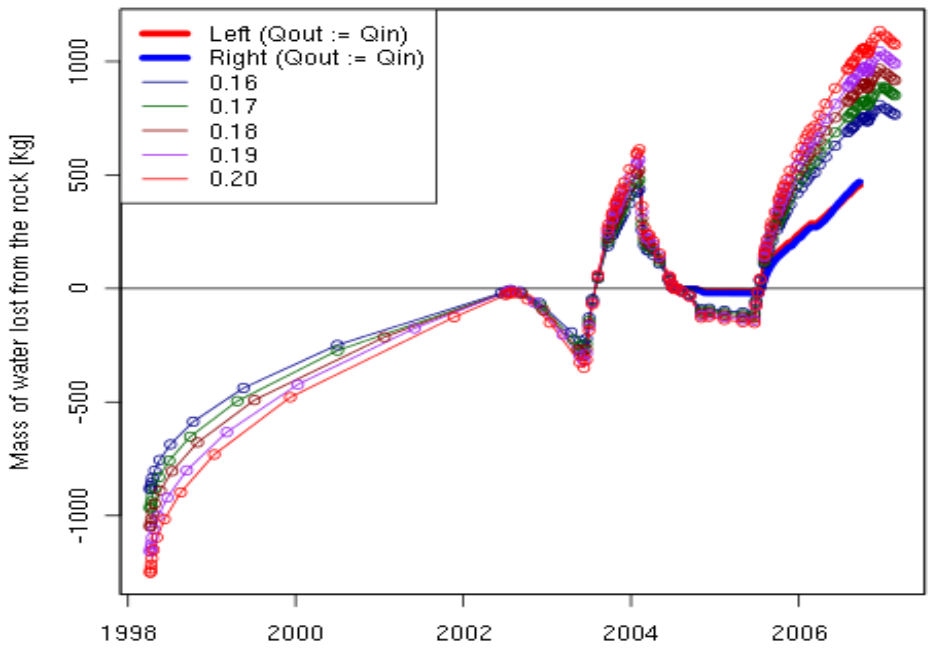


Figure 6.27: Porosity sensitivity analysis (1D model) and the new mass balance.

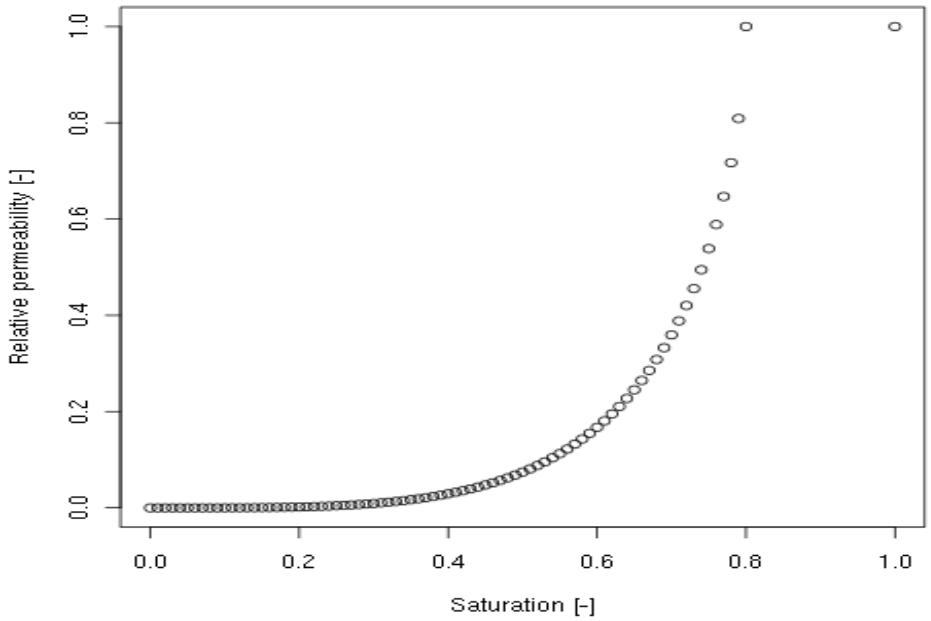


Figure 6.28: A trial relative permeability curve. The curve has a flat top showing $k_{rel} = 1$ between the saturation range 1.0 – 0.8.

linear model than the axisymmetric. This part of the target curve cannot be recreated from the data, because of missing data for flow at the inflow (labelled 'flow in' on figure 6.23), so it is inconclusive which geometry is most appropriate at this last desaturation period. If the target curve is indeed representative of the situation then it could be said that the geometry of water movement is more linear than radial.

While the difference in behaviour is interesting to note in the scope of this thesis, it could be useful in a study of anisotropy.

After the change from 1D to axisymmetry the intrinsic permeability had to be reduced significantly in order to bring the mass balance curve back down to a comparable position. The corollary of this observation is that part of the intrinsic permeability value may compensate for real variation in the geometry of the flow regime between being perfectly radial to linear.

#### Mechanical deformation

The modelled mechanical behaviour (figure 6.18) is fairly close to that shown in the experimental results. An average of all the sensor data looks approximately like the displacement evolution shown by `BVE-47`. Comparing the model with this gauge it can be seen that:

- a slight positive displacement at the start of the data is not seen in the model,
- the subsequent decreasing displacement is not quite steep enough,
- the increase in displacement occurs too early,
- the flattening out occurs to soon.

Refining, or replacing, the capillary pressure boundary condition further (by including a tunnel model) would effect all these features. The sensitivity of the relative displacement to changes in the compressibility, porosity and intrinsic permeability would be worth investigating. This would require minor redesigning of some of the postprocessing functions to accommodate multiple sets of model results.

The simplified mathematical model, although it neglects changes in the stress state of the rock and assumes equilibrium at all times, is a useful approximation of coupled hydraulic and mechanical processes.

#### Chloride concentration

Changing the tortuosity and apparent diffusion coefficient had little effect on the results. The shape of the model's curves vary greatly in time, with results in adjacent time steps looking very different. This observation means that it would be difficult to improve the match with the experimental results without first improving on the hydrodynamic model. The sensitivity of the chloride porosity parameter was not investigated because of this.

#### Relevance of results in the repository context

The shape of the water saturation close to the tunnel wall largely follows the shape of the Dirichlet boundary condition. That this boundary condition is specified at the tunnel wall instead of at each end of the tunnel means that the behaviour of the tunnel/rock system is not captured in such a way as to be directly useful during the construction phase of a repository.

A representation of the behaviour of the tunnel is needed. For this reason the linked model idea developed (see section 5.3.4). Other teams in the DECOVALEX project used computational fluid dynamics (CFD) of the tunnel to try to reproduce the boundary condition at points along the tunnel wall but concluded that the simulation was very sensitive to obstructions in the tunnel, the position of the inlet and outlet pipes. For the linked models, the representation of the boundary condition at the tunnel wall needs some refinement to control the rate of transfer of water mass and to check for conservation of mass between the two models. The run time of the linked models is long so it would be necessary to run parts of OpenGeoSys in parallel. This has already been implemented (by UFZ Leipzig) for standalone models, and would need integrating with the linking scheme.

## 6.2 DECOVALEX Step 0: modelling the Drying Test

Section 3.6.7 made reference to the Drying Test. It was the precursor to the VE, used for scoping parameter values. As such, a brief description is given here. The model setup is shown in figure 6.32.

The application of the Kelvin equation (equation 4.6) results in the $P_c$ boundary condition equivalent to that shown in figure 6.33.

Three cylindrical samples of Opalinus Clay, assumed to be identical[1], are dried for 21 days, 99 days and 142 days, after which times a sample is dissected to determine the saturation at different depths and thereby the profile of water content $wc$ (% dry mass) given by Floría et al. (2002):

$$wc = S\frac{\phi}{(1-\phi)}\frac{\rho_w}{\rho_s} \text{ x } 100\,, \tag{6.7}$$

where $\rho_s$ is the density of the soil.

The responses of all three samples (figure 6.34) were *generally* reproducible using one set of model parameters. At first this would seem like a result that supports the assumption that the samples are homogeneous, however, curves produce by using several different combinations of relative permeability model, intrinsic permeability, and initial saturated permeability could be fitted (figure 6.35). Individual curves were not *exactly* reproducible with a single set of parameters which suggests the samples may be heterogenous (C. McDermott, 2009).

The high sensitivity of a good fit to the choice of relative permeability functions means that other physical processes may be modelled to provide greater mathematical accuracy, however this would not result in more accurate predictions (C. McDermott, 2009). This is similar to findings from modelling the VE in that the uncertainty in the water mass balance determination is masked by the choice of relative permeability function.

[1] There is no data to suggest heterogeneity.

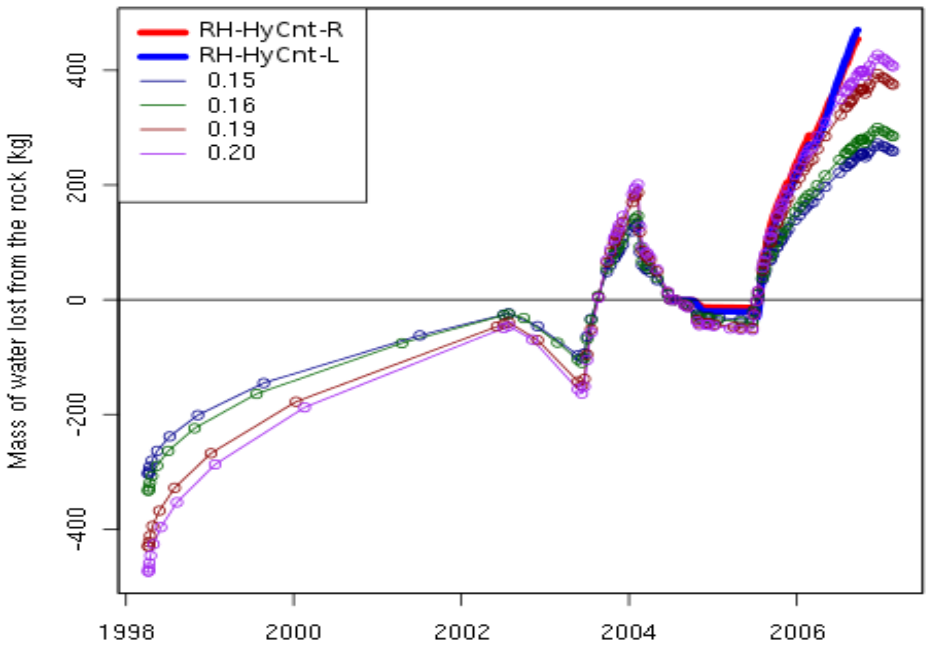


Figure 6.29: Comparison of mass balance with porosity sensitivity analysis using the trial relative permeability vs saturation curve.

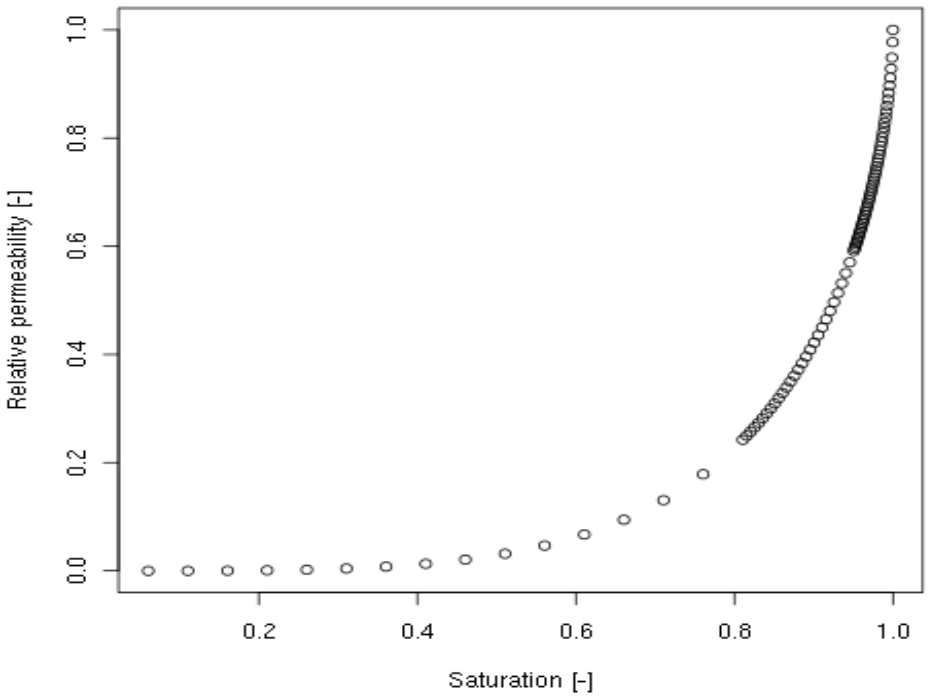


Figure 6.30: Relative permeability curve.

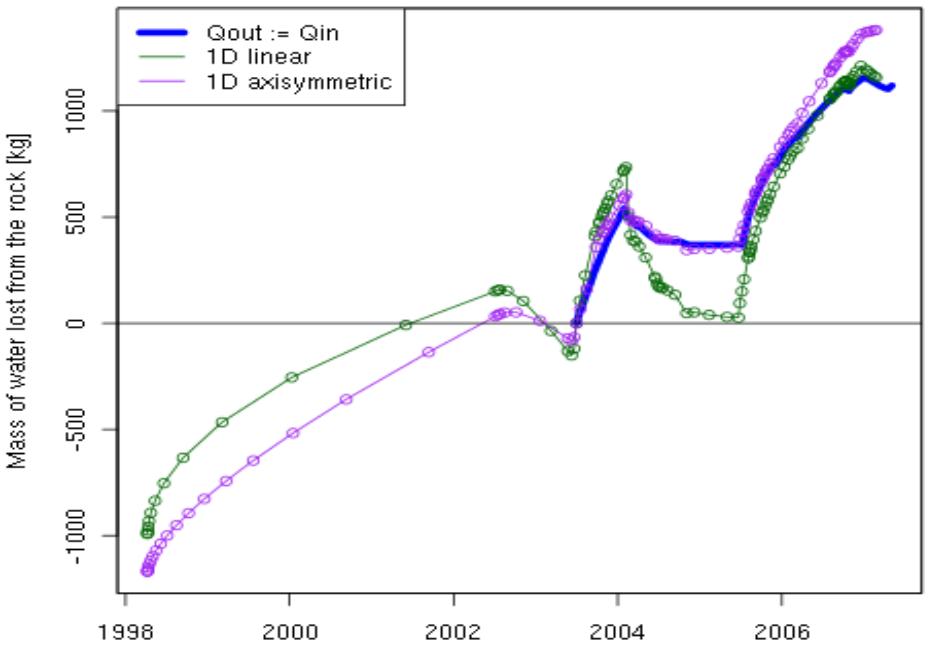


Figure 6.31: Comparison of 1D axisymmetric and 1D linear models. The two have been calibrated to fit the VE results so have different material properties and is not due only to differing geometries.

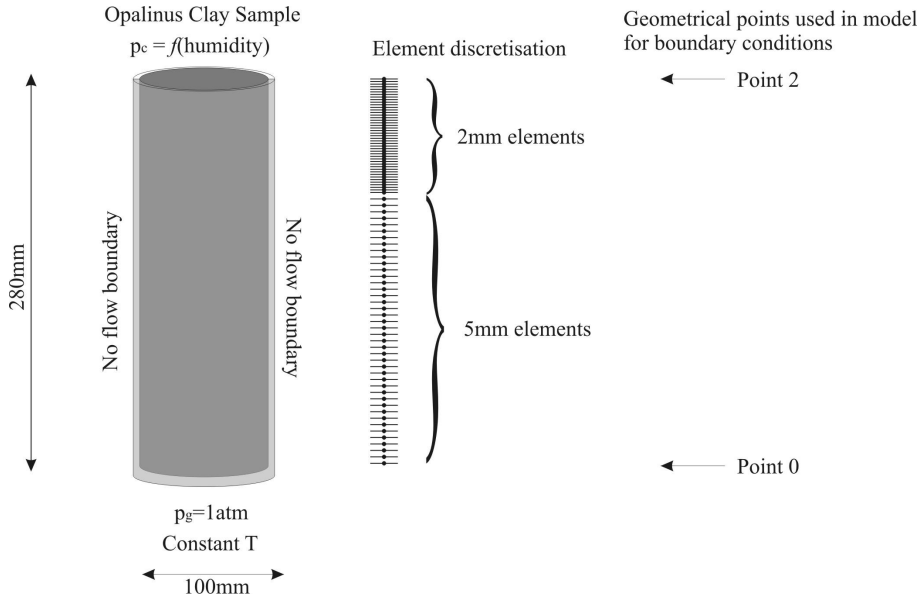


Figure 6.32: Drying Test model setup. Shows the model design, mesh representation and geometrical points used for modelling. Being a one-dimensional (1D) model, the finite element 'mesh' consists of line elements connected by a node at each end. The elements are shorter (2mm) at the drying end of the sample because that is where the changes in parameter values are most dynamic and numerical stability criteria (see section 4.3.4) are critical. *(From C. McDermott, 2009).*

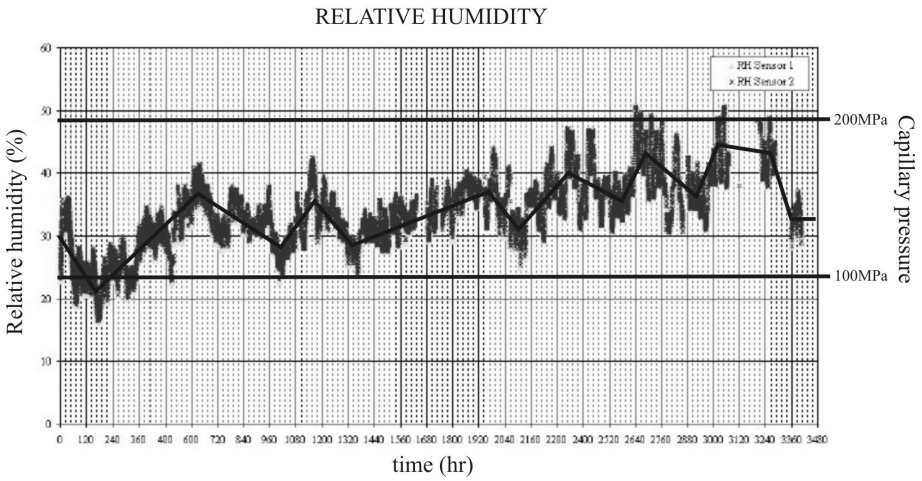


Figure 6.33: Boundary condition of $P_c$ *(RHS y axis)* superimposed on the applied relative humidity. *(From C. McDermott, 2009).*

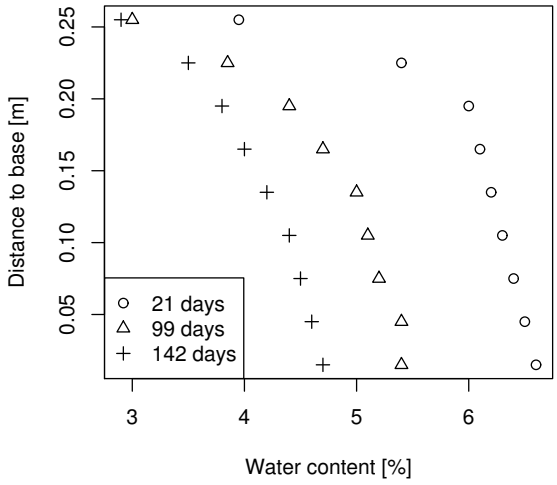


Figure 6.34: Drying Test: Results, water content against distance to base of the drying sample. From equation 6.7, with $\phi = 0.15, \rho_w = 1000, \rho_s = 2700$, and fully saturated ($S = 1$) the water content is 6.54 %. (Although this porosity value is not used consistently, the shape of the curves would not change.) The objective of modelling the Drying Test is to recreate these curves. *(After Floría et al., 2002).*

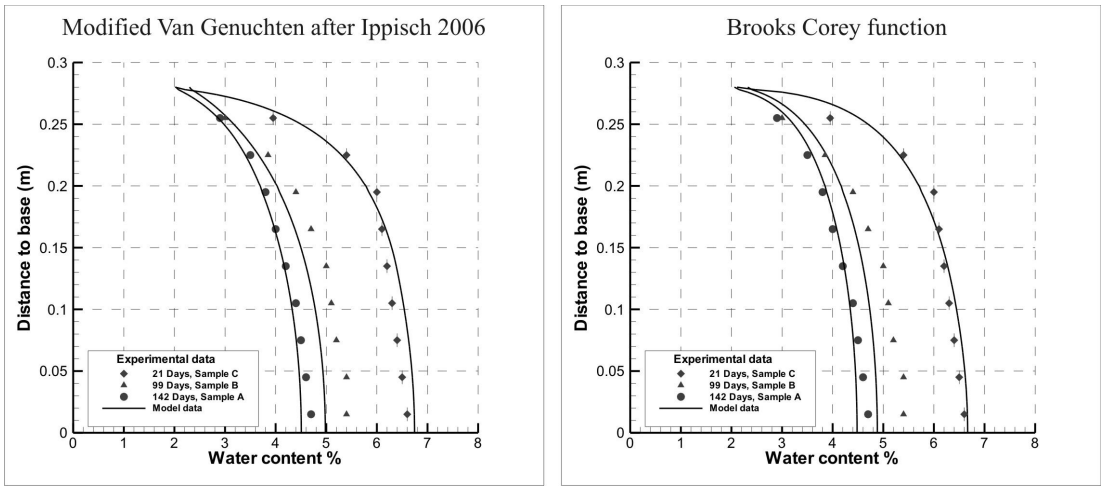


Figure 6.35: Drying Test: Comparison of drying curves for model results based on different functions for $k_{rel} = f(S)$. Both are equally valid and are reasonable matches to the data points (symbols). *(From C. McDermott, 2009).*

Chapter 7

# CONCLUSIONS

The hydrodynamic aspects of the Ventilation Experiment can be modelled satisfactorily, within the uncertainties in the data, using a simple 1D axisymmetric finite element approximation of Richards' Equation, implemented in OpenGeoSys. The mechanical deformation can be derived from this by using a simple postprocessing step and has a good fit with the experimental results. Parameters from the Drying Test were used with some reduction in intrinsic permeability and a change in the formulation used. Chloride concentrations have been reproduced accurately by modelling the conservative mass transport boundary condition at the tunnel wall and OpenGeoSys was developed to achieve this. In completing this work, the most significant coupled processes that would be active during the construction phase of a repository have been characterised, quantified and tested against the results of the field scale experiment.

The water mass balance of the VE was fully explored and an alternative water mass balance curve has been presented and the model fits the results well. A suitable model depends on the right choice of mathematical model, space and time discretisation, domain shape and dimension, software and solver, as well as the data available for comparison of results.

Many different models and variations were investigated and many software utilities were developed around the workflow of developing models and reporting of results. The progress of work to model the VE was significantly influenced by software issues and so ensuring the reproducibility of model results was an important aspect of the work.

An endeavour to replace the tunnel wall boundary with a model of a tunnel, caused OpenGeoSys to be developed to provide new functionality. The two distinct advantages of the method are that the existing code needs only be changed a little and that the program data for the two models are kept separate at the operating system level and only communicate through a strict interface. Among some remaining deficiencies, the application of this coupling method to the final VE model has not been made yet, however the scheme has been shown working in a basic form, but with possible numerical stability issues.

Furthermore, the hydrodynamic VE results are constrained by the availability of calibration targets and the accuracy of the measured water mass balance, and the modelled mechanical response is not coupled with the pore pressure due to software issues.

The most significant uncertainty, with parameters that are the most difficult to measure and with the largest effect on the results, is in the determination of the relative permeability curve. For Step 0, the choice of relative permeability curve parameters was found to be critical. More can be learnt about the underlying processes of multiphase flow through porous media by the investigation of relative permeability functions and it is this topic that has scope for future work, with the potential to increase the accuracy of coupled process models whether applied to nuclear waste disposal or other reservoir engineering challenges.

# BIBLIOGRAPHY


Alonso, E. E. and J. Alcoverro (2005). "The FEBEX test as a benchmark case for THM modelling. Historical perspective and lessons learned". In: *Advances in understanding engineered clay barriers*. International Symposium on Large Scale Field Tests in Granite. Sitges, Barcelona, Spain: Taylor & Francis, p. 3 (cit. on pp. 3, 31).

Anon (Mar. 2008). *The 2007 UK Radioactive Waste Inventory - A Summary of Information for International Reporting*. Pöry Energy Ltd. (cit. on p. 16).

Barnichon, J.-D. and G. Volckaert (2003). "Observations and predictions of hydromechanical coupling effects in the Boom clay, Mol Underground Research Laboratory, Belgium". In: *Hydrogeology journal* 11 (1). Cited by 0022, 193–202 (cit. on p. 12).

Bennethum, L. S., M. A. Murad, and J. H. Cushman (1997). "Modified Darcy's law, Terzaghi's effective stress principle and Fick's law for swelling clay soils". In: *Computers and Geotechnics* 20 (3-4), pp. 245–266 (cit. on pp. 7, 10, 30).

Blümling, P. et al. (2007). "The excavation damaged zone in clay formations time-dependent behaviour and influence on performance assessment". In: *Physics and Chemistry of the Earth, Parts A/B/C* 32 (8-14), pp. 588–599 (cit. on pp. 12, 27).

Blunt, M. J. (2001). "Flow in porous media – pore-network models and multiphase flow". In: *Current Opinion in Colloid & Interface Science* 6 (3), pp. 197–207 (cit. on pp. 9, 11, 44).

Bock, H. (July 2001). *RA Experiment-Rock Mechanics Analyses and Synthesis: Data Report on Rock Mechanics*. Technical Report TR 2000-02 by Q+ S Consult, Mont Terri Underground Rock Laboratory (cit. on p. 26).

Bond, A. E. et al. (Dec. 1, 2012). "Coupled hydro-mechanical—chemical process modelling in argillaceous formations for DECOVALEX-2011". en. In: *Mineralogical Magazine* 76 (8), pp. 3131–3143 (cit. on p. v).

Bond, A. (June 2011). *Decovalex 2011 - Task A, Steps 2 and 3 Report*. QRS-1378J-6 v1.0. Quintessa (cit. on p. 72).

Bond, A., C. McDermott, and M. English (May 2009). *DECOVALEX-2011: TaskA, Step 0 results*. Version 1.0 Draft QRS-1378J-2. Quintessa and University of Edinburgh (cit. on pp. 68, 69, 72).

Bond, A., S. Benbow, et al. (Feb. 2013). "Reactive and non-reactive transport modelling in partially water saturated argillaceous porous media around the ventilation experiment, Mont Terri". In: *Journal of Rock Mechanics and Geotechnical Engineering* 5 (1), pp. 44–57 (cit. on p. v).

Börgesson, L. and J. Hernelind (2005). "Hydraulic bentonite/rock interaction in FEBEX experiment". In: *Advances in understanding engineered clay barriers: proceedings of the International Symposium on Large Scale Field Tests in Granite, Sitges, Barcelona, Spain, 12-14th November 2003*. Taylor & Francis, p. 353 (cit. on pp. 3, 4).

Bossart, P. et al. (Aug. 2004). "Structural and hydrogeological characterisation of the excavation-disturbed zone in the Opalinus Clay (Mont Terri Project, Switzerland)". In: *Applied Clay Science* 26 (1-4), pp. 429–448 (cit. on pp. 12, 27).

Boudreau, B. (1997). *Diagenetic models and their implementation: modelling transport and reactions in aquatic sediments*. Vol. 414. Springer (cit. on p. 72).

Bourgeat, A., M. Jurak, and F. Smaï (2009). "Two-phase, partially miscible flow and transport modeling in porous media; application to gas migration in a nuclear waste repository". In: *Computational Geosciences* 13 (1), 29–42 (cit. on p. 5).

Chan, T. et al. (2005). "DECOVALEX III BMT3/BENCHPAR WP4: The thermo-hydro-mechanical responses to a glacial cycle and their potential implications for deep geological disposal of nuclear fuel waste in a fractured crystalline rock mass". In: *International Journal of Rock Mechanics and Mining Sciences* 42 (5-6), pp. 805–827 (cit. on p. 16).

Chijimatsu, M., H. Kurikami, and Y. Sugita (2005). "Coupled thermo-hydro-mechanical analysis of the Prototype Repository Project using numerical code THAMES". In: *Advances in understanding engineered clay barriers: proceedings of the International Symposium on Large Scale Field Tests in Granite, Sitges, Barcelona, Spain, 12-14th November 2003*. Taylor & Francis, p. 451 (cit. on pp. 4, 9).

Class, H., R. Helmig, and P. Bastian (May 2002). "Numerical simulation of non-isothermal multiphase multicomponent processes in porous media.: 1. An efficient solution technique". In: *Advances in Water Resources* 25 (5), pp. 533–550 (cit. on p. 6).

Couture, F., W. Jomaa, and J.-R. Puiggali (June 1, 1996). "Relative permeability relations: A key factor for a drying model". In: *Transport in Porous Media* 23 (3), pp. 303–335 (cit. on p. 9).

Croisé, J. et al. (2004). "Hydrogeological investigations in a low permeability claystone formation: the Mont Terri Rock Laboratory". In: *Physics and Chemistry of the Earth, Parts A/B/C* 29 (1), pp. 3–15 (cit. on p. 27).

Darcy, H. (1856). "Les fontaines publiques de la ville de Dijon". In: *Dalmont, Paris* 647 (cit. on p. 30).

Degroote, J., K.-J. Bathe, and J. Vierendeels (June 2009). "Performance of a new partitioned procedure versus a monolithic procedure in fluid-structure interaction". In: *Computers & Structures* 87 (11-12), pp. 793–801 (cit. on p. 42).

Dewiere, L., F. Plas, and C. Tsang (1996). "Lessons learned from DECOVALEX". In: *Coupled Thermo-Hydro-Mechanical Processes of Fractured Media - Mathematical and Experimental Studies*. In collab. with L. J. Ove Stephansson and C.-F. Tsang. Vol. Volume 79. Elsevier, pp. 495–504 (cit. on p. 104).

Donea, J. and A. Huerta (June 9, 2003). *Finite Element Methods for Flow Problems*. Wiley. 362 pp. (cit. on p. 39).

DTI (May 2007). *The future of nuclear power: The Role of nuclear power in a low carbon economy*. Consultation Document DTI/Pub 8519/4k/05/07/NP. URN 07/970. Department of Trade and Industry, p. 207 (cit. on p. 16).

Faisal Anwar, A. H. M., M. Bettahar, and U. Matsubayashi (2000). "A method for determining air–water interfacial area in variably saturated porous media". In: *Journal of contaminant hydrology* 43 (2), 129–146 (cit. on p. 9).

Feng, X. T., J. Liu, and L. Jing (2004). "Research and application on coupled THMC processes of geological media in China-A review". In: *Coupled Thermo-Hydro-Mechanical-Chemical Processes in Geo-systems: Fundamentals, Modelling, Experiments and Applications*, p. 37 (cit. on p. 4).

Fernández, A. et al. (Mar. 30, 2007). *Geochemical characterisation of the rock samples for the VE-Test before a second cycle of drying. Draft. NF PRO RTD C4 WP 4.3, EDZ short term evolution: Task 1 (Contract Number: FI6W-CT-2003-02389) Ventilation Test, Phase II, Deliverable 4.3.5* (cit. on pp. 12, 18, 22, 23, 26, 69, 71, 72, 74).

Fernàndez-Garcia, D., J. Jaime Gómez-Hernández, and J.-C. Mayor (2007). "Estimating hydraulic conductivity of the Opalinus Clay at the regional scale: Combined effect of desaturation and EDZ". In: *Physics and Chemistry of the Earth, Parts A/B/C* 32 (8-14), pp. 639–645 (cit. on pp. 12, 13).

Fetter, C. W. (1994). *Applied Hydrogeology*. 3rd. University of Wisconsin-Oshkosh: Prentice Hall. 691 pp. (cit. on p. 44).

Fischer, U. and M. A. Celia (Apr. 1999). "Prediction of relative and absolute permeabilities for gas and water from soil water retention curves using a pore-scale network model". In: *Water Resources Research* 35 (4), pp. 1089–1100 (cit. on pp. 11, 44).

Floría, E., F. Sanz, and J. García-Siñeriz (Jan. 2002). *Ventilation Experiment (VE) Drying test: evaporation rate from core samples of "Opalinus clay" under controlled environmental conditions. Unpublished report. Project Deliverable 6. EC contract FIKW-CT2001-00126* (cit. on pp. 26, 90, 93).

Freiboth, S. et al. (Nov. 16, 2008). "A model for multiphase flow and transport in porous media including a phenomenological approach to account for deformation—a model concept and its validation within a code intercomparison study". In: *Computational Geosciences* (cit. on p. 7).

Freivogel, M. and P. Huggenberger (2003). "Modellierung bilanzierter Profile im Gebiet Mont Terri–La Croix (Kanton Jura)". In: *Mont Terri Project–Geology, paleohydrogeology and stress field of the Mont Terri region. Federal Office for Water and Geology Rep* 4, pp. 7–44 (cit. on p. 20).

Frieg, B. et al. (Dec. 15, 1998). "In situ resin impregnation for investigating radionuclide retardation in fractured repository host rocks". In: *Journal of Contaminant Hydrology* 35 (1-3), pp. 115–130 (cit. on p. 12).

Garavito, A., H. Kooi, and C. Neuzil (Mar. 2006). "Numerical modeling of a long-term in situ chemical osmosis experiment in the Pierre Shale, South Dakota". In: *Advances in Water Resources* 29 (3), pp. 481–492 (cit. on p. 5).

Garitte, B. et al. (Feb. 2013). "Analysis of hydro-mechanical processes in a ventilated tunnel in an argillaceous rock on the basis of different modelling approaches". In: *Journal of Rock Mechanics and Geotechnical Engineering* 5 (1), pp. 1–17 (cit. on pp. v, 13, 26).

Gawin, D., P. Baggio, and B. A. Schrefler (1995). "Coupled heat, water and gas flow in deformable porous media". In: *International Journal for numerical methods in fluids* 20 (7), 967–87 (cit. on p. 7).

Gawin, D. and L. Sanavia (May 24, 2009). "Simulation of Cavitation in Water Saturated Porous Media Considering Effects of Dissolved Air". In: *Transport in Porous Media* (cit. on p. 7).

Gens, A. A. et al. (1998). "Analysis of a full scale in situ test simulating repository conditions". In: *International Journal for Numerical and Analytical Methods in Geomechanics* 22 (7), pp. 515–548 (cit. on p. 7).

Gens, A. et al. (2002). "Factors controlling rock–clay buffer interaction in a radioactive waste repository". In: *Engineering Geology* 64 (2-3), pp. 297–308 (cit. on p. 5).

Genuchten, M. T. van (1980). "A closed-form equation for predicting the hydraulic conductivity of unsaturated soils". In: *Soil Sci. Soc. Am. J* 44 (5), pp. 892–898 (cit. on pp. 33, 69).

Gessner, K. et al. (June 1, 2009). "Coupled Process Models as a Tool for Analysing Hydrothermal Systems". In: *Surveys in Geophysics* 30 (3), pp. 133–162 (cit. on p. 4).

Gibb, F. G. F. (1999). "High-temperature, very deep, geological disposal: a safer alternative for high-level radioactive waste?" In: *Waste management* 19 (3), pp. 207–211 (cit. on pp. 15, 16).

Gray, W. G. (1999). "Thermodynamics and constitutive theory for multiphase porous-media flow considering internal geometric constraints". In: *Advances in Water Resources* 22 (5), 521–547 (cit. on pp. 8, 10).

Gray, W. G. and S. M. Hassanizadeh (May 1991a). "Paradoxes and realities in unsaturated flow theory". In: *Water Resources Research* 27 (8) (cit. on p. 9).

— (May 1991b). "Unsaturated flow theory including interfacial phenomena". In: *Water Resources Research* 27 (8), 1855–1863 (cit. on p. 9).

Gray, W. G. and C. T. Miller (2005). "Thermodynamically constrained averaging theory approach for modeling flow and transport phenomena in porous medium systems: 1. Motivation and overview". In: *Advances in water Resources* 28 (2), 161–180 (cit. on p. 10).

Guo, R. and D. Dixon (June 21, 2006). "Thermohydromechanical simulations of the natural cooling stage of the Tunnel Sealing Experiment". In: *Engineering Geology* 85 (3-4), pp. 313–331 (cit. on pp. 3, 4).

Harrer, H. and K. Maix (1976). *The White Spider: The Story of the North Face of the Eiger*. en. HarperCollins Publishers Limited. 324 pp.

Hassanizadeh, M. and W. G. Gray (1979). "General conservation equations for multi-phase systems: 1. Averaging procedure". In: *Adv. Water Resour* 2 (3), 131–144 (cit. on p. 7).

Hassanizadeh, M. and W. G. Gray (1980). "General conservation equations for multi-phase systems: 3. Constitutive theory for porous media flow". In: *Advances in Water Resources* 3 (1), p. 25 (cit. on p. 7).

Hassanizadeh, S. M., M. A. Celia, and H. K. Dahle (Aug. 1, 2002). "Dynamic Effect in the Capillary Pressure-Saturation Relationship and its Impacts on Unsaturated Flow". In: *Vadose Zone J* 1 (1), pp. 38–57 (cit. on p. 10).

Horseman, S. T. et al. (1996). *Water, Gas and Solute movement through argillaceous media, NEA*. OECD, Report CC-96/1, Paris (cit. on pp. 18, 19, 37).

Horseman, S., J. Harrington, and D. Noy (2007). "Swelling and osmotic flow in a potential host rock". In: *Physics and Chemistry of the Earth, Parts A/B/C* 32 (1-7), pp. 408–420 (cit. on pp. 12, 27).

Hudson, J. A. et al. (Jan. 2001). "Coupled T-H-M issues relating to radioactive waste repository design and performance". In: *International Journal of Rock Mechanics and Mining Sciences* 38 (1), pp. 143–161 (cit. on pp. 4, 17).

Istok, J. (1989). "Groundwater modeling by the finite element method". In: *Water Resources Monograph 13. American Geophysical Union, Washington. 1989. 495* (cit. on p. 40).

Jackson, A. S., C. T. Miller, and W. G. Gray (2009). "Thermodynamically constrained averaging theory approach for modeling flow and transport phenomena in porous medium systems: 6. Two-fluid-phase flow". In: *Advances in Water Resources* 32 (6), 779–795 (cit. on p. 10).

Jerauld, G. R. and S. J. Salter (1990). "The effect of pore-structure on hysteresis in relative permeability and capillary pressure: pore-level modeling". In: *Transport in Porous Media* 5 (2), pp. 103–151 (cit. on pp. 8, 9).

Jiao, Y. and J. A. Hudson (July 1995). "The fully-coupled model for rock engineering systems". In: *International Journal of Rock Mechanics and Mining Science & Geomechanics Abstracts* 32 (5), pp. 491–512 (cit. on p. 6).

Jing, L., C. .-.-F. Tsang, and O. Stephansson (July 1995). "DECOVALEX–An international co-operative research project on mathematical models of coupled THM processes for safety analysis of radioactive waste repositories". In: *International Journal of Rock Mechanics and Mining Science & Geomechanics Abstracts* 32 (5), pp. 389–398 (cit. on pp. 18, 104).

Johnson, L. and F. King (Sept. 2008). "The effect of the evolution of environmental conditions on the corrosion evolutionary path in a repository for spent fuel and high-level waste in Opalinus Clay". In: *Journal of Nuclear Materials* 379 (1-3), pp. 9–15 (cit. on p. 5).

El-Kadi, A. I. and G. Ling (1993). "The Courant and Peclet Number Criteria for the Numerical Solution of the Richards Equation". In: *Water Resources Research* 29 (10), pp. 3485–3494 (cit. on pp. 6, 43, 44).

Kalbacher, T., R. Mettier, et al. (Mar. 1, 2007). "Geometric modelling and object-oriented software concepts applied to a heterogeneous fractured network from the Grimsel rock laboratory". In: *Computational Geosciences* 11 (1), pp. 9–26 (cit. on p. 3).

Kalbacher, T., W. Wang, et al. (2008). "Parallelization Concepts and Applications for THM Coupled Finite Element Problems". In: *Journal of Environmental Science for Sustainable Society* 2, pp. 35–46 (cit. on p. 46).

Kolditz, O., S. Bauer, et al. (Sept. 1, 2012). "OpenGeoSys: an open-source initiative for numerical simulation of thermo-hydro-mechanical/chemical (THM/C) processes in porous media". en. In: *Environmental Earth Sciences* 67 (2), pp. 589–599 (cit. on p. 2).

Kolditz, O. and J. De Jonge (2004). "Non-isothermal two-phase flow in low-permeable porous media". In: *Computational Mechanics* 33 (5), pp. 345–364 (cit. on pp. 5, 6, 34, 38, 42).

Kolditz, O., M. Beinhorn, et al. (Jan. 2008). *GeoSys/RockFlow Version 4.5.10(WW) Open Source Software Design Proposal* (cit. on p. 45).

Kolditz, O. and H. Shao, eds. (Jan. 2010). *OpenTHMC Developer Benchmark Book OGS0-DBB 4.10.07*. In collab. with O.-J. Delfs et al. (cit. on p. 68).

Korsawe, J. et al. (Feb. 2006). "Finite element analysis of poro-elastic consolidation in porous media: Standard and mixed approaches". In: *Computer Methods in Applied Mechanics and Engineering* 195 (9-12), pp. 1096–1115 (cit. on p. 6).

Krabbenhøft, K. (Mar. 2007). "An alternative to primary variable switching in saturated-unsaturated flow computations". In: *Advances in Water Resources* 30 (3), pp. 483–492 (cit. on p. 6).

Lawrence, J., J. Schneider, and P. Zuidema (2002). *Project Opalinus Clay–Safety Report. Demonstration of Disposal Feasibility for Spent Fuel, Vitrified High-level Waste and Long-lived Intermediate-level Waste (Entsorgungsnachweis)*. Nagra Technical Report NTB 02-05, Nagra, Wettingen, Switzerland (cit. on pp. 16, 27).

Logg, A., K.-A. Mardal, G. N. Wells, et al. (2012). *Automated Solution of Differential Equations by the Finite Element Method*. Springer (cit. on p. 73).

Mariner, P. (2004). *In-Drift Precipitates/Salts Model*. ANL-EBS-MD-000045 (cit. on p. 3).

Mason, G. and N. R. Morrow (1991). "Capillary behavior of a perfectly wetting liquid in irregular triangular tubes". In: *J. Colloid Interface Sci* 141 (1), pp. 262–274 (cit. on p. 11).

Maßmann, J. et al. (May 1, 2009). "Investigation of desaturation in an old tunnel and new galleries at an argillaceous site". In: *Environmental Geology* 57 (6), pp. 1337–1345 (cit. on p. 4).

Matray, J. M. and F. Coste (2003). "The Ventilation Experiment at Mont Terri: Preliminary Results and Interpretation of the low humidity-air Phase". In: *Seminar 3 Waste Management,* Eurosafe. Paris, pp. 45–54 (cit. on pp. 20, 21).

Mayer, A. S. and C. Huang (1999). "Development and application of a coupled-process parameter inversion model based on the maximum likelihood estimation method". In: *Advances in Water Resources* 22 (8), pp. 841–853 (cit. on p. 6).

Mayer, G., G. Klubertanz, and J. Croisé (2007). "Modelling of an in situ ventilation experiment in the Opalinus Clay". In: *Physics and Chemistry of the Earth* 32 (8-14), pp. 629–638 (cit. on p. 13).

Mayor, J. C. et al. (2005). "Ventilation experiment in Opalinus Clay for the management of radioactive waste". In: *Publicación técnica.(Empresa Nacional de Residuos Radiactivos)* 1 (7), 1–82 (cit. on p. 20).

Mayor, J.-C., M. Velasco, and J.-L. García-Siñeriz (2006). "Ventilation experiment in the Mont Terri underground laboratory". In: *Physics and Chemistry of the Earth, Parts A/B/C* 32 (8-14), pp. 616–628 (cit. on pp. 20, 27).

Mazurek, M. et al. (2008). *Transferability of geoscientific information from various sources (study sites, underground rock laboratories, natural analogues) to support safety cases for radioactive waste repositories in argillaceous formations.* Uncorrected proof (cit. on pp. 12, 27).

McDermott, C. I., M. Xie, et al. (Jan. 22, 2007). "Geomechanical facies concept and the application of hybrid numerical and analytical techniques for the description of HMC coupled transport in fractured systems". In: *Proceedings of the Thirty-Second Workshop on Geothermal Reservoir Engineering.* Workshop on Geothermal Reservoir Engineering. Stanford University, Stanford, California (cit. on p. 6).

McDermott, C. (Feb. 2007). "Reservoir Engineering and System Analysis: Hydraulic, Thermal and Geomechanical Coupled Processes in Geosystems". Habilitation. Universität Tübingen (cit. on p. 19).

— (Mar. 1, 2009). *TaskA, Step _ 0 Report* (cit. on pp. 13, 26, 29, 90, 92–94).

McDermott, C. I., A. R. Randriamanjatosoa, et al. (June 2006). "Simulation of heat extraction from crystalline rocks: The influence of coupled processes on differential reservoir cooling". In: *Geothermics* 35 (3), pp. 321–344 (cit. on p. 4).

McDermott, C. et al. (Dec. 17, 2008). "Hybrid analytical and finite element numerical modeling of mass and heat transport in fractured rocks with matrix diffusion". In: *Computational Geosciences* (cit. on pp. 3, 42).

Meakin, P. and A. M. Tartakovsky (July 14, 2009). "Modeling and simulation of pore-scale multiphase fluid flow and reactive transport in fractured and porous media". In: *Reviews of Geophysics* 47, RG3002 (cit. on p. 10).

Meijerink, J. A. and H. A. v. d. Vorst (Jan. 1977). "An Iterative Solution Method for Linear Systems of Which the Coefficient Matrix is a Symmetric $M$-Matrix". In: *Mathematics of Computation* 31 (137). ArticleType: primary_article / Full publication date: Jan., 1977 / Copyright © 1977 American Mathematical Society, pp. 148–162 (cit. on p. 43).

Miller, C. T. and W. G. Gray (2005). "Thermodynamically constrained averaging theory approach for modeling flow and transport phenomena in porous medium systems: 2. Foundation". In: *Advances in water resources* 28 (2), 181–202 (cit. on p. 10).

Miller, C. T., G. Christakos, et al. (Mar. 1998). "Multiphase flow and transport modeling in heterogeneous porous media: challenges and approaches". In: *Advances in Water Resources* 21 (2), pp. 77–120 (cit. on pp. 7, 9, 30, 31, 34).

Miller, R. D. (May 1994). "Comment on "Paradoxes and realities in unsaturated flow theory" by WG Gray and SM Hassanizadeh". In: *Water Resources Research* 30 (5), pp. 1623–1624 (cit. on p. 9).

Muñoz, J., A. Lloret, and E. Alonso (May 2003). *Characterization of hydraulic properties under saturated and non saturated conditions. Version 1.0. Project deliverable 4, Unpublished Technical Report, CIMNE.* (Cit. on pp. 12, 26, 32, 71, 72).

NDA (Apr. 2008). *National policies on the long-term management of higher activity wastes.* Update to Nirex Technical Note (Doc number 436003v9). Nuclear Decommissioning Agency, p. 4 (cit. on p. 16).

Neretnieks, I. (2004). "Predicting solute transport in fractured rocks-processes, models and some concerns". In: *Coupled Thermo-Hydro-Mechanical-Chemical Processes in Geo-systems: Fundamentals, Modelling, Experiments and Applications*, p. 19 (cit. on p. 1).

Neuzil, C. E. (1986). "Groundwater Flow in Low-Permeability Environments". In: *Water Resources Research* 22 (8), pp. 1163–1195 (cit. on p. 1).

Nguyen, T. S. et al. (Jan. 2001). "Hydro-mechanical response of a fractured granitic rock mass to excavation of a test pit – the Kamaishi Mine experiment in Japan". In: *International Journal of Rock Mechanics and Mining Sciences* 38 (1), pp. 79–94 (cit. on p. 3).

Nirex (Sept. 2005). *Technical Note: Outline design for a reference repository concept for UK high level waste/spent fuel.* Technical note 502644. Nirex Ltd (cit. on p. 17).

Noy, D. et al. (2004). "An Experimental and modelling study of chemico-osmotic effects in the Opalinus Clay of Switzerland". In: *Mont Terri Project-Hydrogeological Synthesis, Osmotic Flow. Reports of the Federal Office for Water and Geology (FOWG), Geology Series (6)*, 95–126 (cit. on p. 26).

OECD Nuclear Energy Agency (2003). *Features, Events and Processes (FEPs) for Geologic Disposal of Radioactive Waste: An International Database* (cit. on pp. 12, 19, 27).

Pearson, F. J. et al. (2003). *Mont Terri project: Geochemistry of water in the opalinus clay formation at the Mont Terri rock laboratory.* Synthesis Report 5. Bern, Switzerland: Suisse Office Fédéral des Eaux et de la Géologie OFEG. (cit. on pp. 12, 27).

PostgreSQL Global Development Group (2012). *PostgreSQL: The world's most advanced open source database.* PostgreSQL (cit. on pp. 23, 47).

Pruess, K. (1991). *TOUGH2 A general purpose numerical simulator for multiphase fluid and heat flow* (cit. on p. 13).

R Core Team (2012). *R: A Language and Environment for Statistical Computing.* ISBN 3-900051-07-0. R Foundation for Statistical Computing. Vienna, Austria (cit. on p. 47).

Reeves, P. C. and M. A. Celia (1996). "A functional relationship between capillary pressure, saturation, and interfacial area as revealed by a pore-scale network model". In: *Water Resources Research* 32 (8), pp. 2345–2358 (cit. on pp. 10, 11, 32).

Reggiani, P. et al. (1999). "A unifying framework for watershed thermodynamics: constitutive relationships". In: *Advances in Water Resources* 23 (1), 15–39 (cit. on p. 9).

Romero, E., A. Gens, and A. Lloret (Oct. 1999). "Water permeability, water retention and microstructure of unsaturated compacted Boom clay". In: *Engineering Geology* 54 (1-2), pp. 117–127 (cit. on p. 8).

Rutqvist, J., D. Barr, et al. (2005). "Coupled thermal–hydrological–mechanical analyses of the Yucca Mountain Drift Scale Test—Comparison of field measurements to predictions of four different numerical models". In: *International Journal of Rock Mechanics and Mining Sciences* 42 (5-6), pp. 680–697 (cit. on p. 104).

Rutqvist, J., L. Börgesson, M. Chijimatsu, A. Kobayashi, et al. (Jan. 2001). "Thermohydromechanics of partially saturated geological media: governing equations and formulation of four finite element models". In: *International Journal of Rock Mechanics and Mining Sciences* 38 (1), pp. 105–127 (cit. on p. 6).

Rutqvist, J., L. Börgesson, M. Chijimatsu, J. Hernelind, et al. (May 1, 2009). "Modeling of damage, permeability changes and pressure responses during excavation of the TSX tunnel in granitic rock at URL, Canada". In: *Environmental Geology* 57 (6), pp. 1263–1274 (cit. on pp. 3, 17).

Sanavia, L., F. Pesavento, and B. Schrefler (Mar. 1, 2006). "Finite element analysis of non-isothermal multiphase geomaterials with application to strain localization simulation". In: *Computational Mechanics* 37 (4), pp. 331–348 (cit. on pp. 7, 34, 36, 38).

Schaap, M. G. and M. T. van Genuchten (Dec. 16, 2005). "A Modified Mualem-van Genuchten Formulation for Improved Description of the Hydraulic Conductivity Near Saturation". In: *Vadose Zone J* 5 (1), pp. 27–34 (cit. on pp. 33, 44).

Schembre, J. M. and A. R. Kovscek (Aug. 2003). "A technique for measuring two-phase relative permeability in porous media via X-ray CT measurements". In: *Journal of Petroleum Science and Engineering* 39 (1-2), pp. 159–174 (cit. on p. 9).

Senger, R., P. Marschall, and S. Finsterle (2008). "Investigation of two-phase flow phenomena associated with corrosion in an SF/HLW repository in Opalinus Clay, Switzerland". In: *Physics and Chemistry of the Earth* 33, pp. 317–326 (cit. on p. 5).

Shao, H. et al. (July 2009). "Modeling reactive transport in non-ideal aqueous-solid solution system". In: *Applied Geochemistry* 24 (7), pp. 1287–1300 (cit. on p. 5).

Soler, J. M. (2001). "The effect of coupled transport phenomena in the Opalinus Clay and implications for radionuclide transport". In: *Journal of Contaminant Hydrology* 53 (1-2), pp. 63–84 (cit. on p. 5).

Solexperts (Sept. 2003). *Ventilation Experiment in Opalinus Clay, VE Experiment Hydraulic pulse injection tests, Boreholes of section SA1 to SA2 (phase 1). Deliverable D14a - Solexperts, EC contract FIKW-CT2001-00126* (cit. on pp. 21, 26).

Su, K. (2007). *Development of Hydro-mechanical Models of the Callovo-Oxfordian Argillites for the Geological Disposal of Radioactive Waste (MODEX-REP).* Final FIKW-CT-2000-00029. EC Directorate General for Research Euratom, p. 71 (cit. on p. 12).

Thury, M. (2002). "The characteristics of the Opalinus Clay investigated in the Mont Terri underground rock laboratory in Switzerland". In: *Comptes rendus-Physique* 3 (7-8), pp. 923–933 (cit. on pp. 27, 28).

Traber, D. (Aug. 2003). *Ventilation Experiment in Opalinus Clay "VE" Experiment Initial sample laboratory results Geochemical characterisation of samples from drill core BVE82.* Rock Water Interaction Group, Institute of Geological Sciences, University of Bern, Switzerland (cit. on pp. 23, 26).

— (June 2004). *Geochemical Characterisation of Core Samples for Borehole BVE-85 and BVE-86 (Post Desaturation Phase)-Geochemical Process Evaluation. Project Deliverable D5c&d/D22. EC contract FIKW-CT2001-00126* (cit. on pp. 23, 26, 74).

Tsang, C. F. (1991). "Coupled hydromechanical-thermochemical processes in rock fractures". In: *Reviews of Geophysics* 29 (4), pp. 537–551 (cit. on p. 18).

Tsang, C. F. et al. (2009). "DECOVALEX Project: from 1992 to 2007". In: *Environmental Geology* 57 (6), pp. 1221–1237 (cit. on pp. 17, 105).

Tsang, C.-F. (May 1, 2009). "Introductory editorial to the special issue on the DECOVALEX-THMC project". In: *Environmental Geology* 57 (6), pp. 1217–1219 (cit. on p. 104).

Tsang, C.-F. et al. (2005). "The DECOVALEX III project: A summary of activities and lessons learned". In: *International Journal of Rock Mechanics and Mining Sciences* 42 (5-6), pp. 593–610 (cit. on pp. 3, 15, 104).

Wang, W., G. Kosakowski, and O. Kolditz (Aug. 2009). "A parallel finite element scheme for thermo-hydro-mechanical (THM) coupled problems in porous media". In: *Computers & Geosciences* 35 (8), pp. 1631–1641 (cit. on p. 46).

Wang, W., C.-H. Park, and O. Kolditz (June 23, 2009). *Programming notes: Equations of multiphase flow in porous media.* (Cit. on p. 34).

Xie, M. et al. (Feb. 1, 2007). "Numerical Modelling of Swelling Pressure in Unsaturated Expansive Elasto-Plastic Porous Media". In: *Transport in Porous Media* 66 (3), pp. 311–339 (cit. on pp. 6, 7).

Zhang, G., J. Samper, and L. Montenegro (2008). "Coupled thermo-hydro-bio-geochemical reactive transport model of CERBERUS heating and radiation experiment in Boom clay". In: *Applied Geochemistry* 23 (4). Cited by 0013, 932–949 (cit. on p. 3).

Zheng, L. et al. (2004). "Flow and reactive transport model of a ventilation experiment in Opalinus Clay". In: *month* 29, p. 1 (cit. on p. 13).

— (2008). "Multiphase flow and multicomponent reactive transport model of the Ventilation Experiment in Opalinus Clay". In: *Physics and Chemistry of the Earth, Parts A/B/C* 33 (Supplement 1), S186–S195 (cit. on pp. 2, 13).

Zhou, Y. (1998). "Thermo-hydro-mechanical models for saturated and unsaturated flow in porous media". PhD Thesis. University of Manitoba (cit. on p. 6).

Zhu, W. et al. (Oct. 2007). "Analysis of coupled gas flow and deformation process with desorption and Klinkenberg effects in coal seams". In: *International Journal of Rock Mechanics and Mining Sciences* 44 (7), pp. 971–980 (cit. on p. 4).

Zienkiewicz, O. C., R. L. Taylor, and J. Z. Zhu (2005). *The finite element method: its basis and fundamentals. 2005*. Elsevier Butterworth Heinemann, Oxford (cit. on pp. 18, 39).

Appendix A

# THE DECOVALEX PROJECT

Overviews and summaries of the project so far can be found in Dewiere et al. (1996); Jing et al. (1995); Rutqvist, Barr, et al. (2005); C.-F. Tsang (2009); C.-F. Tsang et al. (2005) and in table A.1. A loose acronym of *DEvelopment of COupled process models and VAlidation against EXperiments*, the project has now spanned 17 years or so. The objectives are to (C.-F. Tsang, 2009):

- support development of numerical simulators for THM and THMC[1] processes in geological systems,
- investigate and implement suitable algorithms for THM and THMC modeling,
- compare model calculations with results from field and laboratory experiments,
- design new experiments to support code and model development, and
- study the application of THM and THMC modelling to performance and safety assessment of nuclear waste repositories.

The most recently completed project, 'DECOVALEX 2011', is comprised of three Tasks:

**Task A** Modelling the Ventilation Experiment.

**Task B** Pillar stability and fracturing near excavation rock surfaces expeeriments of SKB[2].

**Task C** Modelling fluid flow, rock stress evolution and contaminant transport in fractured rock.

[1] Thermal, Hydraulical, Mechanical, Chemical.
[2] Svensk Kärnbränslehantering AB — Swedish Nuclear Fuel and Waste Management Co.

| Phase/time period | Benchmark test (BMT), test case (TC) and Task | References to results |
|---|---|---|
| DECOVALEX I, 1992–1995 | BMT 1: Fractured rock with two orthogonal sets of persistent fractures and a heat source<br>BMT 2: Fractured rock with four discrete fractures and a finite-length heat source<br>BMT 3: Fractured rock with a realistic fracture network of 6,580 fractures from Stripa mine data<br>TC 1: Laboratory shear-flow test on rock core sample with a single joint<br>TC 2: Field experiment in fractured rock at Fanay-Augeres, France<br>TC 3: Large-scale laboratory experiment of engineered buffer material (Big-Ben experiment, Japan)<br>TC 4: Laboratory stress flow tests on rock fractures<br>TC 5: Laboratory shear-flow experiment of a rock block with a single joint<br>TC 6: Field experiment of hydraulic injection test on fractures at 356 m depth | Book: Coupled T-H-M processes of fractured media (Stephansson et al. 1996) (27 papers) and Special issue of Int J Rock Mech Min Sci Geomech Abstr vol 32 No.5, 1995 (9 papers) |
| DECOVALEX II, 1995–2000 | Task 1: Numerical study of Nirex's Rock Characterization Facility (RCF) shaft excavation at Sellafield, UK<br>Task 2: Numerical study of PNC's in situ THM experiments in Kamaishi Mine, Japan<br>Task 3: Review of the state-of-the-art of the constitutive relations for rock joints<br>Task 4: Current understanding of the coupled THM processes related to design and PA[a] of radioactive waste repositories | Special issue of Int J Rock Mech Min Sci vol 38 No.1, 2001 (12 papers) |
| DECOVALEX III, 2000–2003 | Task 1: FEBEX (Full-scale engineered barriers experiment in crystalline host rock)<br>Task 2: The drift scale test (DST) at Yucca Mountain<br>BMT 1: Implications of THM coupling on the near-field safety of a nuclear waste repository<br>BMT 2: Upscaling of the THM properties in a fractured rock mass and its significance for large-scale repository PA<br>BMT 3: The THM responses to a glacial cycle and their potential implications for deep geological disposal of nuclear fuel waste in a fractured crystalline rock mass | Proceedings GeoProc 2003; Coupled T-H-M-C processes in geosystems (Stephansson et al. 2004) (33 papers); Special issue of IntJ Rock Mech Min Sci vol 42 No. 5–6, 2005 (18 papers) |
| DECOVALEX-THMC, 2004–2007 | Task A: Influence of near field coupled phenomena on the performance of a spent fuel repository 2007<br>Task B: Understanding and characterizing the excavation damaged zone (EDZ)<br>Task C: Excavation damaged zone (EDZ) in the argillaceous Tournemire Site (France)<br>Task D: Long-term permeability/porosity changes in the EDZ and near field, due to THM and THC processes in volcanic and crystalline-bentonite systems<br>Task E: THM processes associated with long-term climate change: glaciation case study | Proceedings GeoProc 2006 (Xu et al.) (24 papers) and Special issue of Environ Geol 57(6) (12 papers) |

Table A.1: The DECOVALEX Project: phases, tasks, and results (C. F. Tsang et al., 2009, Pg. 1224, Table. 2).

[a]Performance Assessment

Appendix B

# SOURCE CODE, MODEL FILES AND UTILITIES – CD-ROM

The attached CD-ROM[1] includes the final VE model and source code.

## B.1 `models/` – OpenGeoSys model input files

**1D_horiz** the current VE model

**axial_rock** rock model for linked models

**axial_tunnel** tunnel model for linked models

## B.2 `sources/` – OpenGeoSys source code

A git repository with three branches:

**clneuman** includes chloride boundary condition developed

**linkDev** development domain linking branch

**UoE@7537** trunk plus some development, the stable branch.

## B.3 `linked_nodes/` – linked nodes module for OpenGeoSys

When combined with the rest of the OpenGeoSys source code, these modules provide the functionality for the linked nodes method described in section 5.3.4.

`link_model.h`

`link_model.cpp`

`rf_st_new.h.diff` patch against rf_st_new.h

`rf_st_new.cpp.diff` patch against rf_st_new.cpp

## B.4 `tools/` – tools for use with OpenGeoSys models

**tagWithMetadata.sh** prints provenance metadata for a model and source tree

**importResultsToDB.sh** used in the first postprocessing step, imports the results into the database

[1] md5sum: 9d99f22c19d46513923c0a0af2166a95

## B.5 ogs_template.sql

A database schema for managing OpenGeoSys model results.

## B.6 mechanics.sql

Mechanical deformation calculation in the database. The query (or 'view' in PostgreSQL) `getDisplacements` calls all of the other views to calculate the displacement.

## B.7 fenics - FEniCS implementation of the VE

`taska_fenics.py` main model

`tunnel_bc.py` tunnel boundary condition